Mariella Polino

Master of Science in Chemistry and Pharmaceutical Technologies

Ion-exchange membranes for protein crystallization and protein crystals' derivatization

Dissertation for obtaining the degree of

Doctor of Philosophy in
Membrane Engineering

Adviser: João Paulo Serejo Goulão Crespo, Full Professor, NOVA University of Lisbon

Co-advisers: Isabel Maria Rôla Coelhoso, Assistant Professor with Habilitation, NOVA University of Lisbon

Reyes Mallada, Associate Professor, University of Zaragoza

Han Gardeniers, Full Professor, University of Twente

Examination Committee

Chairperson: Prof. Maria João Romão, Universidade Nova de Lisboa
Raporteurs: Prof. João Pedro Estrela Rodrigues Conde, University of Lisbon
Dr. Gianluca di Profio, Istituto per la Tecnologia delle Membrane (ITM)
Members: Prof. Maria João Romão, Universidade Nova de Lisboa
Prof. João Paulo Serejo Goulão Crespo, Universidade Nova de Lisboa

FACULDADE DE CIÊNCIAS E TECNOLOGIA
UNIVERSIDADE NOVA DE LISBOA

March, 2019

Ion-exchange membranes for protein crystallization and protein crystals' derivatization

This document was created using the (pdf)LaTeX processor, based in the "novathesis" template[1], developed at the Dep. Informática of FCT-NOVA [2].
[1] https://github.com/joaomlourenco/novathesis [2] http://www.di.fct.unl.pt

To my Family.

Acknowledgements

Pursuing a PhD was for me, so far, the most amazing experience. It was the best way to challenge myself, learn and perform different things every day. I was blessed with the possibility to carry out my own research work in three different universities in three different countries and benefit from the support and advice of many supervisors. The help received from all of them was crucial for both my professional and personal development. Hence, I would like to dedicate here few lines of acknowledgements to each one of them.

First of all, I would like to express my sincere gratitude to Prof. João Crespo, for giving me the opportunity to carry out my PhD in his research group and for the guidance, the constant encouragement and support, especially in the last phase of the PhD.

I would like to profoundly thank Prof. Isabel Coelhoso, for her kindness, constant availability and for being an important reference point since my first day in the Faculdade de Ciências e Tecnologia, Universidade Nova de Lisboa. I also would like to sincerely acknowledge Dr. Carla Portugal for the scientific advices that enhanced the value and quality of my work.

I am deeply grateful to Prof. Reyes Mallada, for the constant motivation and the energy she transmitted to me, during the time I spent at the Instituto de Nanociencia de Aragón, Universidad de Zaragoza. I owe my gratitude also to Prof. María Pilar Pina for teaching me the importance of small details in doing a good job and also for the interest and excitement towards my work.

I would like to greatly acknowledge Prof. Han Gardeniers, for welcoming me in the Mesoscale Chemical Systems Group at University of Twente and for providing me the opportunity to learn about microfluidics. I am definitely grateful to Dr. Hoon Sook Rho for the patience in teaching me about microfluidics and all the advices that helped me improve my work.

Apart from the supervisors, I feel other people too contributed to the development of my thesis and should be acknowledged here.

I would like to acknowledge all the members of Erasmus Mundus Doctorate in Membrane Engineering for the support during the program and the annual meetings.

At Nova University of Lisbon, I would like to express my gratitude to:

Prof. Maria João Romao for allowing me to collaborate with her research group. Prof. Ana Luisa de Carvalho and Dr. Ramesh Pandian for their constant availability and help during the crystallographic analysis. Dr. Lina Juknaité for the assistance during the process of structure resolution of my crystals. Joana Monte for being a reference point in the lab, and for helping me always with a smile. Dª Maria Jose and Dª Palmina for the kindness and help whenever I needed it. Nuno from the cafeteria for all the pasteis de nata and the jokes that turned my grumpy face into a smile during difficult days.

At the University of Zaragoza, I would like to acknowledge:

Nuria Navascues for the constant support in the lab. Marta Lafuente for helping me with the nanoimprint lithography equipment and the spotting machine. All the technicians from the Cleanroom and SEM for their kindness and patience during the trainings.

At the University of Twente, I extend my gratitude to:

Stephan for preparing my devices and for the patience in showing me all the processes in the cleanroom. Pino for his availability and constant help. Brigitte Boogaard and Susan for the assistance during bureaucratic issues.

Besides the desire to challenge myself with science, one of the main reasons that motivated me to join the EUDIME program was the concept of experiencing life in three different countries. The very first moment my brain processed the idea of pursuing this PhD, I could picture myself not just in the lab but also travelling, having international friends and speaking new languages.

After 4 years, I can say reality did not disappoint my expectations. I am grateful for all the trips and experiences I had. But mostly, for all the amazing friends that supported me during the difficult moments of my journey and/or shared with me the good times.

I am grateful to my conference companion and desk neighbour Carla Martins, for the daily encouragements, the scientific and life related discussions and the amazing trips. I owe my gratitude also to Paloma, (the only "pigeon" I can ever befriend) for supporting and tolerating me during the most difficult months of my work. Many thanks to Giorgia, for bearing with me the emotions and the stress of writing a PhD thesis and the proposition for a healthy life.

I would like to thank Costa for all the talks at "the bar" with a *copo de vinho verde* or a bottle of super bock, and also Mani, Alex and Yen for always being there to take care of me and cheer me up! I definitely want to thank Inês and Rafael for all the funny moments in the office and outside and for improving my culture about Marvel movies.

I wish to thank Roberta, the most generous and kind person, for making me feel at home in Zaragoza and for sharing lots of hard-working moments with me. I am thankful to Thijs for being a good friend, for the road trip he planned for me just because I wanted to see the seals and for introducing me to Trap music. My gratitude goes also to Amaia, Yannick, Michela, Sho, Peter and Pieter, Yiyuan, Hanky and Brigitte Bruijns that made my days at UTwente better and funnier!

When I got my acceptance to this PhD, I had no idea that I was going to be part of a big family: the Eudime Family. My Eudimates were a crucial part of this experience and I cannot fail to acknowledge them:

I would like to thank Magda for the constant support and motivation, all the skype-calls and the beard jokes that only We can understand; Usman for taking care of me whenever I needed and for cheering me up during difficult moments; also my good friends Sergio Santoro, Nayan and Lakshmeesha for all the help, the jokes, the trips and the good time spent together.

I met many amazing friends also outside the university and I feel they also supported me during all these years. I am definitely grateful to my first Portuguese friend Alda, for welcoming me in Portugal, helping during my initial days here, and for being an inspiring person to me.

I feel grateful to Sergio Casimiro for helping me when I reached Lisbon for the first time, Elisa for the funny and crazy moments we shared, Paulo and Catia, always kind and helpful, Nichin and Marie, for the veggy dinners on Thursday night and for teaching me amazing words like *Kudlapura* and *Yelito Kopito Platito*!

Many thanks to my old friend Cinzia *Uncol* for always being present in my life and being supportive despite the distance. I wish to acknowledge Bianca, my best roomie ever, for all the *Credence Clearwater Revival* sessions of house cleaning and the karaoke in the kitchen with *Abba*'s songs.

Lastly, but definitely not because of lesser importance, I express my deepest gratitude to my family who has always taken care of me and in particular my brothers Mario and Nico for all the advices and support and my parents, the first people who believed in

me and never failed to show their encouragement during the challenges I undertook and their pride for my achievements.

Ever tried. Ever failed. No matter. Try Again.

Fail again. Fail better.

- Samuel Beckett -

Abstract

This PhD thesis is focused on the application of ion-exchange membranes for protein crystallization and protein crystals derivatization. The experimental work is divided in three parts. The first part of the work is focused on the understanding of the effect of topography on nucleation. Soft lithography is used to modify the surface topography of Nafion® membranes with target designs, avoiding changes of surface chemistry that might mask the effect of topography on nucleation. The imprinted membranes are characterized by Atomic Force Microscopy (AFM), Scanning Electron Microscopy (SEM) and contact angle and tested for the crystallization of Trypsin from Bovine Pancreas. Nucleation and crystals growth are followed over time by optical microscope. Experimental results are compared with theoretical calculations of the ratio of change of Gibbs free energy of heterogeneous to homogeneous nucleation. The second part of the work is focused on the development of a method for performing a gentle derivatization of protein crystals using ion-exchange membranes. Nafion® and Neosepta 01 were selected after an initial screening of several membranes, due to their ability of promoting nucleation. The kinetics of ion-transport for Br^-, $PtCl_4^{2-}$ and Hg^{2+} is evaluated and used for modelling the transport in the derivatization set-up. Stability of crystals derivatized by ion-exchange membranes over time is compared with the stability of crystals derivatized by the conventional soaking method. The crystals derivatized by the help of the ion-exchange membranes are analysed by synchrotron and protein structure resolved with the Isomorphous Replacement technique. The third part of the work involves the integration of the ion-exchange membrane derivatization concept in a Polydimethylsiloxane (PDMS) microdevice. A microdevice composed of two compartments, one with channels and one with wells is designed and built by photolithography and soft-lithography. Bonding of the membrane to the PDMS parts is done by grafting. Transport modelling of water, NaCl and Hg^{2+} transport in the microdevice, crystallization experiments where

supersaturation is achieved by osmosis and evaluation of the crystals' diffraction quality are performed.

Keywords: Crystallization, Derivatization, Protein, Ion-exchange membranes ...

Resumo

Nesta tese de doutoramento foi investigada a utilização de membranas de permuta iónica, para cristalização de proteínas e derivatização dos cristais de proteínas. O trabalho experimental está dividido em três partes. A primeira parte do trabalho está focada na compreensão do efeito da topografia no processo de nucleação. A *soft*-litografia é usada para modificar a topografia de superfície das membranas Nafion® com padrões específicos, evitando alterações da composição química de superfície que possam mascarar o efeito da topografia na nucleação. As membranas impressas são caracterizadas por Microscopia de Força Atómica (AFM), Microscopia Eletrónica de Varrimento (SEM) e ângulo de contacto e testadas para a cristalização de Tripsina de Pâncreas de Bovino. A nucleação e o crescimento dos cristais são controlados ao longo do tempo através de microscopia óptica. Os resultados experimentais são comparados com cálculos teóricos da razão de variação de energia livre de Gibbs de nucleação heterogénea e homogénea. A segunda parte do trabalho está focada no desenvolvimento de um método para realizar uma *soft*-derivatização de cristais de proteína usando membranas de permuta iónica. Nafion® e Neosepta 01 foram selecionadas após uma triagem inicial de várias membranas devido à sua capacidade de promover a nucleação. A cinética de transporte de iões Br^{-}, $PtCl_4^{2-}$ e Hg^{2+} foi avaliada e usada para modelar o transporte na célula de derivatização. A estabilidade dos cristais derivatizados com a membrana de permuta iónica ao longo do tempo foi comparada com os cristais derivados pelo método convencional de imersão. Os cristais obtidos com as membranas de permuta iónica foram analisados por sincrotrão e a estrutura proteica resolvida com a técnica de substituição isomórfica. A terceira parte do trabalho envolveu a integração do conceito de derivatização da membrana de permuta iónica num microdispositivo de polidimetilsiloxano (PDMS). Um microdispositivo composto por dois compartimentos, um com canais e outro com poços, foi desenhado e construído por fotolitografia e *soft*-litografia. A ligação da membrana ao PDMS foi feita por *grafting*.

Foi realizada a modelação do transporte de água, NaCl e Hg^{2+} no microdispositivo, bem como ensaios de cristalização onde a supersaturação foi obtida por osmose e a qualidade de difração dos cristais foi avaliada.

Palavras-chave: Cristallização, Derivatização, Proteínas, Membranas de permuta iónica ...

Resumen

Esta tesis doctoral se centra en la aplicación de membranas de intercambio iónico para la cristalización de proteínas y la derivatización de cristales de proteínas. El trabajo experimental se divide en tres partes. La primera parte del trabajo se centra en la comprensión del efecto de la topografía en la nucleación. La *soft*-litografía se utilizó para modificar la topografía superficial de las membranas Nafion® con diseños específicos, evitando así cambios en la química de la superficie que pueden enmascarar el efecto de la topografía en la nucleación. Las membranas impresas se caracterizaron por microscopia de fuerza atómica (AFM), microscopia electrónica de barrido (SEM) y ángulos de contacto, y se analizó la cristalización de tripsina de páncreas bovino. La nucleación y el crecimiento de los cristales se controlaron a lo largo del tiempo mediante el uso de microscopía óptica. Los resultados experimentales se compararon con los cálculos teóricos del ratio de la variación de la energía libre de Gibbs de nucleación heterogénea y homogénea. La segunda parte del trabajo se centró en una *soft*-derivatización de cristales de proteínas utilizando membranas de intercambio iónico. Nafion® y Neosepta 01 se seleccionaron entre varias membranas por su capacidad de facilitar la nucleación. La cinética del transporte de iones para Br^-, $PtCl_4^{2-}$ y Hg^{2+} se evaluó para modelar el transporte en la celda de derivatización. La estabilidad de los cristales derivatizados por membranas de intercambio iónico a lo largo del tiempo fue comparada con la estabilidad de los cristales derivatizados por el método convencional de inmersión. Los cristales derivatizados con las membranas de intercambio iónico se analizaron mediante sincrotrón y la estructura de la proteína se resolvió con la técnica de reemplazo isomorfo. La tercera parte del trabajo consistió en la integración del concepto de derivatización con membranas de intercambio iónico en un microdispositivo de polidimetilsiloxano (PDMS). El microdispositivo se diseñó y construyó mediante las técnicas de fotolitografía y *soft*-lithography. La unión de la membrana al PDMS se realizó mediante *grafting*. Se realizaron la modelización del transporte de agua,

NaCl y Hg^{2+} en el microdispositivo, los experimentos de cristalización donde la sobresaturación se conseguió mediante ósmosis, y la evaluación de la calidad de difracción de los cristales se realizó.

Palavras-llave: cristalizacion, derivatizacion, proteinas, membranas de intercambio ionico . . .

Abstract

Dit PhD proefschrift gaat over de applicatie van non-ion-wisselende membranen voor proteïne kristallisatie en proteïne kristal derivatisering. Het experimentele deel is onderverdeeld in drie delen. Het eerste deel van het onderzoek is gefocust op het begrijpen van het effect van oppervlakte topografie op nucleatie. Zachte lithografie wordt gebruikt om de oppervlaktetopografie van Nafion® membranen met specifieke ontwerpen te modificeren, terwijl veranderingen in de oppervlaktechemie van het membraan, die de effecten van de topografiemodificering zouden kunnen maskeren, worden vermeden. De gemodificeerde membranen worden gekarakteriseerd door middel van Atomic Force Microscopy (AFM), Scanning Electron Microscopy (SEM) en contacthoekmetingen. Ook worden ze getest op de kristallisatie van rundertrypsine. De experimentele resultaten worden vergeleken met theoretische berekeningen over de Gibbs vrije energie van heterogene tot homogene nucleatie. Het tweede deel van het onderzoek richt zich op de ontwikkeling van een methode voor zachte derivatisering van proteïne kristallen via het gebruik van ionuitwisselende membranen. Na een eerste screening van membranen zijn Nafion® en Neosepta 01 geselecteerd, omdat deze membranen nucleatie kunnen bevorderen. De kinetiek van iontransport voor Br^-, $PtCl_4^{2-}$ en Hg^{2+} wordt geëvalueerd en gebruikt voor het modelleren van het iontransport in de derivatie opstelling. De stabiliteit van de kristalderivatie door ionuitwisselende membranen over tijd is vergeleken met de stabiliteit van kristallen die zijn gederiveerd via de tradionele weekmethode. De eiwitstructuur van de met behulp van ionenuitwisselingsmembranen gederivatiseerde kristallen worden geanalyseerd door middel van synchrotron, waarna de vergaarde data verwerkt is met behulp van de isomorfe vervangingstechniek. Het derde deel van het onderzoek bestaat uit de integratie van ionuitwisselingsmembranen in een concept apparaat bestaande uit polydimethylsiloxaan (PDMS). Dit apparaat bestaat uit twee compartimenten, een met kanalen en een met putjes, wordt ontworpen en gefabriceerd door middel van zachte lithografie

en fotolithografie. Het hechten van het membraan aan de PDMS-delen gebeurt via enten. Ook worden het transport van water, NaCl en Hg^{2+} in het apparaat, de kristallisatie experimenten waarbij superverzadiging plaatsvind door middel van osmose en de evaluatie van de diffractie kwaliteit van de kristallen gemodelleerd.

Sleutelwoorden: kristallisatie, derivatisering, proteïne, ion-wisselende membranen ...

Contents

List of Figures

List of Tables

List of Acronyms

Abbreviations

AFM atomic force microscopy.

BPT bovine pancreatic trypsin.

BSA bovine serum albumin.

$CC_{1/2}$ Pearson's correlation coefficient.

CNI compact nano imprint.

DMF N,N-dimetilformammide.

CNT classic nucleation theory.

DSC differential scanning calorimetry.

F feeding compartment.

GA glutaraldehyde.

HEWL hen egg white lysozyme.

I reflection intensity.

IEM ion-exchange membrane.

MAC membrane-assisted crystallization.

MD membrane distillation.

MEMS micro electro-mechanic systems.

MIR multiple isomorphous replacement.

MR molecular replacement.

PDB protein data bank.

PDMS polydimethylsiloxane.

PEG polyethylene glycol.

PEGDE poly(ethylene glycol) diglycidyl ether.

pI isoelectric point.

PTFE Polytetrafluoroethylene.

PVA polyvinyl alcohol.

PVDF polyvinylidene difluoride.

R receiving compartment.

Ra average of absolute values of profile height deviations from the mean line.

R$-factor$ discrepancy between experimental data and the model.

R$_{free}$ discrepancy between experimental data and the model for 1000 random diffracted beams.

RH relative humidity.

R$_{meas}$ multiplicity-corrected version of R$_{merge}$.

R$_{merge}$ spread of multiple measurements of a given reflection.

RMS root-mean-square.

R$_{work}$ R$-factor$ for the larger "working" set of reflections.

SAD single-wavelength anomalous dispersion.

SAM self-assembled monolayer.

SCA static contact angle.

SEM scanning electron microscopy.

SLS Swiss light source.

TCDB 1,3,5-tris(10-carboxydecyloxy) benzene.

TFOCS tridecafluoro-1,1,2,2-tetrahydrooctyl-1-trichlorosilane.

VTES triethoxyvinylsilane.

Variables

A area $\left(m^2\right)$ or $\left(cm^2\right)$ or $\left(\mu m^2\right)$.

C concentration $\left(\frac{mol}{L}\right)$.

d specific mass $\left(\frac{g}{cm^3}\right)$.

D diffusion coefficient $\left(\frac{m^2}{s}\right)$.

f fraction.

G Gibbs free energy (J).

h depth (μm).

J molar flux $\left(\frac{mol}{m^2 s}\right)$.

K mass transfer coefficient $\left(\frac{m}{s}\right)$.

l thickness (μm).

M_w molecular weight $\left(\frac{g}{mol}\right)$.

n number of wells.

p vapour pressure (Pa).

Q volumetric flow rate $\left(\frac{mL}{h}\right)$.

R^* critical nucleation radius (m).

R gas constant $\left(\frac{m^3 Pa}{K mol}\right)$.

t time (s) or (min) or (h).

T temperature $(°C)$.

Tg glass transition temperature $(°C)$.

V volume of solution (μL) or (mL) or (m^3).

Greek symbols

γ interfacial energy between nucleus and liquid $\left(\frac{J}{m^2}\right)$.

μ chemical potential $\left(\frac{J}{mol}\right)$.

Ω molar volume $\left(\frac{m^3}{mol}\right)$.

ϕ ratio between Gibbs free energy variation of heterogeneous to homogeneous nucleation.

σ estimated error.

Γ ratio between actual and projected surface.

θ contact angle (°).

Subscripts

0 initial.

c critical.

cb Cassie-Baxter.

eq equilibrium.

Het heterogeneous nucleation.

Hom homogeneous nucleation.

i compound i.

N nucleus.

NL nucleus-liquid.

NS nucleus-substrate.

rep repetition unit.

SL substrate-liquid.

tri triangle.

w water.

wz Wenzel.

Y Young.

Chapter 1

Introduction: motivation and thesis outiline

1.1 Motivation

Proteins are biological macromolecules able to carry out several important functions in the human body: they can act as enzymes, transporters, messengers, structural components, provide energy and so on. Therefore, understanding the three-dimensional structure of protein molecules represents an important step for the investigation of metabolic pathways involved in physiological and pathological processes and for the design of more selective drugs [1]. So far, the main technique used for protein structure resolution is X-ray crystallography: when a monochromatic beam of x-rays shoots a crystal, the interaction of the waves with the electrons of the matter produces a light scattering in different directions. The scattered waves can be collected by a film sensitive to x-rays where a diffraction pattern (dispersed black spots) is generated. Each spot of the diffraction pattern is the result of all the interactions between the initial wave and the matter. The intensity and the scattering angle of the waves are strictly related to the orientation of the molecules in the space, in respect to the x-ray beam. Hence, from the analysis of the diffraction pattern, the electron density map of the unit molecule can be recovered and finally the molecular structure can be resolved. Bearing in mind the importance of molecules' orientation in the data collection, it becomes clear that molecules in a powder

or in a solution with a random orientation lighted with x-rays will not give a diffraction pattern useful for structure determination. Instead, using a repeating organized unit (a crystal) it is possible to generate constructive interferences between the waves that will amplify the signal generated by a single molecule. At this point we can understand how crucial it is for this technique to obtain well-diffracting crystals.

The process of formation of protein crystals is called protein crystallization. Protein crystallization is an event unlikely to occur and only specific conditions may lead to the formation of crystals. Hence, being able to induce nucleation is the first important milestone to achieve in order to obtain well-diffracting crystals. Playing with the types of additives and concentration, temperature, pH, among others helps to find out a range of conditions where crystallization is more likely to occur [2]. Trial-and-error is therefore the most used strategy when a protein has to be crystallized, and finding a way to explore uncommon conditions, investigating the effect of new techniques or materials and developing methods to increase the control of the protein crystallization process is important to amplify the chances of success.

Membrane technology contributed so far to protein crystallization by controlling the solvent removal rate with hydrophobic porous membranes and using the membrane surface as an heterogeneous nucleation promoter, by adjusting their chemistry and topography[3, 4]. In the last years, several studies are pointing out how the chemical interactions can be enhanced by a suitable topography. Indeed, topographical features may affect surfaces' wettability and create physical obstacles for protein molecules creating local supersaturation spikes [5–8]. Different approaches have been used to create surfaces with different topography (functionalization [9], coatings [10], oxidation treatments [11] and so on). However, the topographical change was, in these cases, always promoted as a consequence of a chemical treatment; therefore, it was always difficult to distinguish whether the effects of these surfaces on nucleation were due to the chemistry or to the topography of the surfaces.

Considering this situation, the first part of this thesis is dedicated to the understanding of the effect of pure topographical differences on the nucleation process. To do so, membranes were modified by soft lithographic techniques to imprint specific topographies. The advantages of such techniques, besides the affordability and ease of use, are the possibility to design the target topography and minimise changes in the surface chemistry of the material. Several geometries were designed, and the crystallization results obtained

with the imprinted membranes were compared based on theoretical calculations of the ϕ values, which correspond to the ratio between heterogeneous and homogeneous Gibbs free energy variation of nucleation, using a model that takes into consideration the topographical features.

In some situations, despite all efforts and attempts, when the crystals obtained diffract poorly, or in some other cases such as for completely unknown protein molecules, routine diffraction analysis (Molecular Replacement Techniques) are not able to solve the structure. It becomes essential, in these cases, the introduction of heavy atoms into the crystal (derivatization), in order to facilitate the resolution process by means of Isomorphous Replacement Techniques [12–16]. The crystals derivatization is effective and useful only when the introduction of the heavy atoms occurs without changing the orientation of macromolecules in the space group of the native crystal (isomorphism)[12]. To diffuse those species into the protein crystals and keep the crystalline lattice isomorphous, the native preformed crystals are soaked in a solution containing low concentrations of these compounds, so they can diffuse into the solvent channels of the crystals. The main problems of this procedure are related with the sensitivity of the crystals to abrupt environmental changes. To perform soaking, crystals have to be harvested, removed from their native environment and brought in contact with a solution with a different composition from the growing buffer. All these steps may easily damage the crystals. For this reason, soaking has to be performed in several stages involving the use of several solutions with an increasing concentration of the halide or metal ion to be incorporated[12],being therefore time consuming and involving laborious procedures.

Hence, the second part of this PhD thesis is devoted to the development of a new membrane-based derivatization method able to overcome the most common problems faced by crystallographers in derivatizing protein crystals. Ion-exchange membranes were chosen for this work because they have suitable characteristics for performing derivatization: they are semipermeable barriers, where fixed charged groups are attached to a hydrophobic backbone (usually made of polystyrene)[17]. The hydrophobic backbone guarantees that the protein solution remains on the top of the membrane, and it is not absorbed by the support. At the same time, the presence of charged groups allows the selective transport of the desirable ions across the membrane. Furthermore, controlling protein and derivatization solutions concentration it is possible to have a controlled diffusion avoiding abrupt

changes of the environment, preserving and/or improving diffraction quality of the crystals.

Developing a system where the operator can control the processes involved in x-ray crystallography brings numerous advantages: mostly, the possibility of exploring crystallization conditions with a rational that might bring improvements in the diffraction quality. However, prediction capabilities are still limited, and a screening of conditions is still very important. Besides the time and human work needed for screening conditions, the very limiting requirement is represented by the amount of protein available for performing experiments [18].

For this reason, the last part of this PhD thesis is focused on the design and development of a microfluidic device that can integrate ion-exchange membranes and guarantee a control of both crystallization and derivatization process with a low consumption of reagents.

1.2 Thesis outline

This thesis consists of six chapters. The content of the chapters is the following:

Chapter 1 Introduction: motivation and thesis outline. It describes the motivation and aim of the work and the PhD thesis outline.

Chapter 2 Membrane-assisted crystallization for structure elucidation by x-ray diffraction. It describes the current state of the art on which this thesis is based. The content of this chapter was submitted to Crystal Growth and Design

Chapter 3 Structured Nafion® membranes for protein crystallization. It describes the surface topography modification of ion-exchange membranes by nanoimprint lithography and their effect on protein crystallization compared with theoretical calculations.

Chapter 4 Ion-exchange-membranes for protein crystals derivatization. It describes the development of an ion-exchange membrane contactor to perform derivatization of protein crystals. The content of this chapter was published in Crystal Growth and Design, 2017, 17 (9),4563–4572.

Chapter 5 Ion-exchange membrane-integrated microdevice for protein crystallization and protein crystals derivatization. It describes the design and development of a

microdevice integrating an ion-exchange membrane to be used for protein crystallization and protein crystals derivatization.

Chapter 6 Outlook and future work. It describes the general conclusions of this Ph.D. thesis and suggestions for future work.

References

[1] R. Giegé. "A historical perspective on protein crystallization from 1840 to the present day." In: *FEBS Journal* 280.24 (2013), pp. 6456–6497. DOI: 10.1111/febs.12580.

[2] J. Newman. "A review of techniques for maximizing diffraction from a protein crystal in stilla." In: *Acta Crystallographica Section D: Biological Crystallography* 62.1 (2006), pp. 27–31. DOI: 10.1107/S0907444905032130.

[3] G. Di Profio, A. Caridi, R. Caliandro, A. Guagliardi, E. Curcio, and E. Drioli. "Fine dosage of antisolvent in the crystallization of L-histidine: Effect on polymorphism." In: *Crystal Growth and Design* 10.1 (2010), pp. 449–455. DOI: 10.1021/cg901038g.

[4] E. Curcio, G. Di, and E. Drioli. "Microporous Hydrophobic Membranes for Crystallization of Biomolecules." In: *Chemical Engineering Transactions* 47.2 (2016), pp. 421–426. DOI: 10.3303/CET1647071.

[5] A. S. Ghatak and A. Ghatak. "Precipitantless Crystallization of Protein Molecules Induced by High Surface Potential." In: *Crystal Growth & Design* 16 (2016), pp. 5323–5329. DOI: 10.1021/acs.cgd.6b00833.

[6] A. S. Ghatak, G. Rawal, and A. Ghatak. "Precipitant-Free Crystallization of Protein Molecules Induced by Incision on Substrate." In: *Crystals* 7.8 (2017), p. 245. DOI: 10.3390/cryst7080245.

[7] U. V. Shah, N. H. Jahn, S. Huang, Z. Yang, D. R. Williams, and J. Y. Heng. "Crystallisation via novel 3D nanotemplates as a tool for protein purification and bioseparation." In: *Journal of Crystal Growth* 469 (2017), pp. 42–47. DOI: 10.1016/j.jcrysgro.2016.09.029.

[8] U. V. Shah, D. R. Williams, and J. Y. Heng. "Selective crystallization of proteins using engineered nanonucleants." In: *Crystal Growth and Design* 12.3 (2012), pp. 1362–1369. DOI: 10.1021/cg201443s.

[9] Y. X. Liu, X. J. Wang, J. Lu, and C. B. Ching. "Influence of the roughness, topography, and physicochemical properties of chemically modified surfaces on the heterogeneous nucleation of protein crystals." In: *Journal of Physical Chemistry B* 111.50 (2007), pp. 13971–13978. DOI: 10.1021/jp0741612.

[10] W. De Poel, J. A. W. Mu, J. A.A. W. Elemans, W. J. P. Van Enckevort, A. E. Rowan, and E. Vlieg. "Surfaces with Controllable Topography and Chemistry Used as a Template for Protein Crystallization." In: *Crystal Growth & Design* 18 (2018), pp. 763–769. DOI: 10.1021/acs.cgd.7b01174.

[11] H. Hou, B. Wang, S.-Y. Hu, M.-Y. Wang, J. Feng, P.-P. Xie, and D.-C. Yin. "An investigation on the effect of surface roughness of crystallization plate on protein crystallization." In: *Journal of Crystal Growth* 468.October 2016 (2017), pp. 290–294. DOI: 10.1016/j.jcrysgro.2016.10.007.

[12] A. C. W. Pike, E. F. Garman, T. Krojer, F. von Delft, and E. P. Carpenter. "An overview of heavy-atom derivatization of protein crystals." In: *Acta crystallographica. Section D, Structural biology* 72.Pt 3 (2016), pp. 303–318. DOI: 10.1107/S2059798316000401.

[13] G. L. Taylor. "Introduction to phasing." In: *Acta Crystallographica Section D: Biological Crystallography* 66.4 (2010), pp. 325–338. DOI: 10.1107/S0907444910006694.

[14] M. Dauter and Z. Dauter. "Phase determination using halide ions." In: *Methods in molecular biology (Clifton, N.J.)* 364.9 (2007), pp. 149–158. DOI: 10.1385/1-59745-266-1:149.

[15] J. P. Morth, T. L. M. Sørensen, and P. Nissen. "Membrane's eleven: Heavy-atom derivatives of membrane-protein crystals." In: *Acta Crystallographica Section D: Biological Crystallography* 62.8 (2006), pp. 877–882. DOI: 10.1107/S0907444906023547.

[16] C. Giacovazzo, M. Ladisa, and D. Siliqi. "The approach of the joint probability distribution functions: the SIR-MIR, SAD-MAD and SIRAS-MIRAS, cases." In: *Zeitschrift für Kristallographie - Crystalline Materials* 217.12 (2002), pp. 703–709. DOI: 10.1524/zkri.217.12.703.20660.

[17] T. Xu. "Ion exchange membranes: State of their development and perspective." In: *Journal of Membrane Science* 263.1-2 (2005), pp. 1–29. DOI: 10.1016/j.memsci.2005.05.002.

[18] L. Li and R. F. Ismagilov. "Protein Crystallization Using Microfluidic Technologies Based on Valves, Droplets, and SlipChip." In: *Annu. Rev. Biophys* 39 (2010), pp. 139–58. DOI: 10.1146/annurev.biophys.050708.133630.

Chapter 2

Protein crystallization by membrane-assisted technology

Submitted as: Mariella Polino, Carla A.M. Portugal, Gianluca Di Profio, Isabel M.R. Coelhoso, João G. Crespo, Protein crystallization by membrane-assisted technology, 2019, Crystal Growth & Design*

Summary

In recent years, membrane technology has improved the control of protein crystallization and post-crystallization treatment of protein crystals. Many advancements have been achieved regarding solvent evaporation control, heterogeneous nucleation modulation, diffusion of ligands, and the attainment of a protective environment from the combination of membranes with hydrogel materials. Indeed, membranes allow for finer control of the supersaturation rate and nucleation at lower degrees of supersaturation while also enhancing crystallization kinetics, providing greater stability, and decreasing crystal handling during post-crystallization. This comprehensive view addresses the concept of membrane-assisted crystallization with particular focus on proteins and the impact of the process on the quality of crystal diffraction. Furthermore, it advocates for the benefits of combining membranes with microfabrication technologies and encourages the innovation of new membrane-devices with high throughput for crystallographic purposes.

2.1 Introduction

Protein crystallization is the limiting step for elucidating the tri-dimensional structure of protein molecules by X-ray diffraction analysis. There are numerous parameters that can affect final diffraction resolution and the steps required to obtain well-diffracting crystals: the supersaturation rate, types of additives and concentrations, temperature, pH, protein-surface interactions, and the modification of crystals, among others [1–3]. Moreover, the complex nature of proteins makes it difficult to predict the adequate conditions for promoting nucleation and obtaining well-diffracting crystals [4]. Therefore, there is no single technique that ensures crystallization for all protein types. That is why it is crucial that new methods of generating supersaturation and controlling all parameters of crystal growth be sought out[5]. The most common methods for achieving supersaturation are: the batch method (protein and precipitant solution are mixed under oil and reach the supersaturation state immediately), vapor diffusion (protein and precipitant are mixed and placed in a closed system; part of the solvent migrates in vapor phase towards a stripping solution that determines a slow increase of protein concentration), and liquid-liquid diffusion (protein and precipitant slowly mix by diffusion inside a capillary, thereby creating a concentration gradient) [6].

Membrane-assisted crystallization (MAC) was developed almost 20 years ago and research has looked at how membranes contribute to the fine control of crystallization of both inorganic and macro molecules [7–10]. Membranes were firstly used to control evaporation rates, but, in recent years, many advances have been accomplished by studying surface-protein interactions [11, 12], improving crystal stability during post-crystallization and their effect on crystal diffraction quality [1]. Hydrogel-composite membranes combine the transport properties of a microporous hydrophobic membrane with the ability of the gel to promote specific polymer-solute interactions and to protect crystals from environmental stress. Thus, they have contributed to significant improvement in crystal diffraction quality [13, 14].

The efficiency of membrane technology has also increased recently due to coupling with microfabrication techniques. The use of small volumes, laminar flow, and the low-cost fabrication processes of micro-devices have generated several benefits for the most common membrane processes [15, 16]. However, few studies are yet available regarding the use of micro-technology for improving membranes' properties and processes of

protein crystallization.

This review deals with the development of membrane-assisted crystallization processes of protein molecules, in order to obtain crystals for structure solution. It discusses membrane assisted crystallization and the effect of topography and chemistry on heterogeneous nucleation. Emerging topics such as the use of membranes to improve post-crystallization are also addressed. It goes on to highlight the potential advantages of microfabrication for this field. Finally, it provides an overview of all the roles that membranes can play in crystallization and post-crystallization processes in order to promote further advancements and turn membrane-assisted crystallization into a routine methodology for protein crystallography.

2.2 Principle of protein crystallization

Protein crystallization is the process of forming protein crystals. This happens when molecules are able to organize themselves into an ordered lattice maintained by different types of protein-protein interactions (hydrogen bonding, ionic interactions, and hydrophobic interactions). The process starts when an under-saturated solution reaches the unstable supersaturated state (i. e., when solute concentration surpasses the solubility limit). The supersaturated state is conventionally achieved by removing the solvent to the vapor phase (vapor diffusion techniques) [3–5] and using additives to lower the protein solubility (these additives are therefore called precipitants) using a range of mechanisms: salts such as $(NH_4)_2SO_4$ or NaCl interact with water molecules, decreasing their availability for the solvation of the protein and also creating protein-ion interactions that affect morphology and diffraction quality; organic solvents such as ethanol reduce the polarization of the medium, promoting attraction between the protein molecules; polymers, such as polyethylene glycol, force protein molecules into a restricted space, thus promoting their interaction [3].

As the solvent is removed, both protein and precipitant concentrations increase and the supersaturated zone is achieved, where nucleation can finally start. As protein concentration in solution decreases due to nuclei formation, the system can reach the metastable zone where nucleation stops and only crystal growth takes place (Figure 2.1).

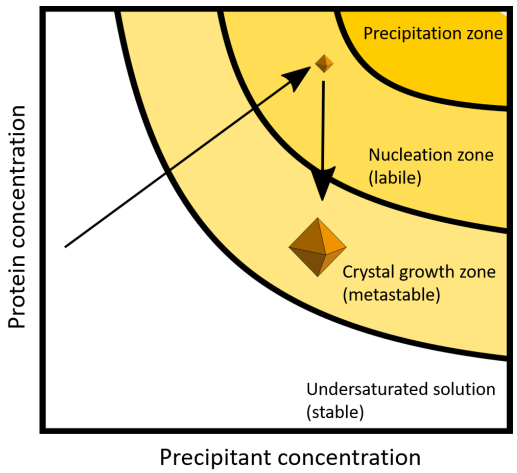

Figure 2.1: Solubility diagram. Four zones can be identified: under-saturated zone where no nucleation or crystal growth can occur, a supersaturated metastable zone where only crystal growth can occur but no nucleation, a supersaturated labile zone where both nucleation and crystal growth can occur, a precipitation zone.

2.3 Membrane-assisted protein crystallization

The term membrane crystallizer appeared for the first time in 2001, when Curcio *et al.* [8] applied the concept of membrane distillation (MD) to the crystallization of sodium chloride. Soon the idea of using membranes to control nucleation and the growth rate of small inorganic molecules was applied to protein crystallization. Indeed, in 2002, lysozyme molecules were successfully crystallized with the help of a membrane contactor [17]. Membrane crystallization was born as an extension of the concept of MD. Hence, it was initially associated with hydrophobic micro-porous membranes intended to serve as a mere separation wall, rather than a selective barrier. In previous works other types of membranes have been used to generate supersaturation in protein crystallization. As example, in the work of Todd *et al.* [18] in 1991, a reverse osmosis (RO) membrane was employed to control the supersaturation of a lysozyme solution by osmosis. In another work, dialysis membranes were exploited [19]. Moreover, it was promptly realized that membrane crystallizers had an important role to play in controlling nucleation and growth, given the heterogeneous effect that different types of surfaces are likely to induce [20]. Indeed, the topography and the chemistry of the membrane materials have proved to be highly useful in crystallization [21]. New composite materials combined with hydrogels have also been tested in the control of crystallization kinetics and the preservation of protein bioactivity [13]. The use of different membrane configurations and set-ups have

been demonstrated to yield finer control of supersaturation rates, crystal morphology, and size distribution. Three main aspects of membranes that may affect crystallization kinetics and diffraction quality will be discussed below:

- solvent removal: principle and effect on crystallization kinetics
- heterogeneous nucleation: effect of topography and chemistry
- set-up configurations

2.3.1 Solvent removal: principle and effect on crystallization kinetics

In membrane-assisted crystallization (MAC), the removal of the solvent to reach supersaturation is controlled by membrane transport properties and is normally performed in membrane modules. The membrane separates two compartments, one for the protein solution and another for the stripping solution (the hypertonic solution used to drive the solvent removal process) (Figure 2.2).

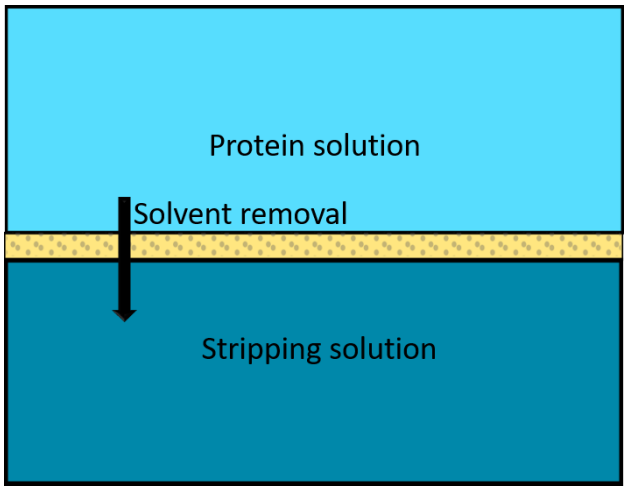

Figure 2.2: Membrane generation of supersaturation.

Solvent transfer can be obtained using either dialysis, reverse osmosis (RO), or via evaporation in microporous hydrophobic membranes. The solvent removal mechanism is different in each case, depending on the membranes' structural and chemical properties. A dialysis membrane is a porous barrier with a molecular cut-off weight that allows water to permeate, together with small components such as salts, additives, and crystallization reagents, while preventing transport of macromolecules. However, it is difficult to control crystallization kinetics during dialysis, due to the fact that equilibrium is reached quickly

and often needs to be slowed down by using long capillaries or intermediate solutions [19, 22].

Reverse Osmosis (RO) membranes can also bring about protein crystallization. Their dense structures regulate the selective diffusion of water, thereby preventing the transport of other molecules by size-exclusion effect [23]. Water transport can be adjusted by regulating two aspects on either side of the membrane, namely: the relative height of the liquid (hydrostatic pressure); and the relative water concentration (osmotic pressure gradient). Hydrostatic pressure is generally negligible, hence water flux ($J_{(H_2O)}$) can be defined as:

$$J_{H_2O} = P_{H_2O}\Delta[H_2O] \tag{2.1}$$

where P_{H_2O} is the permeability of water through the membrane, and $\Delta[H_2O]$ is the difference in water concentration between the protein and the stripping solution. According to this equation, the water removal rate can be controlled by adjusting permeability or the driving force of the process [18, 24, 25].

Microporous hydrophobic membranes (such as PP, PVDF, PTFE) may also be used between an under-saturated protein solution and a hypertonic stripping one. The hydrophobic character of the membrane combined with a pore size ranging from 0.01-1 µm, narrow pore size distribution, and a highly porous surface [9, 26] prevent water from entering the pores in the liquid phase, and water transport only occurs during the vapor phase [23, 27].

Solvent transport is driven by partial pressure gradient across the two sides of the membrane (Figure 2.3). The driving force can be generated by temperature or concentration differences or the addition of an anti-solvent [27–29]. However, in order to avoid thermal degradation, variations in concentration are most commonly used for protein crystallization.

The transport of solvent through the membrane pores depends on: the membrane's morphological characteristics; and the driving force (vapor pressure gradient). Hence, the flux (J_i) of solvent i can be calculated according to the Dusty Gas Model Theory:

$$J_i = -\frac{D}{RT}\nabla p_i \tag{2.2}$$

where D represents the effective diffusion coefficient inside the pores, R is the gas constant, T is temperature, and ∇p_i is the difference in the partial vapor pressure of compound i,

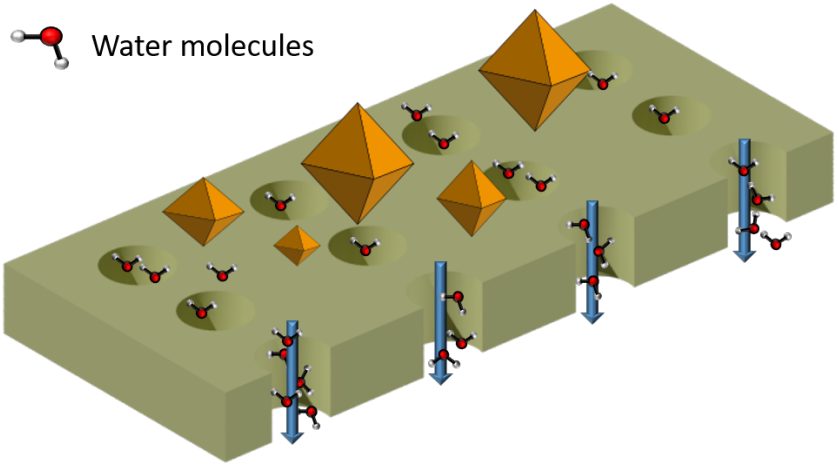

Figure 2.3: Membrane-assisted crystallization principle. Protein and stripping solution are on different sides of the membrane. The volatile solvent is removed from the protein solution in vapour phase, supersaturation is reached and crystals formation occurs.

generated across the two sides of the membrane [30, 31]. The effective diffusion coefficient of the Dusty Gas Model takes into account surface diffusion (adsorption of molecules on the surface), Knudsen diffusion (when molecule-wall interactions are predominant), molecular diffusion (when molecule-molecule interactions dominate), and viscous flow (for differences in total pressure) [32]. However, simplifications can be applied for protein crystallization: surface diffusion can be considered negligible for pore sizes greater than 0.01μm, and viscous flow can be considered null, since no external pressure is applied [26, 33, 34]. Hence, the effective diffusion coefficient (D) can be defined as a combination of Knudsen and molecular diffusion coefficients:

$$D = \frac{\epsilon}{\tau}\left(\frac{3}{2r}\sqrt{\frac{\pi M_i}{8RT}}) + \frac{(1-y_{air})}{D^0_{\frac{i}{air}}}\right)^{-1} \tag{2.3}$$

where ϵ is porosity, τ is tortuosity, r is the average pore radius of the membrane, y_{air} is the mole fraction of air in the membrane pores, M_i is the molecular weight of compound i, and $D^0_{\frac{i}{air}}$ represents the diffusion coefficient in air of the compound i [30]. Crystallization process kinetics can be affected by the transmembrane flux, and can hence be modulated by altering the membrane's morphological characteristics and differences in vapor pressure.

Generally speaking, high levels of transmembrane flux lead to greater rates of nucleation [35]. This can be seen in greater detail not only in equation 2 but also from experimental results [35]: high rates of porosity combined with large pores lead to an

elevated diffusion coefficient, hence faster mass transfer rates and, consequently, quick induction times and high nucleation rates.

The vapor pressure difference can be altered by changing the concentrations of the stripping and precipitant solutions. In both cases, the induction time, and rates of nucleation and growth may be affected: Increasing salt concentration in the stripping solution leads to shorter induction times and greater nucleation rates. Indeed, this determines a higher gradient of vapor pressure and promotes higher rates of transmembrane flux [20, 26]. Boosting the precipitant concentration in the protein solution may have opposite effect, depending on the magnitude of the change: a small increase leads to a decrease in the solution activity and a fall in solvent evaporation with higher induction times and lower nucleation and growth rates. Greater increments result in a decrease in protein solubility, promoting protein-protein aggregation with a consequent slowdown in induction times, together with higher rates of nucleation and growth [20, 26, 31].

2.3.2 Heterogeneous nucleation: effect of topography and chemistry

The growth of crystals of inorganic molecules from the interaction with mineral substrates by epitaxial nucleation led McPherson [36] to hypothesize in 1988 that the same concept might be applied to macromolecules. Since then, several studies have investigated the effect of protein-surface interactions on nucleation and crystal growth. During membrane-assisted crystallization, the protein solution is in contact with the membrane surface, therefore, membranes may also act as heterogeneous nucleants. Surface chemistry and topography are the main membrane parameters that can affect nucleation. A summary of their effects follows.

Topography. Since 2001, Chayen and co-workers have been demonstrating the effectiveness of using porous silicon films with a pore size within the dimension range of the protein molecule to induce the nucleation of proteins such as lysozyme, trypsin, thaumatin, catalase, and phicobiliprotein. This has been provoked by trapping protein molecules inside the narrow pores where they accumulate over time, thereby increasing local concentrations [37–39]. The confinement effect is also supported by the formation of submicron protein crystals within square shaped pores in silicon substrates with sizes between 100 to 1000 nanometers [40]. Therefore, using porous surfaces might lead to the local accumulation of protein molecules for a variety of pore-sizes. Indeed, it was

assumed that a surface with a wide range of pore-sizes might increase the likelihood of finding the adequate dimension to promote nucleation [41]. Shah, on the contrary, set a preferential pore size for inducing crystallization that was related to the size of the protein gyration radius [42]. Hydrophobic microporous PP [17, 20, 43] and PVDF [35] membranes have been shown to reduce induction time relative to the same supersaturation level in conventional vapor diffusion experiments. Curcio et al. [35] developed a mathematical model to correlate the free energy nucleation ratio between heterogeneous and homogeneous nucleation and the porosity of the membrane. They found that increased porosity lowered the energetic activation barrier for nucleation to occur. The effect of roughness was investigated by Liu et al. [44]. Their model included the roughness effect in calculating the Gibbs free energy variation of heterogeneous to homogeneous nucleation. They assumed rough surfaces to be formed of uniform cones, and included their geometry in the model, and then validated their model by forming different topographies on glass slides using different types of oxidation. In 2010 Curcio et al. [11] simulated nucleation on rough surfaces (PVDF, PDMS and hyflon membranes) and showed that their predictions were in agreement with theoretical calculations of classical nucleation theory (CNT) [45]. Salehi et al. [46] recently demonstrated the effect of roughness on nucleation. Hydrogel-composite membranes were designed using differing concentrations of iron oxide nanoparticles determining several degrees of roughness. The increased nanoparticle concentration in Poly(vinyl alcohol) (PVA) hydrogel, crosslinked with poly(ethylene glycol) diglycidyl ether (PEGDE) or glutaraldehyde (GA), led to a higher probability and density of nucleation. The effect was more pronounced for the gel crosslinked with PEGDE, since higher numbers of interactive groups provided more interaction sites with protein molecules. Both the type of crosslinker and the presence of nanoparticles affected crystal diffraction quality. PVA crosslinked with PEGDE is highly flexible due to the long crosslinker chain. Hence, during crystal growth, it reassembled, adapting its position to the growing crystals. PVA crosslinked with GA has a high mechanical stability, therefore cannot be distorted by the crystal. Instead, it was forced to incorporate the gel fibers into the crystalline lattice to continue growing. Adding gel raised the growth rate and size of the crystals, but with higher levels of internal disorder (higher mosaicity) and changes in the unit cell. This effect was more evident with higher concentrations of iron oxide nanoparticles. However, no influence on crystal mosaicity was found for crystals grown in a more flexible gel. The general consensus regarding roughness is that the obstacles

formed by surface irregularities form cavities where protein molecules can accumulate and form local supersaturation spikes. According to these models and most experimental data available, increasing roughness is directly related to higher levels of nucleation. Moreover, studying the oxidation of crystallization plates, Hou et al. [47] recently hypothesized the potential existence of an ideal roughness size. Indeed, cavities smaller than the proteins may exclude accumulation, while larger ones might have the same effect as flat surfaces. Cavities capable of accommodating a few protein molecules might be the actual promoters of nucleation.

The ideal topographical size and shape is not yet obvious. However, it can be argued that crystallization on surfaces with hillocks or pores might be advantageous for achieving supersaturation at lower protein concentrations, due to the ability to accumulate protein molecules in tight spaces. There may also be a preferential degree of porosity/roughness determined by the size of any specific protein.

Chemistry. Proteins contain several functional groups that might interact not only with other protein molecules but also with functional groups available on membranes or surfaces in general, thereby reducing the activation energy needed for nucleation [21]. For example, the functionalization of microporous PVDF membranes with sulfonamide groups led to the formation of additional protein-surface interactions that, in turn, produced protein orientation and agglomeration. This resulted in faster nucleation and higher crystal numbers than in the case of unmodified PVDF crystallization [48]. Hydrophobic microporous membranes were also used to tune the interactions between protein molecules and ligands, such as ions, in order to improve the crystal diffraction resolution. Lysozyme crystallization on polypropylene membranes in the presence of $CuCl_2$ allowed protein crystals to form with a different space group than that obtained with $CuCl_2$ but without a membrane, suggesting that membrane-protein interactions might also drive crystal polymorphism [49]. In order to combine the control provided by membrane-assisted nucleation (control of solvent-removal rate and faster nucleation rate) with the advantages of gel crystallization (such as mechanical stability, size increase, lack of convection and reproducibility), porous polypropylene membranes coated with hydrogel were used. Lysozyme and concanavalin A crystals, obtained on the composite membranes, were more stable and better diffracting than those obtained on conventional plates and plain polypropylene, thanks to the protective environment created by the gel. Shah et

al. [50] demonstrated that the pore size effect could be enhanced using surface chemistry. Indeed, mesoporous glass substrates with different pore sizes (3 to 12 nm diameter) and functional groups (-OH, -CH_3, -NH_3, etc.) were applied for the crystallization of lysozyme, concanavalin A, thaumatin, catalase and human serum albumin. The hypothesis of enhanced nucleation results from a combined effect of small pores, which leads to entrapment and restricted protein mobility with subsequent nuclei formation, and the functional groups that helped stabilize the nuclei by interacting with a specific crystal face. Protein side chains determine the final folded molecule in terms of specific surface charge and hydrophilicity or hydrophobicity levels. Therefore, it can be concluded that each protein type may establish a unique interaction with an external substrate and with other protein molecules. Indeed, the effect of surface properties on the crystallization of different proteins oftentimes precludes explanation by a single general correlation. The same surface might induce different effects, depending on protein type. De Poel [51], for example, looked at insulin, lysozyme, talin and bovine serum albumin crystallization on mica surfaces functionalized with 1,3,5-tris(10-carboxydecyloxy) benzene (TCDB). They found different degrees of hydrophilicity/hydrophobicity and roughness. Each protein showed distinct behavior, and protein crystal formation seemed to have been affected in varying levels depending on distinct surface characteristics. For instance, insulin crystallization occurred preferentially at surfaces with greater topographical relief. The surface roughness seemed to have had greater influence than surface chemistry. In contrast, surface chemistry appeared to have exerted greater control than topography on nucleation, in the formation of lysozyme and talin crystals, while no significant variations appeared on the BSA crystallization on different surfaces.

Environmental conditions, particularly pH, may change the charge of the protein depending on its isoelectric point (pI): at pH less than pI the molecule will be positively charged, while a negative charge will be exhibited when the environmental pH is higher than the pI. The total charge of the molecule will affect its solubility: two uncharged molecules will be more likely to interact than similarly charged ones. Hence, it might be easier to nucleate a neutral protein than a charged one: Lysozyme crystallization (PI=10.5– 11.2) occurs with a lower induction time at pH=8.5 than at pH=4.5 [51]. Environmental factors such as pH and temperature can also be used to fine tune the properties of hydrogel composite membranes made of stimuli-sensitive monomers, such as NIPAM. Changes in the buffer pH and/or the temperature may induce differences in

swelling properties, ion-adsorption and supersaturation, leading to lysozyme crystals of diverse shapes, from rod-like to flower-shaped [52]. Electrically charged amino-acids can easily form ionic interactions or repulsions with electrically charged surfaces, leading to improved protein crystallization, given suitable control of protein-surface ionic interactions. Protein crystallization studies have been conducted using electrically charged films. In 2001, Fermani et al. [53], looked at the crystallization of concanavalin A and lysozyme on positively (silk-fibroin films with poly-L-lysine) and negatively (sulfonated polystyrene and silk-fibroin films with poly-L-aspartate) charged surfaces. Concanavalin A (negatively charged at experimental pH) interacted with charged substrates leading to nucleation with quicker induction times and at lower protein concentrations than conventional hanging drop experiments. However, no effect was found for lysozyme (positively charged at experimental pH). Moreover, in 2008 Tosi et al. [54] tested positively and negatively charged polystyrene on proteins (insulin and ribonuclease A) with different net charges. They explained protein crystallization according to two different mechanisms depending on the relationship between the charge at the membrane surface and that of the protein molecules:

- Surface-induced crystallization: the protein molecules and the surface repulsed each other, resulting in a thin layer of concentrated protein above the surface, that led to lower crystallization at lower protein concentrations.
- Surface-controlled crystallization: the protein and the surface attracted each other, leading to the accumulation of a thin layer of protein on the surface contributing to a quicker nucleation at lower protein concentrations.

Hence, although through a different mechanism, both cases (with the same or opposite charges) might lead to crystals at lower protein concentration. This is advantageous, because it enables crystals to form in the metastable region, where moderate supersaturation slows their growth and increases the chance of obtaining well-diffractive examples [54]. Ghatak et al. [55, 56] recently tested protein crystallization on patterned and electrically charged films. PDMS films with charges, surface wrinkles, and a combination of the two were tested in lysozyme crystallization. When charges and wrinkles acted together, lysozyme crystals were obtained without the need of precipitants. In fact, electric charges combined with topographical features led to the formation of surface potential due to the orientation of the water hydrogen bonds that facilitated the self-organization of the

protein molecules. Successful crystallization without precipitant was obtained both for single proteins and for mixtures. They were shown, by X-ray diffraction, to have unit cell dimensions very similar to reference crystals produced with precipitant. Therefore, these types of surfaces may be profitably used for screening crystallization conditions without precipitants, thereby simplifying the search for the optimal combination of ingredients. Studies to date have shown that the complex nature of proteins precludes identifying any general rule for the design of an optimal surface chemistry to promote nucleation. Instead, conditions must be adapted to each protein. However, synergistic effects of topography and chemistry have been found that may potentially aid in the design of surfaces that better promote nucleation.

2.3.3 Set-up configurations

In addition to membrane morphology, topography and chemistry, the set up configuration may also affect the crystallization process. Different membrane configurations can be used, for example:

- Capillary/tubular/hollow fiber membranes: the membrane has a tubular shape with an external diameter between 0.2 and 1.8 mm. One of the solutions (stripping or protein) fills the lumen that is wrapped at the extremities; the tube(s) can be placed in a glass container or in a tube filled with the other solution (Figure 2.4)[9, 26, 31].

- Flat membranes: they can be placed in a cell (Figure 2.4) to separate the environment in two compartments, one for the stripping and the other for the protein solution.

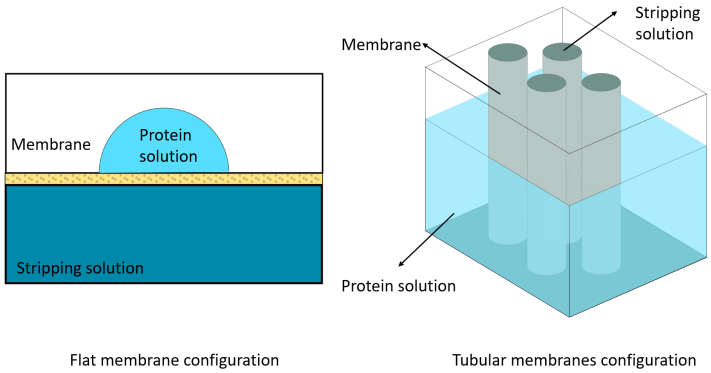

Figure 2.4: Membrane configurations

Moreover, two operation modes are available (Figure 2.5):

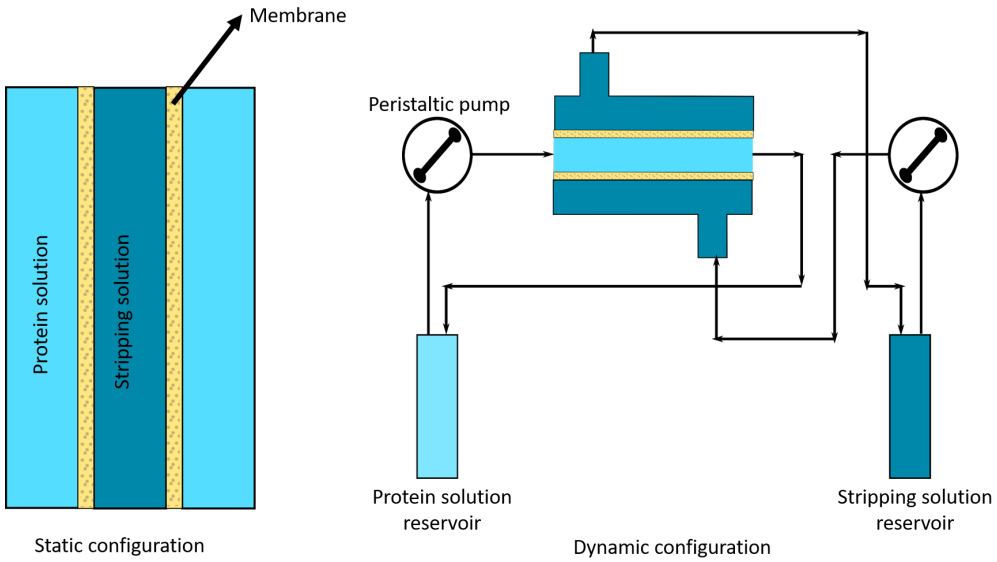

Figure 2.5: Set-up configurations for membrane-assisted protein crystallization: In static configuration, the stripping solution (hypertonic solution to drive solvent removal from the protein solution) is typically located in the lumen of the tubular membrane, while the protein solution is placed outside to facilitate observation. In the dynamic configuration, protein solution may be run through the lumen and the stripping solution flows in counter current on the shell side.

- Static mode: the two solutions are kept in contact with the membrane until equilibrium is achieved and crystals are obtained in a quiescent state [9, 17].
- Dynamic mode: the solutions are pumped in counter-current by a peristaltic micropump; the supersaturated protein solution is collected in a separate vessel, where nucleation occurs [9, 17].

In a static configuration the solvent removal rate, and consequently the rate at which the supersaturated state is obtained, depends on the surface transport area (porosity, in the case of hydrophobic micro-porous membranes, or transport surface, with other membrane types) [17]. When using hollow fibers in a static configuration, the stripping solution is placed in the lumen and the protein solution outside, so as to facilitate monitoring of the process. Upon increasing the number of hollow fibers with stripping solution for the same volume of protein solution, an increased flow rate of solvent extraction was observed, due to the extra active membrane area [43]. Furthermore, the increased number of hollow fibers reduced lower induction time and increased the growth rate of the

crystal's face perpendicular to the membrane surface, which may have been due to the effect of solvent flow rate through the pores rectifying the random Brownian motion of the molecules [43]. The main drawback of the static configuration is that it leads to the accumulation of crystals on the surface over time which lowers the available transport area and process performance [9]. The dynamic configuration not only contributes to supersaturation as a result of membrane transport properties and protein-surface interactions, it also yields increased control by adjusting the flowrates of the stripping and protein solutions. Over time, transmembrane flux tends to fall, as progressive (or gradual) equilibrium is established between the protein and stripping solutions. The replenishment of solution throughout the process leads to higher flow rates and promotes quicker evaporation of the solvent and higher nucleation rates. The convection forces acting on the protein molecules also rise. Excessive flow rate of protein solution may lead to protein denaturation. However, this did not take place at velocities between 10 µm/s [17] and 1500 µm/s [43]. Experimental results have demonstrated that the convective forces affect:

- crystal growth rate. In particular, a critical value of solution velocity ($\mathbf{u}_c$) was observed. Below uc, crystal growth rate went up with the rise of solution velocity, while above $\mathbf{u}_c$ the rate fell as solution velocity grew. The initial increase was justified by an enhanced solute concentration at the solid-liquid interface, while the decrease in crystal growth above the uc was explained by a surge of impurities to the solid-liquid interface [43].

- crystal morphology. In this case as well, the solution velocity around $\mathbf{u}_c$. led to differing behaviors. Below this speed, growth rates were comparable for length and width and yielded square-shaped crystals. Above $\mathbf{u}_c$, growth was longer than it was wide and resulted in crystals stretched along the *c* axis [26, 33, 43]. These results were observed by diffraction analysis: convective flux resulted in a change in the unit cell dimensions *a*,*b* and *c*. Indeed, trypsin crystals grown in a dynamic set up exhibited an increased value for a and b and a decreased value for c, compared to those obtained in the static configuration [9].

- crystal size distribution. Distribution curves were sharper in dynamic systems than those in static configurations.

The diffraction resolution of crystals grown in both static and dynamic systems was excellent: trypsin crystals diffracted at 1.9 Å in the static device and at 2.0 Å in the

dynamic one, demonstrating that the set up does not have a negative effect on crystal diffraction quality. The convective flux also promoted the removal of crystal nuclei from the membrane surface after formation, leaving nucleation sites available and limiting fouling [9].

In summary, the configuration of the membrane and set-up may also lead to significant differences in terms of growth rate, crystal size distribution and morphology. Additionally, the ability to tune the flow velocity enables greater increases in super-saturation at later stages of the process, while also guaranteeing diffraction quality comparable to that of crystals obtained with conventional crystallization techniques.

2.4 Emerging techniques

2.4.1 Membranes and gels for post-crystallization modifications

Once crystals are obtained, they must always be subjected to post-crystallization treatments before undergoing x-ray diffraction, such as cryoprotection (soaking the crystals in glycerol, in order to protect them from ice-ring formation during flash-cooling with liquid nitrogen flux). Sometimes, in spite of all efforts to control crystal packing, poor diffraction quality crystals result, which, then, have to undergo some types of modifications, such as dehydration (by solvent evaporation), or annealing (thaw/freeze cycles to stimulate molecule reorganization [1, 2]. Furthermore, in order to solve the unknown structure of macromolecules by multiple isomorphous replacement (MIR), crystals have to be derivatized with some heavy atom (soaking in a heavy atom solution) [57]. However, crystals are highly fragile, and are in equilibrium with the surrounding environment. Therefore, post-crystallization treatments have several drawbacks, namely the risk of breaking the vapor diffusion equilibrium or of wreckage due to handling and/or brusque environmental changes. Membranes and hydrogel media have recently been used to control post-crystallization treatments such as cryoprotection and the derivatization of the crystals with heavy atoms. The gel was found to be a better environment for slower ligand diffusion than solutions, as it avoided the shock of immersing the bare crystals directly in the osmotic solution [58]. As previously mentioned, crystals grown in gel can, in some cases, incorporate the gel fibers into the crystalline lattice [46], leading to higher mosaicity and the distortion of the unit cell [59]. However, the presence of the gel inside the crystal structure has the advantage of improving mechanical stability and

producing greater resistance to osmotic shock when soaking in concentrated solutions of heavy atoms or organic solvents [14]. Ion-exchange membranes have also been used to control the diffusion of heavy metals and halides in ionic formations in lysozyme crystals. The crystals were grown by vapor diffusion in an ion-exchange membrane crystallizer. The protein solution was located on one side. Relative humidity was controlled, and supersaturation was generated by removing water (Figure 2.6A). Once crystallization occurred and the crystals were in equilibrium with the environment (Figure 2.6B), the bottom compartment was filled with the derivatizing solution (Figure 2.6C). The ion-exchange membrane regulated the diffusion of the ions to the protein solution and then diffused into the crystal. The diffusion regulation by the membrane enabled the system to avoid any damage arising from abrupt changes in the environment or disturbances of the vapor diffusion equilibrium or crystal handling. Diffraction analysis showed how unit cell parameters did not change significantly keeping the isomorphism needed for the protein structure solution by multiple isomorphous replacement [60]. Therefore, the use of membranes and hydrogels has been shown to make significant contributions to post-crystallization treatments. The controlled diffusion of molecules performed by selective membranes and hydrogels and the higher mechanical resistance provided by the incorporation of hydrogel fibers in the crystalline lattice have contributed both to the improvement/maintenance of the diffraction quality of the crystals.

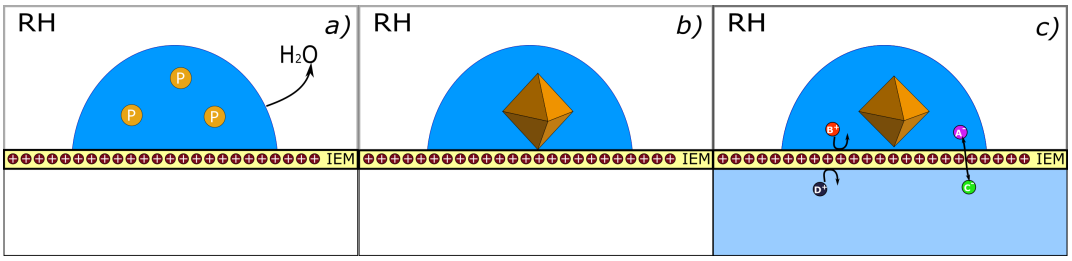

Figure 2.6: Membrane-assisted crystallization with an ion-exchange membrane. a) Supersaturation is generated by controlling relative humidity; b) crystals are formed in equilibrium with the environment; and c) derivatization of the crystals by ion counter-diffusion.

2.4.2 Membrane-assisted protein crystallization and microfabrication technologies

The unpredictable nature and behavior of proteins make protein crystallization a trial-and-error science. When the structure of an unknown protein has to be unraveled, several

combinations of compounds and compositions have to be tested in order to identify (when possible) the right recipe for well-diffracting crystals. Therefore, the limitations in protein crystallization (apart from the difficulties represented by the protein structure itself) are the large selection of reagents and the time required to perform extensive screenings.

Microfluidic science and technology has had a great impact in recent years on protein crystallography, yielding creative designs (valve based, droplet based [61, 62], slip chip [63] or centrifugal design [64]) for minimizing the consumption of reagents and, at the same time, maximizing the number of conditions screened [65, 66]. Investigations about protein phase change behaviour [67], crystallization kinetics [68, 69], mixing effect [70] have been also performed in microfluidic devices. In addition, efforts are underway to develop x-ray transparent materials that might be used to perform in-situ diffraction analysis so as to limit the need for crystal manipulation [71, 72].

The main characteristic of microfluidics is their capacity for working with very small volumes of fluids. They are currently used in a range of fields, from analytical techniques, to bioreactors, to electro-mechanic systems (MEMS). Thanks to their small size, not only can reagent use be limited but also procedures can be carried out under laminar flow conditions and automated, using a series of valve and pump systems. Moreover, throughput can be raised [73] at lower fabrication costs. Uses of membrane-based micro-devices for protein crystallization have been reported where the gas permeability of PDMS has been exploited to control supersaturation. Indeed, by adjusting the thickness of the PDMS layer and the surrounding relative humidity, evaporation rates were controlled and different crystal sizes were obtained [74, 75].

The main material used was polydimethylsiloxane (PDMS), which is optically transparent, non-toxic and inexpensive. When mixed with a crosslinking agent, it can be cast and shaped on micro-structured molds and a wide range of topographic details with high resolution can be shaped into it. That is why it is used to build microfluidic devices or as a mold in the preparation of patterned solid substrates for crystallization (membranes) by soft lithography [76, 77]. Indeed, soft lithography is a group of low-cost microfabrication techniques that use an elastomeric stamp (PDMS) to imprint a pattern onto another substrate. The main soft lithography techniques (represented in Figure 2.7) for transferring a pattern are:

- microcontact printing. The PDMS mold can be set into an ink that will be released

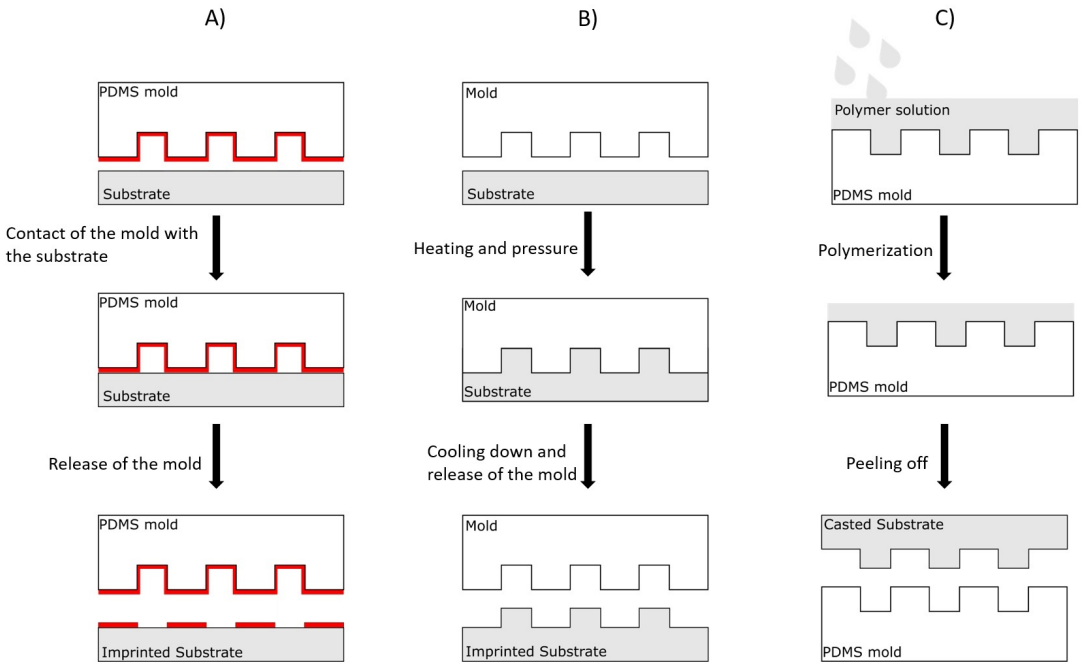

Figure 2.7: Soft lithographic techniques for surface patterning. A) Microcontact Printing; B) Embossing; C) Casting

onto the surface by contact. During this step, the ink forms a self-assembled monolayer that can be used for patterning membranes for cell cultures [78, 79].

- embossing. The substrate is softened with heat and by pressurized contact, and the shape of the mold is transferred onto the substrate. Several types of membranes have been successfully molded with micro and nano structures such as PDMS [80], Nafion® [81–84], Polypropilene [85] etc. Membrane patterning has been used for improving transport properties of membrane processes like microfiltration and ultrafiltration membranes [86], for fouling mitigation [87], flux enhancement, and control deposition [88].

- casting. The PDMS mold can be used to cast a polymer solution that will take the mold's shape after polymerization.

Patterning of membrane material for protein crystallization may enable the fabrication of tailored shaped or functionalized surfaces that aid the investigation of heterogeneous nucleation effects. Furthermore, using casting or embossing to create specific surface topographies would avoid chemical modifications, allowing for a more reliable comparison of different structures, while producing a deeper understanding of the strict topographical effect on nucleation. Microcontact printing would also create chemical

patterns that might induce localized interactions with protein molecules and thereby produce supersaturation spikes.

2.5 Overview and conclusions

Membranes have shown, to date, great potential for controlling and improving protein crystallization and post-crystallization treatments. Membranes can play several roles, serving as:

- a separation barrier, for the fine control of solvent (usually water) removal rate;
- heterogeneous support, modulating protein-surface interactions and, ultimately, driving protein-protein interactions;
- a selective barrier, controlling the diffusion of components from/to the protein solution; and
- a protective environment for protein conformation / bioactivity against osmotic shock when combined with hydrogels.

A complete list of works with the type and role of the membrane in the crystallization process, protein, and use appears in Table 3.1.

Furthermore, various advantages can be outlined to using membranes for protein crystallization, such as:

- enhanced crystallization kinetics due to tuning the transport properties of the membrane;
- nucleation at lower degrees of supersaturation, resulting either from the formation of local concentration spikes during physical entrapment in the membrane's asperities and/or from enhanced chemical interaction between protein molecules and the membrane; and
- greater crystal stability and diffraction quality due to the protective and convection-free environment created by hydrogel-composite membranes or the in-situ, selective and controlled diffusion of ligands provided by ion-exchange membranes during post-crystallization treatments.

Table 2.1: List of membrane-assisted crystallization works with their role, target compound, type of membrane and application

Title	Protein	Membrane	Membrane role	Application	Ref.
Membrane crystallization of macromolecular solutions	HEWL	Tubular PP membrane	Separation barrier	X-ray analysis	[17]
A new membrane-based crystallization technique: tests on lysozyme	HEWL	Tubular PP membrane	Separation barrier	X-ray analysis	[25]
Membrane crystallization of lysozyme: kinetic aspects	HEWL	Tubular PP membrane	Separation barrier and Heterogeneous effect	X-ray analysis	[20]
Trypsin crystallization by membrane-based techniques	Trypsin from Bovine Pancreas	Tubular PP membrane	Separation barrier	Bio-catalytitc applications	[43]
Influence of the structural properties of poly(vinylidene fluoride) membranes on the heterogeneous nucleation rate of protein crystals	HEWL	Flat PVDF	Separation barrier and heterogeneous effect	Crystallization in general	[35]
Preparation of enzyme crystals with tuneable morphology in membrane crystallizers	Trypsin from Bovine and Porcine Pancreas	PP hollow fibres	Separation barrier	X-ray analysis	[9]
Membrane crystallization of lysozyme under forced solution flow	HEWL	PP hollow fibres	Separation barrier	X-ray analysis	[33]
Polymeric hydrophobic membranes as a tool to control polymorphism and protein–ligand interactions	HEWL	PP hollow fibres	Separation barrier and heterogeneous nucleation	Polymorphism and x-ray diffraction	[49]

Title	Protein	Membrane	Membrane role	Application	Ref.
Energetics of protein nucleation on rough polymeric surfaces	HEWL	Flat PVDF-PDMS-Hyflon	Heterogeneous nucleation	Nucleation studies	[11]
Tailored hydrogel membranes for efficient protein crystallization	HEWL and CONA	Flat hydrogel-PP	Heterogeneous nucleation and protection	X-ray diffraction	[13]
Hydrogel composite membranes incorporating iron oxide nanoparticles as topographical designers for controlled hetero-nucleation of proteins	HEWL	Flat hydrogel-PP with iron oxide nanoparticles	Heterogeneous nucleation and protection	X-ray diffraction	[46]
The study of continuous membrane crystallization on lysozyme	HEWL	PVDF hollow fibres	Separation barrier	crystallization in general	[31]
Precipitants and additives for membrane crystallization of lysozyme	HEWL	PP hollow fibres	Separation barrier and heterogeneous nucleation	X-ray diffraction	[89]
Tailored robust hydrogel composite membranes for continuous protein crystallization with ultrahigh morphology selectivity	HEWL	Flat hydrogel-PP	Heterogeneous nucleation, protection and polymorphism control	X-ray diffraction	[52]
Crystallization of lysozyme in pores of etched heavy-ion tracks	HEWL	Flat PC-PI-Mica	Heterogeneous nucleation	Crystallization in general	[90]
Application of osmotic dewatering to the controlled crystallization of biological macromolecules and organic compounds	HEWL	Tubular RO membranes	Osmosis	Crystallization in general	[18]

Title	Protein	Membrane	Membrane role	Application	Ref.
The growth of yeast thiolase crystals using a polyacrylamide gel as dialysis membrane	3-KetoacylCoA thiolase	Polyacrilammide gel	Dialysis	Crystallization in general	[19]
Colloidal graphene as heterogeneous additives to enhance protein crystal yield	ADH, Catalase, HEWL, trypsin,PSPC1-Nono	Graphene, Graphene-oxide	Heterogeneous nucleation	X-ray diffraction	[91]
Interactive functional poly (vinylidene fluoride) membranes with modulated lysozyme affinity: a promising class of new interfaces for contactor crystallizers	HEWL	Flat microporous PVDF	Heterogeneous nucleation	X-ray diffraction	[48]
Growth of protein crystals in hydrogels prevents osmotic shock	HEWL, Thaumatin, Elastase	Hydrogel	Protection of the environment	X-ray diffraction	[14]
Ion-exchange membranes for stable derivatization of protein crystals	HEWL	Nafion®-Neosepta AX01	Selective diffusion of ions	X-ray diffraction	[60]
Protein crystallization on polymeric film surfaces	HEWL and CONA	Polystirene, silk fibroin, Gelatine	Heterogeneous nucleation	X-ray diffraction	[53]
Precipitant-free crystallization of protein molecules induced by incision on substrate	HEWL and proteinase K	Wrinkled PDMS	Heterogeneous nucleation	X-ray diffraction	[55]
Precipitantless crystallization of protein molecules induced by high surface potential	HEWL, Ferritin, Thaumatin, Proteinase K, Glucose Isomerase	Wrinkled PDMS	Heterogeneous nucleation	X-ray diffraction	[56]

Title	Protein	Membrane	Membrane role	Application	Ref.
Porous silicon: an effective nucleation-inducing material for protein crystallization	catalase, CONA, HEWL, a phycobiliprotein, thaumatin and trypsin	Porous silicon	Heterogeneous nucleation	X-ray diffraction	[39]
Nucleation of sub-micrometer protein crystals in square-shaped macroporous silicon structures	HEWL	Porous silicon	Heterogeneous nucleation	X-ray diffraction	[40]
Experiment and theory for heterogeneous nucleation of protein crystals in a porous medium	HEWL, Thaumatin, porcine pancreas trypsin	Porous silicon	Heterogeneous nucleation	X-ray diffraction	[41]
Selective crystallization of proteins using engineered nanonucleants	HEWL, Thaumatin, Trypsin, Human serum albumin, CONA, catalase, ferritin	Mesoporous glass	Heterogeneous nucleation	X-ray diffraction	[50]
Crystallization of proteins at ultralow supersaturations using novel three-dimensional nanotemplates	CONA, HEWL, Thaumatine, Catalase, Human Serum Albumin	Functionalized nanoporous glasses	Heterogeneous nucleation	X-ray diffraction	[42]

Title	Protein	Membrane	Membrane role	Application	Ref.
A technique for high-throughput protein crystallization in ionically cross-linked polysaccharide gel beads for x-ray diffraction experiments	HEWL, catalase from bovine liver, a-ribazole 59-phosphate phosphatase mutant L38M from Thermus thermophilus HB8, diphthine synthase mutant Y175H from Pyrococcus horikoshii OT3, conserved hypothetical protein from Pyrococcus horikoshii OT3, Glucose isomerase	Alginic acid and carragenan	Protection of the environment and heterogeneous nucleation	X-ray diffraction	[58]
Crystalline quality of lysozyme crystals grown in agarose and silica gels studied by X-ray diffraction techniques	HEWL	Silica gel	Protection of environmen t	X-ray diffraction	[59]
Design and application of a microfluidic device for protein crystallization using an evaporation-based crystallization technique	HEWL	PDMS in a microfluidic device	Separation barrier	X-ray diffraction	[74]

Membrane-assisted crystallization and post-crystallization treatments might be joined so as to develop a system that is able to, firstly, control nucleation and crystal growth and then to potentially perform post-crystallization modifications. In this sense, membrane-assisted protein crystallization might yield benefits when introduced into a microfluidic device, not only for improved throughput but also for process automation. In addition, microfabrication techniques might help to develop surfaces with well-defined characteristics so as to contribute to more intensive screening of parameters (inherent to heterogeneous nucleation), which would enable systematic studies of their impact on the different steps of protein crystallization (e.g. nucleation and crystal growth). Furthermore, most of these studies have been conducted on model proteins. Investigations into real case studies should be performed in order to start thinking about membrane-assisted protein crystallization as a routine methodology for x-ray crystallography.

References

[1] B. Heras and J. L. Martin. "Post-crystallization treatments for improving diffraction quality of protein crystals." In: *Acta Crystallographica Section D: Biological Crystallography* 61.9 (2005), pp. 1173–1180. DOI: 10.1107/S0907444905019451.

[2] J. Newman. "A review of techniques for maximizing diffraction from a protein crystal in stilla." In: *Acta Crystallographica Section D: Biological Crystallography* 62.1 (2006), pp. 27–31. DOI: 10.1107/S0907444905032130.

[3] A. McPherson and J. A. Gavira. "Introduction to protein crystallization." In: *Acta Crystallographica Section F:Structural Biology Communications* 70.1 (2014), pp. 2–20. DOI: 10.1107/S2053230X13033141.

[4] R. Giegé. "A historical perspective on protein crystallization from 1840 to the present day." In: *FEBS Journal* 280.24 (2013), pp. 6456–6497. DOI: 10.1111/febs.12580.

[5] J. A. Gavira. "Current trends in protein crystallization." In: *Archives of Biochemistry and Biophysics* 602 (2016), pp. 3–11. DOI: 10.1016/j.abb.2015.12.010.

[6] M. R. Sanderson and J. V. Skelly. *Macromolecular Crystallography: Conventional and high-throughput methods*. Vol. 9780198520. 2007, pp. 1–304. DOI: 10.1093/acprof:oso/9780198520979.001.0001.

[7] G. Di Profio, E. Fontananova, E. Curcio, and E. Drioli. "From tailored supports to controlled nucleation: Exploring material chemistry, surface nanostructure, and wetting regime effects in heterogeneous nucleation of organic molecules." In: *Crystal Growth and Design* 12.7 (2012), pp. 3749–3757. DOI: 10.1021/cg3005568.

[8] E. Curcio, A. Criscuoli, and E. Drioli. "Membrane crystallizers." In: *Industrial and Engineering Chemistry Research* 40.12 (2001), pp. 2679–2684. DOI: 10.1021/ie000906d.

[9] G. D. Profio, G. Perrone, E. Curcio, A. Cassetta, D. Lamba, and E. Drioli. "Preparation of Enzyme Crystals with Tunable Morphology in Membrane Crystallizers." In: *Ind Eng Chem Res* (2005), pp. 10005–10012. DOI: 10.1021/ie0508233.

[10] E. Drioli, E. Curcio, A. Criscuoli, and G. D. Di Profio. "Integrated system for recovery of CaCO3, NaCl and MgSO 4·7H2O from nanofiltration retentate." In: *Journal of Membrane Science* 239.1 (2004), pp. 27–38.

[11] E. Curcio, V. Curcio, G. D. Profio, E. Fontananova, and E. Drioli. "Energetics of Protein Nucleation on Rough Polymeric Surfaces." In: *Journal of Physical Chemistry B* 114 (2010), pp. 13650–13655.

[12] R.-B. Zhou, H.-L. Cao, C.-Y. Zhang, and D.-C. Yin. "A review on recent advances for nucleants and nucleation in protein crystallization." In: *CrystEngComm* 19.8 (2017), pp. 1143–1155. DOI: 10.1039/C6CE02562E.

[13] G. D. Profio, M. Polino, F. P. Nicoletta, B. D. Belviso, R. Caliandro, E. Fontananova, G. De Filpo, E. Curcio, and E. Drioli. "Tailored hydrogel membranes for efficient protein crystallization." In: *Advanced Functional Materials* 24.11 (2014), pp. 1582–1590. DOI: 10.1002/adfm.201302240.

[14] S. Sugiyama, M. Maruyama, G. Sazaki, M. Hirose, H. Adachi, K. Takano, S. Murakami, T. Inoue, Y. Mori, and H. Matsumura. "Growth of protein crystals in hydrogels prevents osmotic shock." In: *Journal of the American Chemical Society* 134.13 (2012), pp. 5786–5789. DOI: 10.1021/ja301584y.

[15] X. Chen and J. Shen. "Review of membranes in microfluidics." In: *Journal of Chemical Technology and Biotechnology* 92.2 (2017), pp. 271–282. DOI: 10.1002/jctb.5105.

[16] J. De Jong, R. G. Lammertink, and M. Wessling. "Membranes and microfluidics: A review." In: *Lab on a Chip* 6.9 (2006), pp. 1125–1139. DOI: 10.1039/b603275c.

[17] E. Curcio, G. Di Profio, and E. Drioli. "Membrane crystallization of macromolecular solutions." In: *Desalination* 145.1-3 (2002), pp. 173–177. DOI: 10.1016/S0011-9164(02)00404-6.

[18] P. Todd, S. K. Sikdar, C. Walker, and Z. R. Korszun. "Application of osmotic dewatering to the controlled crystallization of biological macromolecules and organic compounds." In: *Journal of Crystal Growth* 110.1-2 (1991), pp. 283–292. DOI: 10.1016/0022-0248(91)90897-E.

[19] R. K. Wierenga. "The growth of yeast thiolase crystals using a polyacrylamide gel as dialysis membrane." In: *Journal of Crystal Growth* 122 (1992), pp. 194–198.

[20] G. D. Di Profio, E. Curcio, A. Cassetta, D. Lamba, and E. Drioli. "Membrane crystallization of lysozyme: Kinetic aspects." In: *Journal of Crystal Growth* 257.3-4 (2003), pp. 359–369. DOI: 10.1016/S0022-0248(03)01462-3.

[21] U. V. Shah, C. Amberg, Y. Diao, Z. Yang, and J. Y. Heng. "Heterogeneous nucleants for crystallogenesis and bioseparation." In: 8 (2015), pp. 69–75. DOI: 10.1016/j.coche.2015.03.002.

[22] S. S. J. Lee and R. Cudney. "A modified microdialysis button for use in protein crystallization." In: *J. Appl. Cryst* 37 (2004), pp. 504–505. DOI: 10.1107/S0021889804007174.

[23] G. Di Profio, E. Curcio, and E. Drioli. "Supersaturation control and heterogeneous nucleation in membrane crystallizers: Facts and perspectives." In: *Industrial and Engineering Chemistry Research* 49.23 (2010), pp. 11878–11889. DOI: 10.1021/ie100418z.

[24] C.-y. Lee, M. G. Sportiello, S. P. Cape, S. Ferree, P. Todd, C. E. Kundrot, S. Lietzke, and C. Barnes. "Characterization and Application of Osmotic Dewatering to the Crystallization of Oligonucleotides." In: *Biotechnology Progress* 13 (1997), pp. 77–81.

[25] C.-Y. Lee, S. R. Mcentyre, P. Todd, K. Schaefer, and C. E. Kundrot. *Control of nucleation in oligonucleotide crystallization by the osmotic dewatering method with kinetic water removal rate control*. Tech. rep. 1998, pp. 490–498.

[26] E. Curcio, G. Di, and E. Drioli. "A new membrane-based crystallization technique : tests on lysozyme." In: *Jornal of Crystal Growth* 247 (2003), pp. 166–176. DOI: 10.1016/S0022-0248(02)01794-3.

[27] E. Drioli, G. D. Profio, E. Curcio, W. S. W. Ho, and K Li. "Progress in membrane crystallization." In: *Current Opinion in Chemical Engineering* 1 (2012), pp. 178–182. DOI: 10.1016/j.coche.2012.03.005.

[28] G. Di Profio, C. Stabile, A. Caridi, E. Curcio, and E. Drioli. "Antisolvent Membrane Crystallization of Pharmaceutical Compounds." In: *Journal of Pharmaceutical Sciences* 98.12 (2009), pp. 4902–4913. DOI: 10.1002/jps.

[29] G. Di Profio, A. Caridi, R. Caliandro, A. Guagliardi, E. Curcio, and E. Drioli. "Fine dosage of antisolvent in the crystallization of L-histidine: Effect on polymorphism." In: *Crystal Growth and Design* 10.1 (2010), pp. 449–455. DOI: 10.1021/cg901038g.

[30] E. Curcio, G. Di, and E. Drioli. "Microporous Hydrophobic Membranes for Crystallization of Biomolecules." In: *Chemical Engineering Transactions* 47.2 (2016), pp. 421–426. DOI: 10.3303/CET1647071.

[31] C. Y. Zhang, D. C. Yin, Q. Q. Lu, Y. Z. Guo, W. H. Guo, X. K. Wang, H. S. Li, H. M. Lu, and Y. J. Ye. "Cycling temperature strategy: A method to improve the efficiency of crystallization condition screening of proteins." In: *Crystal Growth and Design* 8.12 (2008), pp. 4227–4232. DOI: 10.1021/cg800689j.

[32] E Drioli, E Curcio, and G Di Profio. "State of the art and recent progresses in membrane contactors." In: *Trans IChemE, Part A* 83.March (2005), pp. 223–233. DOI: 10.1205/cherd.04203.

[33] E. Curcio, S. Simone, G. Di, E. Drioli, A. Cassetta, and D. Lamba. "Membrane crystallization of lysozyme under forced solution flow." In: *Jornal of Membrane Science* 257 (2005), pp. 134–143. DOI: 10.1016/j.memsci.2004.07.037.

[34] W Kast and C.-R Hohenthanner. "Mass transfer within the gas-phase of porous media." In: 43 (2000), pp. 807–823.

[35] E. Curcio, E. Fontananova, G. D. Profio, and E. Drioli. "Influence of the Structural Properties of Poly(vinylidene fluoride) Membranes on the Heterogeneous Nucleation Rate of Protein Crystals." In: *Journal of Physical Chemistry B* 4.1 (2006), pp. 12438–12445. DOI: 10.1021/jp061531y.

[36] A. Mcpherson and P. Shlichta. "Heterogeneous and Epitaxial Nucleation of Protein Crystals on Mineral Surfaces." In: *Science* 239 (1988), pp. 385–387. DOI: 10.1126/science.239.4838.385.

[37] S. Khurshid, E. Saridakis, L. Govada, and N. E. Chayen. "Porous nucleating agents for protein crystallization." In: *Nature Protocols* 9.7 (2014), pp. 1621–1633. DOI: 10.1038/nprot.2014.109.

[38] C. N. Nanev, E. Saridakis, and N. E. Chayen. "Protein crystal nucleation in pores." In: *Scientific Reports* 7 (2017), pp. 35821–35829. DOI: 10.1038/srep35821.

[39] N. E. Chayen, E Saridakis, R El-Bahar, and Y Nemirovsky. "Porous silicon: an effective nucleation-inducing material for protein crystallization." In: *Journal of Molecular Biology* 312.4 (2001), pp. 591–595. DOI: 10.1006/jmbi.2001.4995.

[40] U. Salazar-Kuri, J. O. Estevez, E. E. Antunez, B. S. Martinez-Aguila, J. B. Warren, B. Andi, M. L. Cerniglia, V. Stojanoff, and V. Agarwal. "Nucleation of sub-micrometer protein crystals in square-shaped macroporous silicon structures." In: *Crystal Growth and Design* 15.6 (2015), pp. 2801–2808. DOI: 10.1021/acs.cgd.5b00243.

[41] N. E. Chayen, E. Saridakis, and R. P. Sear. "Experiment and theory for heterogeneous nucleation of protein crystals in a porous medium." In: *Proceedings of the National Academy of Sciences of the United States of America* 103 (2006), pp. 597–601. DOI: 10.1073/pnas.0504860102.

[42] U. V. Shah, D. R. Williams, and J. Y. Heng. "Selective crystallization of proteins using engineered nanonucleants." In: *Crystal Growth and Design* 12.3 (2012), pp. 1362–1369. DOI: 10.1021/cg201443s.

[43] G. Di Profio, E. Curcio, and E. Drioli. "Trypsin crystallization by membrane-based techniques." In: *Journal of Structural Biology* 150.1 (2005), pp. 41–49. DOI: 10.1016/j.jsb.2004.12.006.

[44] Y. X. Liu, X. J. Wang, J. Lu, and C. B. Ching. "Influence of the roughness, topography, and physicochemical properties of chemically modified surfaces on the heterogeneous nucleation of protein crystals." In: *Journal of Physical Chemistry B* 111.50 (2007), pp. 13971–13978. DOI: 10.1021/jp0741612.

[45] S. Karthika, T. K. Radhakrishnan, and P. Kalaichelvi. "A Review of Classical and Nonclassical Nucleation Theories." In: *Crystal Growth and Design* 16 (2016), pp. 6663–6681. DOI: 10.1021/acs.cgd.6b00794.

[46] S. M. Salehi, A. C. Manjua, B. D. Belviso, C. A. M. Portugal, I. M. Coelhoso, V. Mirabelli, E. Fontananova, R. Caliandro, Joa, G Crespo, E. Curcio, and G. D. Profio. "Hydrogel Composite Membranes Incorporating Iron Oxide Nanoparticles as Topographical Designers for Controlled Heteronucleation of Proteins." In: *Crystal Growth & Design* 18.6 (2018), pp. 3317–3327. DOI: 10.1021/acs.cgd.7b01760.

[47] H. Hou, B. Wang, S.-Y. Hu, M.-Y. Wang, J. Feng, P.-P. Xie, and D.-C. Yin. "An investigation on the effect of surface roughness of crystallization plate on protein crystallization." In: *Journal of Crystal Growth* 468.October 2016 (2017), pp. 290–294. DOI: 10.1016/j.jcrysgro.2016.10.007.

[48] A. Gugliuzza, C Aceto, and E. Drioli. "Interactive functional poly (vinylidene fluoride) membranes with modulated lysozyme affinity : a promising class of new interfaces for contactor crystallizers." In: *Polym Int* 58 (2009), pp. 1452–1464. DOI: 10.1002/pi.2681.

[49] S. Simone, E. Curcio, G. Di, M. Ferraroni, and E. Drioli. "Polymeric hydrophobic membranes as a tool to control polymorphism and protein – ligand interactions." In: *Jornal of Membrane Science* 283 (2006), pp. 123–132. DOI: 10.1016/j.memsci.2006.06.028.

[50] U. V. Shah, M. C. Allenby, D. R. Williams, and J. Y. Y. Heng. "Crystallization of proteins at ultralow supersaturations using novel three-dimensional nanotemplates." In: *Crystal Growth and Design* 12.4 (2012), pp. 1772–1777. DOI: 10.1021/cg201190c.

[51] W. De Poel, J. A. W. Mu, J. A.A. W. Elemans, W. J. P. Van Enckevort, A. E. Rowan, and E. Vlieg. "Surfaces with Controllable Topography and Chemistry Used as a Template for Protein Crystallization." In: *Crystal Growth & Design* 18 (2018), pp. 763–769. DOI: 10.1021/acs.cgd.7b01174.

[52] L. Wang, G. He, X. Ruan, and D. Zhang. "Tailored Robust Hydrogel Composite Membranes for Continuous Protein Crystallization with Ultrahigh Morphology Selectivity." In: *ACS Applied Materials & Interfaces* 10.31 (2018), pp. 26653–26661. DOI: 10.1021/acsami.8b08381.

[53] S. Fermani, G. Falini, M. Minnucci, and A. Ripamonti. In: *Journal of Crystal Growth* ().

[54] G. Tosi, S. Fermani, G. Falini, J. A. Gavira Gallardo, and J. M. Garcia Ruiz. "Crystallization of proteins on functionalized surfaces." In: *Acta Crystallographica Section D: Biological Crystallography* 64.10 (2008), pp. 1054–1061. DOI: 10.1107/S0907444908025079.

[55] A. S. Ghatak, G. Rawal, and A. Ghatak. "Precipitant-Free Crystallization of Protein Molecules Induced by Incision on Substrate." In: *Crystals* 7.8 (2017), p. 245. DOI: 10.3390/cryst7080245.

[56] A. S. Ghatak and A. Ghatak. "Precipitantless Crystallization of Protein Molecules Induced by High Surface Potential." In: *Crystal Growth & Design* 16 (2016), pp. 5323–5329. DOI: 10.1021/acs.cgd.6b00833.

[57] A. C. W. Pike, E. F. Garman, T. Krojer, F. von Delft, and E. P. Carpenter. "An overview of heavy-atom derivatization of protein crystals." In: *Acta crystallographica. Section D, Structural biology* 72.Pt 3 (2016), pp. 303–318. DOI: 10.1107/S2059798316000401.

[58] M. Sugahara. "A technique for high-throughput protein crystallization in ionically cross-linked polysaccharide gel beads for x-ray diffraction experiments." In: *PLoS ONE* 9.4 (2014), pp. 1–8. DOI: 10.1371/journal.pone.0095017.

[59] O Vidal, M. Robert, B Arnoux, and B Capelle. "Crystalline quality of lysozyme crystals grown in agarose and silica gels studied by X-ray diffraction techniques." In: *Journal of Crystal Growth* 196.2-4 (1999), pp. 559–571. DOI: 10.1016/S0022-0248(98)00917-8.

[60] M. Polino, A. Luísa Carvalho, L. Juknaite, C. A. M Portugal, I. M. Coelhoso, M. J. Romao, and J. G. Crespo. "Ion-Exchange Membranes for Stable Derivatization of Protein Crystals." In: *Crystal Growth & Design* 17 (2017), pp. 4563–4572. DOI: 10.1021/acs.cgd.7b00315.

[61] Y. R. Liang, L. N. Zhu, J. Gao, H. X. Zhao, Y. Zhu, S. Ye, and Q. Fang. "3D-Printed High-Density Droplet Array Chip for Miniaturized Protein Crystallization Screening under Vapor Diffusion Mode." In: *ACS Applied Materials and Interfaces* 9.13 (2017), pp. 11837–11845. DOI: 10.1021/acsami.6b15933.

[62] H. Yamaguchi, M. Maeki, K. Yamashita, H. Nakamura, M. Miyazaki, and H. Maeda. "Controlling one protein crystal growth by droplet-based microfluidic system." In: *Journal of Biochemistry* 153.4 (2013), pp. 339–346. DOI: 10.1093/jb/mvt001.

[63] W. Du, L. Li, K. P. Nichols, and R. F. Ismagilov. "SlipChip." In: *Lab on a Chip* 9.16 (2009), p. 2286. DOI: 10.1039/b908978k.

[64] L. Wang, K. Sun, X. Hu, G. Li, Q. Jin, and J. Zhao. "A centrifugal microfluidic device for screening protein crystallization conditions by vapor diffusion." In: *Sensors and Actuators B: Chemical* 219 (2015), pp. 105–111. DOI: 10.1016/J.SNB.2015.04.105.

[65] L. Li and R. F. Ismagilov. "Protein Crystallization Using Microfluidic Technologies Based on Valves, Droplets, and SlipChip." In: *Annu. Rev. Biophys* 39 (2010), pp. 139–58. DOI: 10.1146/annurev.biophys.050708.133630.

[66] B. Zheng, C. J. Gerdts, and R. F. Ismagilov. "Using nanoliter plugs in microfluidics to facilitate and understand protein crystallization." In: *Current Opinion in Structural Biology* 15.5 (2005), pp. 548–555. DOI: 10.1016/j.sbi.2005.08.009.

[67] J. Ferreira, F. Castro, F. Rocha, and S. Kuhn. "Protein crystallization in a droplet-based microfluidic device: Hydrodynamic analysis and study of the phase behaviour." In: *Chemical Engineering Science* 191 (2018), pp. 232–244. DOI: 10.1016/j.ces.2018.06.066.

[68] P. C. Hansen. "Introduction and Motivation." In: *Discrete Inverse Problems: Insight and Algorithms* (2010), pp. 1–4. DOI: http://dx.doi.org/10.1137/1.9780898718836.

[69] S. V. Akella, A. Mowitz, M. Heymann, S. Fraden, and M. A. Fisher. "Emulsion-Based Technique To Measure Protein Crystal Nucleation Rates of Lysozyme." In: *Crystal Growth & Design* 14 (2014), pp. 4487–4509. DOI: 10.1021/cg500562r.

[70] D. L. Chen, C. J. Gerdts, and R. F. Ismagilov. "Using Microfluidics to Observe the Effect of Mixing on Nucleation of Protein Crystals." In: *Journal of the American Chemical Society* 127 (2018), pp. 9672–9673. DOI: 10.1021/ja052279v.

[71] C. J. J. Gerard, G. Ferry, L. M. Vuillard, J. A. Boutin, L. M. G. Chavas, T. Huet, N. Ferte, and R. Grossier. "Crystallization via tubing microfluidics permits both in situ

and ex situ X-ray diffraction research communications." In: *Acta Crystallographica F* 73 (2017), pp. 574–578. DOI: 10.1107/S2053230X17013826.

[72] M. Heymann, A. Opthalage, J. L. Wierman, S. Akella, D. M. E. Szebenyi, S. M. Gruner, and S. Fraden. "Room-temperature serial crystallography using a kinetically optimized microfluidic device for protein crystallization and on-chip X-ray diffraction." In: *IUCrJ* 1 (2014). DOI: 10.1107/S2052252514016960.

[73] G. M. Whitesides. "The origins and the future of microfluidics." In: *Nature* 442.7101 (2006), pp. 368–373. DOI: 10.1038/nature05058.

[74] Y. Yu, X. Wang, D. Oberthür, A. Meyer, M. Perbandt, L. Duan, and Q. Kang. "Design and application of a microfluidic device for protein crystallization using an evaporation-based crystallization technique." In: *Journal of Applied Crystallography* 45.1 (2012), pp. 53–60. DOI: 10.1107/S0021889811048047.

[75] B. Zheng, L. S. Roach, and R. F. Ismagilov. "Screening of protein crystallization conditions on a microfluidic chip using nanoliter-size droplets." In: *Journal of the American Chemical Society* 125.37 (2003), pp. 11170–11171. DOI: 10.1021/ja037166v.

[76] D. Qin, Y. Xia, and G. M. Whitesides. "Soft lithography for micro- and nanoscale patterning." In: *Nature Protocols* 5.3 (2010), pp. 491–502. DOI: 10.1038/nprot.2009.234.

[77] A. Pimpin and W. Srituravanich. "Review on Micro- and Nanolithography Techniques and their Applications." In: *Engineering Journal* 16.1 (2012), pp. 37–55. DOI: 10.4186/ej.2012.16.1.37.

[78] F. Evenou, J.-M. D. Meglio, B. Ladoux, and P. Hersen. "Micro-patterned porous substrates for cell-based assays †." In: *Lab on a Chip* 12 (2012), pp. 1717–1722. DOI: 10.1039/c2lc20696j.

[79] P. Gao, A. Hunter, S. Benavides, M. J. Summe, F. Gao, and W. A. Phillip. "Template Synthesis of Nanostructured Polymeric Membranes by Inkjet Printing." In: *ACS Applied Materials & Interfaces* 8.5 (2016), pp. 3386–3395. DOI: 10.1021/acsami.5b11360.

[80] T. Köpplmayr, L. Häusler, I. Bergmair, B. Farshchian, S. M. Hurst, J. Lee, and S. Park. "3D molding of hierarchical micro- and nanostructures." In: *Journal of*

Micromechanics and Microengineering 21 (2011), pp. 1–8. DOI: 10.1088/0960-1317/21/3/035016.

[81] Y.-h. Cho, J. Woo, O.-h. Kim, J. Young, N. Jung, K. Shin, H. Choi, H. Choe, Y.-h. Cho, and Y.-e. Sung. "High performance direct methanol fuel cells with micro / nano-patterned polymer electrolyte membrane." In: *Journal of Membrane Science* 467 (2014), pp. 36–40. DOI: 10.1016/j.memsci.2014.03.069.

[82] M. H. Yildirim, J Braake, H. C. Aran, D. F. Stamatialis, and M Wessling. "Micro-patterned Nafion membranes for direct methanol fuel cell applications." In: *Journal of Membrane Science* 349 (2010), pp. 231–236. DOI: 10.1016/j.memsci.2009.11.050.

[83] A Omosebi and R. S. Besser. "Electron Beam Assisted Patterning and Dry Etching of Nafion Membranes." In: *Journal of Electrochemical Society* 158.10 (2011), pp. D603–D610. DOI: 10.1149/1.3615938.

[84] S Cuynet, A Caillard, T Lecas, N Semmar, J Bigarr, and P. Brault. "Membrane patterned by pulsed laser micromachining for proton exchange membrane fuel cell with sputtered ultra-low catalyst loadings." In: *Journal of Power Sources* 298 (2015), pp. 299–308. DOI: 10.1016/j.jpowsour.2015.08.019.

[85] M. Lafuente, E. Martínez, I. Pellejero, M. del Carmen Artal, and M. del Pilar Pina. "Wettability control on microstructured polypropylene surfaces by means of O2 plasma." In: *Plasma Processes and Polymers* 14.8 (2017), pp. 1–6. DOI: 10.1002/ppap.201700019.

[86] J. Hutfles, W. Chapman, and J. Pellegrino. "Roll-to-roll nanoimprint lithography of ultrafiltration membrane." In: *Journal of Applied Polymer Science* 135.11 (2018), pp. 1–12. DOI: 10.1002/app.45993.

[87] O. Heinz, M. Aghajani, A. R. Greenberg, and Y. Ding. "Surface-patterning of polymeric membranes: fabrication and performance." In: *Current Opinion in Chemical Engineering* 20 (2018), pp. 1–12. DOI: 10.1016/j.coche.2018.01.008.

[88] S. H. Maruf, L. Wang, A. R. Greenberg, J. Pellegrino, and Y. Ding. "Use of nanoimprinted surface patterns to mitigate colloidal deposition on ultrafiltration membranes." In: *Journal of Membrane Science* 428 (2012), pp. 598–607. DOI: 10.1016/j.memsci.2012.10.059.

[89] X. Zhang, M. S. El-Bourawi, K. Wei, F. Tao, and R. Ma. "Precipitants and additives for membrane crystallization of lysozyme." In: *Biotechnology Journal* 1.11 (2006), pp. 1302–1311. DOI: 10.1002/biot.200600088.

[90] D Dobrev, D Baur, and R Neumann. "Crystallization of lysozyme in pores of etched heavy-ion tracks." In: 80 (2005), pp. 451–456. DOI: 10.1007/s00339-004-3078-z.

[91] B. S. Gully, J. Zou, G. Cadby, D. M. Passon, K. S. Iyer, and C. S. Bond. "Colloidal graphenes as heterogeneous additives to enhance protein crystal yield." In: *Nanoscale* 4 (2012), pp. 5321–5324. DOI: 10.1039/c2nr31150j.

Chapter 3

Enhanced protein crystallization on Nafion® membranes modified by low-cost surface patterning techniques

3.1 Summary

In this work, the influence of surface topography on protein crystallization over Nafion® is investigated. Two types of Nafion® based membranes were modified by soft lithographic techniques in order to create different topographies at the micro and nano scale and subsequently tested. From the analysis of the induction time, nucleation and crystal growth rate of Trypsin from Bovine Pancreas, all the patterned Nafion® based membranes show an enhanced nucleation and crystal growth. To provide additional insight to the experimental observations, the wettability properties of the prepared samples and the ratio of the Gibbs free energy of heterogeneous nucleation to homogeneous nucleation were evaluated. The crystallization outcome results from the combined effect of both, the structural and chemical properties of the nucleant Nafion® surface.

3.2 Introduction

X-ray crystallography is the main technique used for solving the tri-dimensional structure of proteins. The main limitation of X-rays analysis is the attainment of well-diffracting

crystals of biological macromolecules [1, 2]. The key event for obtaining protein crystals suitable for x-ray diffraction is nucleation. Nucleation is a phase change, occurring in supersaturated solutions that reinstate equilibrium by clustering protein molecules in small solid nuclei. This leads to the formation of an interface between the solid nuclei and the solution creating the need for overcoming an activation energy for the process to occur. In other words, nucleation only becomes effective when the nuclei reach a critical size [3, 4]. It is well known that the interaction of the target solution with external substrates, also denominated as nucleant surfaces, alters the Gibbs free energy of the nucleation process promoting or inhibiting nucleation (heterogeneous nucleation) [5]. Heterogeneous nucleation for protein crystals was first reported in 1988, by McPherson, growing protein crystals onto minerals with a similar crystalline lattice (epitaxy) [6]. From there on, several nucleant surfaces were investigated and several chemical interactions between protein molecules and surfaces were hypothesized as effective control mechanisms: ionic interactions, hydrogen bonding and hydrophobic interactions [7–11]. . Furthermore, an always increasing number of studies are pointing out how combining chemical interactions with a suitable surface topography at the nanoscale might enhance the probability of nucleation. For instance, Shah et al. [12–15] noticed the preferential nucleation of proteins in the pores of nucleant particles, i.e. ordered mesoporous silica with 4-20 nm average pore size, for a given relationship between the protein radius of gyration and specific pore diameter of the nucleant particle. They also hypothesised a further stabilization of the nuclei formed in the nucleant pores induced by the presence of specific chemical moieties (such as –OH, -NH_3 or CH_3) on the pore wall [12, 13]. Ghatak et al. [16, 17], obtained protein crystals without the help of precipitant by combining a wrinkled PDMS surface with an oxidation treatment. Recent efforts are oriented towards the evaluation of topography and roughness effect on nucleation over nucleant surfaces without altering its surface chemistry. According to the literature review, the creation of different topographies at the nanoscale is mainly associated with local changes in the surface chemistry, i.e. induced by plasma or wet oxidation treatments, or specific coatings. Thus, Liu et al. [18]. investigated the performance of chemically modified glass slides with different polymers on the heterogenous nucleation of lysozyme crystals. They found that both, the surface chemistry (by controlling the chemical and physical interactions with the protein molecules), and the surface topography (by increasing the possibility of nucleation compared with that on an ideally flat surface) of the modified glass slide

affect the heterogeneous nucleation to different extents. Recently, a similar study has been reported for several model proteins on muscovite mica substrates modified with multilayers of 1,3,5-tris(10-carboxydecyloxy) benzene (TCDB) grown by evaporation. The surface roughness (up to 3 nm) and wettability properties were correlated with the amount of TCDB deposited [19] and with the protein crystallization outcome. Topography effects were also investigated by modifying the surface of conventional protein crystallization plates with various types of wet oxidation treatments [20] in order to generate different degrees of roughness (up to 32 nm). During the last twenty years, membranes have been used in crystallization processes to control solvent transport and hence the supersaturation rate; and also as heterogeneous nucleation promoters by inducing a reduction in the free energy barrier [21]. Indeed, the physical properties, i.e. porous structure, and chemical nature of the membrane surface control the mass transfer rate of components and provide at the same time the micro-nano environment for crystal nucleation and growth [22–25] . The use of microporous hydrophobic supports covered with an hydrophilic hydrogel layer allows the production of protein crystals with improved diffraction properties due to the convection-free environment of the gel [26]. Recently, the tuning of chemical and topographical features of similar hydrogel composite membranes by incorporating different amounts of iron oxide nanoparticles [27] has been investigated for model proteins crystallization by our group. As the NPs were introduced in the hydrogel composite membrane, the crystal density number increased with the increase of the NPs load. The fabrication of nucleant surfaces with a tunable topography whereas preserving the chemical nature of the pristine material seems to be a priority for a more comprehensive understanding of the nucleation mechanisms. To the best of our knowledge, there are no previous works where the influence of nucleant topography is systematically investigated keeping unaltered the chemical composition of the surface. Nowadays, soft lithography outstands as a convenient, effective, and low-cost method for the formation and manufacturing of micro- and nanostructures. It includes a set of techniques that make use of an elastomeric stamp, namely a PDMS stamp, to generate patterns and structures with feature sizes ranging from 30 nm to 100 μm. Thus, it is possible to design tailored geometries at different scales and transfer them to different surfaces minimizing surface chemistry changes. This approach is cleanroom free and high-throughput process, which makes micro and nano-fabrication affordable for a wide range of applications. Basically, it relies on the fabrication of a silicon master mold that is further used to prepare

the PDMS elastomeric stamp or mold by casting. The PDMS replicas can be then used repeatedly for thermal nanoimprint lithography or microtransfer molding processes [28]. More specifically, thermal nanoimprint lithography (NIL) is a powerful and inexpensive technique for reproducing large patterns onto thermoplastic materials [29–31]. It takes advantage of the ability of materials to become soft and suffer deformation at temperatures higher than their glass transition temperature (Tg) and reinstate their stiffness at temperatures below the Tg. In microtransfer molding (MT) and replica molding (REM), a liquid prepolymer is poured onto the patterned surface of the PDMS mold. In REM, this mold is overloaded with the prepolymer solution; and then, is cured to a solid by illuminating the mold with UV light or by heating it. When the PDMS mold is peeled away carefully, a patterned microstructure is left on the surface of the substrate. In MT approach, the removal of the prepolymer excess poured on the PDMS mold is carefully performed before curing. This work explores the use of soft lithographic techniques for the micro and nanopatterning of Nafion® based membranes. This type of ion-exchange membranes has been selected due to its protein crystal derivatization performance, recently demonstrated by our group [32]. Hence, optimizing a membrane surface suitable for a gentle derivatization, besides a more controlled nucleation, would allow for creating a nucleant support suitable for all steps required for protein X-ray solution. In particular, three different fabrication approaches are herein investigated: i) thermal NIL for the micro and nanopatterning of commercial Nafion® 117 flat membranes using hard molds; ii) MT and REM to pattern microstructures upon thermal curing of the Nafion™ NR50 superacid resin solution spread on the PDMS mold; and iii) the combination of both to obtain a hierarchical structure by hot pressure assembly of single micropatterned (MT) and nanopatterned (NIL) membranes, respectively. The crystallization performance of all the prepared membranes, i.e. induction time, nucleation and growth rate, is evaluated using Trypsin from Bovine Pancreas as protein model and compared to the crystallization on Nafion® 117 flat membrane. Finally, the effect of surface properties on protein crystallization is discussed on the basis of the classical nucleation theory by adapting the model developed by Liu et al. [18] to the designed geometries.

3.3 Materials and Methods

3.3.1 Flat Nafion® membranes

Two types of flat Nafion® membranes are studied in this work: commercially available flat Nafion® 117 membranes (average equivalent weight 1100 g per sulfonic group and 178μm thickness) purchased from Sigma Aldrich; and those prepared from Nafion™ NR50 superacid resin purchased from Ion-Power in the form of beads. Flat Nafion™ NR50 based membranes were obtained by casting on a Petri dish from a diluted solution in N,N-Dimethylformamide (DMF). According to the technical specifications of the suppliers, both Nafion materials possess the same equivalent weight (1100 g/eq). However, the resulting flat membranes exhibit different macroscopic properties, i.e. water uptake: i.e. 15% wt. for Nafion™ NR50 vs. 24% wt. for Nafion® 117, which may be attributed to the membrane formation process. The influence of solvent on the Nafion molecular conformation in dilute solutions is well reported in the literature [33], and thus the morphology and macroscopic properties of the resulting membranes are greatly affected.

3.3.2 Hard molds for Thermal Nanoimprint Lithography (NIL)

Different topographies, with micro or nano features, were created on the surface of commercial Nafion® 117 membranes by thermal nanoimprint lithography. In particular, two rigid silicon molds were used. The nanomold used for the Nafion® 117 nanopatterning was produced by displacement Talbot lithography [34]. This nanomold contains Au/Ti on cone-shaped silicon features 110.7±2 nm in diameter and 115.4±0.5 nm in height with a pitch of 250 nm. The cone-shaped features are displayed in Figure 3.1A and Figure 3.1B before and after the residual resist removal on the top of the pillars (marked with a black line ~18 nm), respectively. All the 117 Nano membranes prepared in this work were imprinted with the mold containing the residual resist coating.

3.3.3 Soft mold for Microtransfer Molding (MT) or Replica Molding (REM)

A similar microscale patterning was transferred to Nafion™ NR50 by casting and curing the Nafion:DMF solution onto the poly(dimethylsiloxane) (PDMS) micromold (shown in Figure 3.2B). This elastomeric mold, with triangular-prism shaped pillars 160μm side and 110μm height and periodically ordered on the surface with a repeating unit of 347μmx182μm, was produced by casting a mixture of PDMS pre-polymer (purchased by

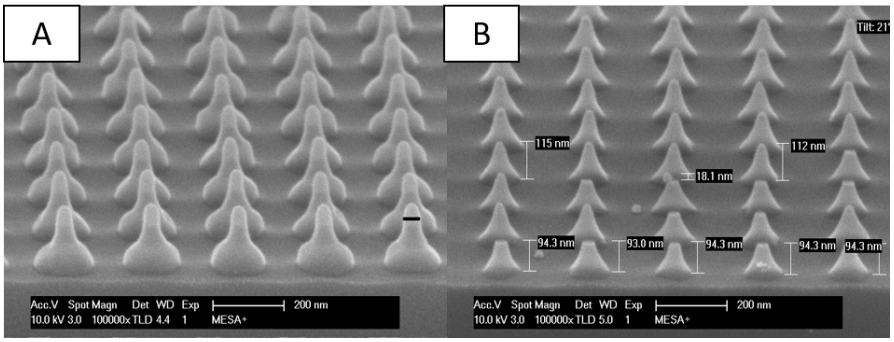

Figure 3.1: SEM images of the fabricated nanomold before (A) and after (B) residual resist removal.

Sylgard 184 Dow Corning, Midland, MI) and curing agent (10:1) onto a SU8-Si master (shown in Figure 3.2A) fabricated by standard photolithography [35]. The PDMS solution casted onto the SU8-Si master was cured by baking at 80°C for 50 minutes and the final elastomeric mold was released by peeling-off.

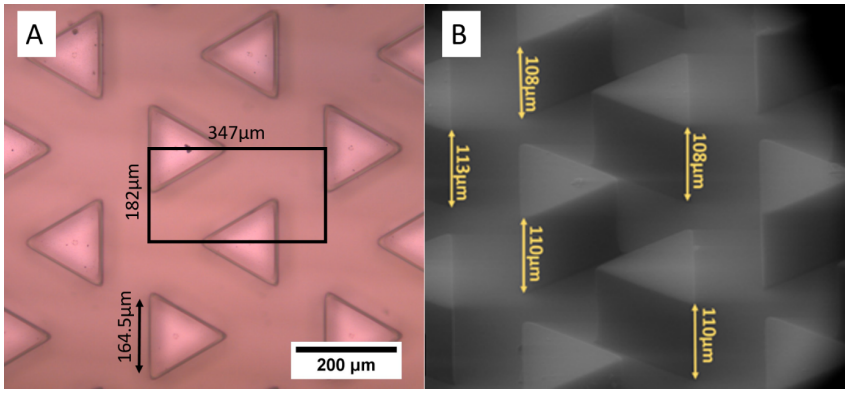

Figure 3.2: SEM images of the SU8-Si micromold (A) and PDMS micromold (B) used to prepare patterned Nafion membranes by NIL and MT respectively.

3.3.4 Patterning of Nafion® based membranes

Three different approaches are herein investigated to prepare 117 Micro, 117 Nano and NR50 Micro Nafion-based membranes (see Figure 3.3). All of them take advantage of the intimate contact of the Nafion substrate with a mold for transferring the designed structure.

The first approach is based on thermal NIL to prepare 117 Micro (when using the hard micro mold) and 117 Nano (when using the hard nano mold) samples, respectively. More specifically, Nafion® 117 flat membranes 178μm thick were patterned using a Compact NanoImprint (CNI) tool from NILT company. Both, the Nafion® 117 substrate and

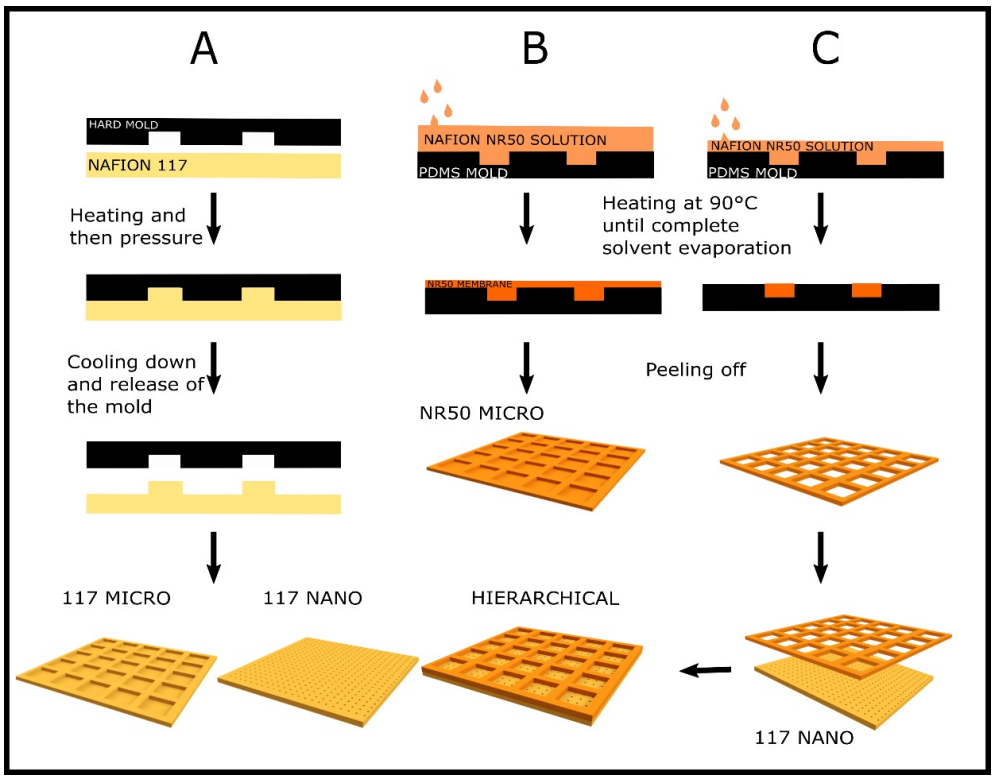

Figure 3.3: Schematics of the fabrication processes for patterned Nafion® membranes: A) thermal nanoimprint lithography (NIL) on Nafion® 117 flat films to prepare 117 Micro and 117 Nano samples; B) replica molding (REM) to prepare NR50 Micro sample; and C) microtransfer molding (MT) to prepare Hierarchical sample by hot pressure assembly with 117 Nano.

the mold were contacted on the top of a ceramic heating plate. The chamber was closed and a program was set in order to firstly rise the temperature to 135°C to soften the membrane, 20°C above the glass transition temperature Tg of Nafion® 117 (referred to Supporting Information for its experimental determination from DSC analyses). Then, a pressure of 6 bar was applied for 6 minutes to improve the contact between the mold and Nafion® 117. Finally, the chamber was cooled down to 60 °C (to freeze the structure of the mold in the substrate) and the pressure released (see schematics in Figure 3.3A). The second strategy relies on REM and leads to NR50 Micro sample. Unlike previously, Nafion™ NR50 beads were, instead, dissolved in N,N-Dimethylformamide (DMF) purchased from Acros, at 240°C for 24h in autoclave, at a concentration of 0.030g/mL (3.2% wt). The Nafion™ solution was casted onto the PDMS mold and left on a hot plate at 90°C until complete evaporation of the solvent (see schematics in Figure 3.3B). Controlling the amount of polymer solution used for casting allows to tune the thickness of the Nafion substrate. When the thickness of the membrane is less than the height of the

pillars (110±2µm), a NR50 Micro membrane with straight pores connecting both sides is obtained (See Figure 3.3C). In order to facilitate the release of the membrane, before Nafion™ NR50 solution casting, the PDMS mold was treated with Tridecafluoro-1,1,2,2-tetrahydrooctyl-1-trichlorosilane (TFOCS, from Sigma Aldrich). Few drops of TFOCS were left evaporating and deposited as a thin layer onto the PDMS mold to make it more hydrophobic [28]. All the NR50 based membranes were carefully washed in boiling water to remove traces of DMF solvent. In the third strategy, a hierarchical structure with the nanowells inside the microwells is obtained by hot pressure assembly of NR-50 Micro (MT) and 117 Nano (NIL) membranes, respectively (see schematics in Figure 3.3C). The final hierarchical membrane combines the microstructured Nafion™ NR50 membrane (90μm thick) with straight pores connecting both sides and the nano imprinted Nafion® 117 membrane (178μm thick).

3.3.5 Characterization Techniques

In order to evaluate the fidelity of master duplication in soft lithography techniques, the molds and the obtained Nafion® membranes were characterized by AFM (Multimode 8 from Veeco/Bruker), SEM (Inspect F50, FEI) and optical microscopy (Nikon Eclipse ci). Samples for SEM were sputtered either with Au/Pd or carbon. AFM images were processed by Gwyddion software [36] and SEM and optical microscopy images by Image J [37]. In order to track chemical changes that may occur during the imprinting process FTIR (Perkin Elemer, Spectrum Two, FT-IR Spectrometer) spectra of the membranes were recorded. The wetting properties of the patterned Nafion based membranes were studied based on the static contact angle (SCA) measurements. These were evaluated by the sessile drop method in a contact angle goniometer (CAM 100, KSV Instruments Ltd., Finland). The solution used for the measurement was the same solution used for the crystallization experiments, hence: Trypsin from Bovine Pancreas 20 mg/mL, Hepes buffer 12.5 mM (pH 7.5), $CaCl_2$ 5mM, Benzamidine 5mg/mL, $(NH_4)_2SO_4$ 0.1M, PEG 8K 10%, Cacodylate 0.05M (pH 6.5). Five independent measurements were performed on each sample to calculate the average value and standard deviation (SD). The drop volume used for the measurements was 9μL.

3.3.6 Crystallization solutions

A solution of Trypsin from Bovine Pancreas (BPT), purchased from Panreac, with initial concentration of 40 mg/mL was prepared in 25mM Hepes buffer (pH 7.5), with 10mM $CaCl_2$ and 10mg/mL Benzamidine (in order to inhibit the protease activity). The precipitant solution, also used as stripping solution, was composed of $(NH_4)_2SO_4$ (purchased from Panreac) 0.2M, PEG 8K 20% wt (purchased from Sigma-Aldrich), and 0.1M of Cacodylate (purchased from Sigma Aldrich) pH 6.5. The final crystallization solution, after mixing the protein and precipitant solutions, was 20 mg/mL.

3.3.7 Crystallization experiments

Crystallization tests were carried out by using 24-well plates (from Qiagen) conventionally used for the vapor diffusion technique [1] and adapted for membrane-assisted crystallization experiments (sitting drop mode). The setup is displayed in Figure 3.4. Briefly, an equal amount (5μL) of protein and precipitant solution was mixed on the top of the nucleant membrane (0.7cmx0.7cm) and left equilibrating with 500μL of stripping solution. The difference in water activity between the crystallization solution and the stripping solution determines solvent migration from the protein solution to the stripping solution, increasing protein concentration until supersaturation is reached promoting nucleation. The crystallization tests were carried out at 20 °C with five replicates for each condition to assure the results reproducibility. Crystallization trials were also carried out using flat Nafion membranes for reference purposes. Data over time, on nucleation and crystal growth, were obtained by monitoring the number of crystals and size with an optical microscope (Nikon Eclipse ci) equipped with a camera and pictures were processed with the ImageJ software [37].

3.4 Results and Discussion

3.4.1 Characterization of the patterned topographies on Nafion® membranes

Figure 5 shows the top view of the 117 Nano and 117 Micro samples prepared by thermal NIL. For the nanostructured membrane (Figure 3.5A), SEM images reveal a repeating

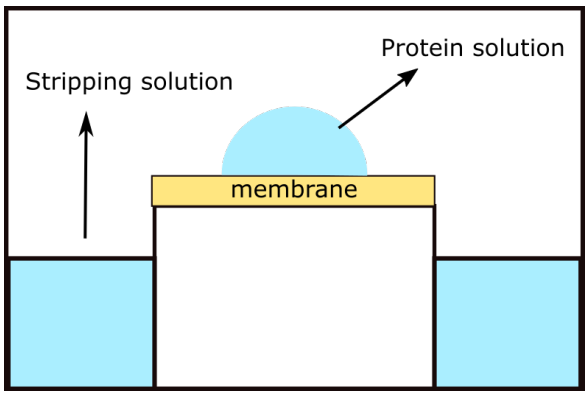

Figure 3.4: Experimental set-up used for crystallization experiments in vapour diffusion mode.

unit of 230 nm x 230 nm with cilindrical-shaped wells 110 nm diameter. Thus, the nanostructures on Nafion 117 replicate almost the inverse pattern of the master with periods smaller than the original of the rigid master due to large thermal expansion coefficient of thermoplastic Nafion (200x 10^{-6} $K^{-}1$) [38]. For the microstructured membrane (Figure 3.5B), optical microscope images indicate triangular-shaped wells 164μm size and a repeating unit of 187μmx355μm. Also in this case, the microstructure on the Nafion® 117 replicates closely the inverse pattern of the master.

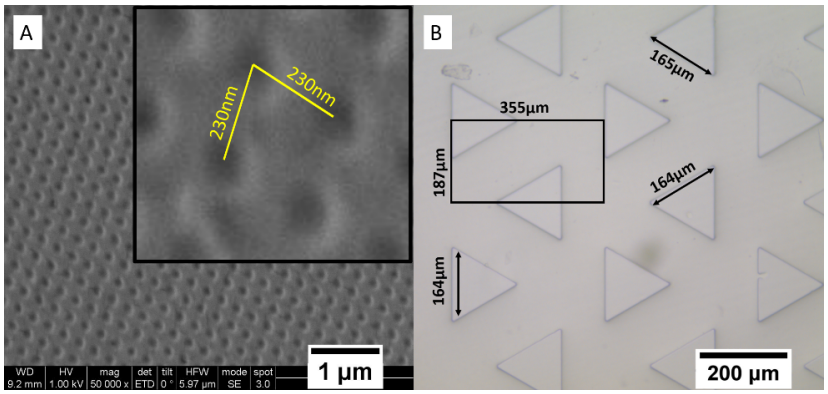

Figure 3.5: Top view images of: A) 117 Nano (SEM) and, B) 117 Micro (optical)

In addition, the imprint depth of the nanofeatures was analysed from 3D AFM images (see Figure 3.7) the depth of the wells was 56±4 nm compared to the rigid master depth, 115.4±0.5 nm.

The AFM scanning was performed over the areas depicted in Figure 3.6. The processing of AFM images from the patterned surfaces by software Gwyddion [36] provides with the roughness parameters shown in Table 1: Ra (average of absolute values of profile height deviations from the mean line) and Rms (root mean square average of the profile

height deviations from mean line).

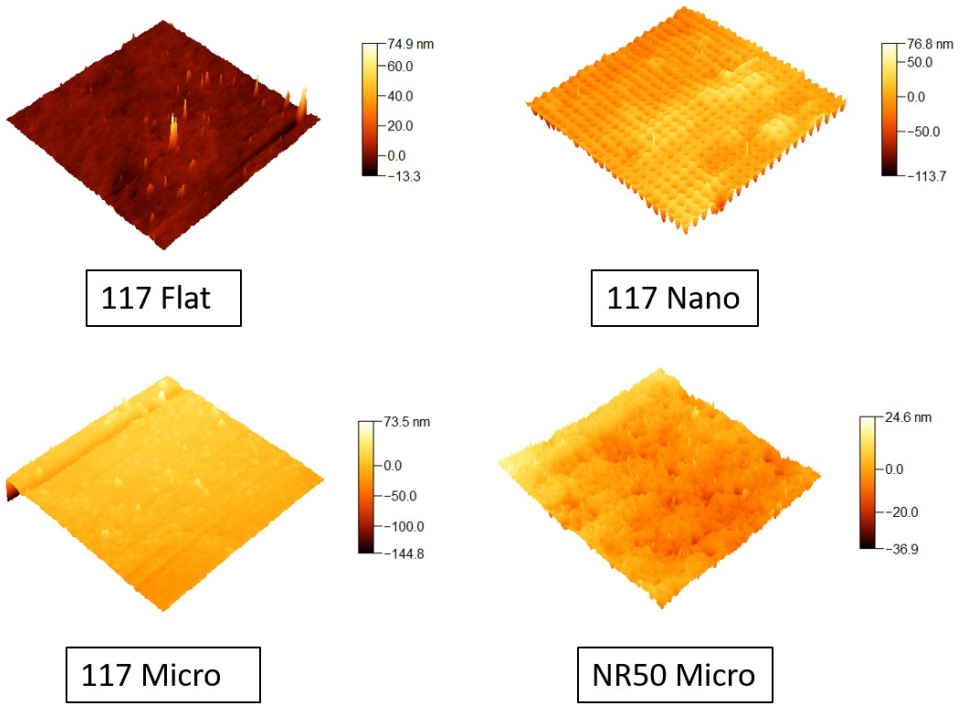

Figure 3.6: AFM images of the Nafion based membranes developed for this work. The scanned area was 5μmx5μm for all the membranes.

Table 3.1: Main characteristics of the Nafion® based membranes studied in this work.

Type of Membrane	Patterning	Thickness (μm)	Contact Angle (°)	Ra (nm)	Rms (nm)
117-Flat	n.a.	178	64.7±2.9	1.0±0.2	3.1±3.4
117-Nano	nano(NIL)	178	63.2±2.4	14.9±4.9	16.8±7.2
117-Micro	micro(NIL)	178	48.1±4.2	4.0±0.4	6.4±1.1
NR50-Flat	n.a.	90	77.7±4.4	22.2±6.0	38.5±21.9
NR50-Micro	micro (REM)	90	100±4	2.8±0.4	3.8±0.6
Hierarchical (117+ NR50)	nano + micro (NIL+MT)	268	87.3±1.6	4.52*	5.07*

Herein, it is worthy to point out that the scanned line for determining the roughness

on sample 117 Nano (as shown in Figure 3.7) was drawn across the hillocks. Consequently, the surface roughness reported in Table 1 for 117 Nano is somehow overestimated when compared with its counterparts due to the periodic nanoholes are included in the averaging. In general, all the Nafion-based membranes show a rather smooth surface with comparable roughness at nanoscopic scale. As an example, 117 Flat and 117 Micro membranes, with clearly different topographies at a microscopic level, exhibit similar Ra values, i.e. 1.0±0.2 nm and 4.0±0.4 nm, respectively. In addition, whatever the soft lithography approach to obtain the desired microstructure, the surface roughess is comparable: 2.8±0.4 nm for NR50 Micro (REM) vs. 4.0±0.4 nm for 117 Micro (NIL).

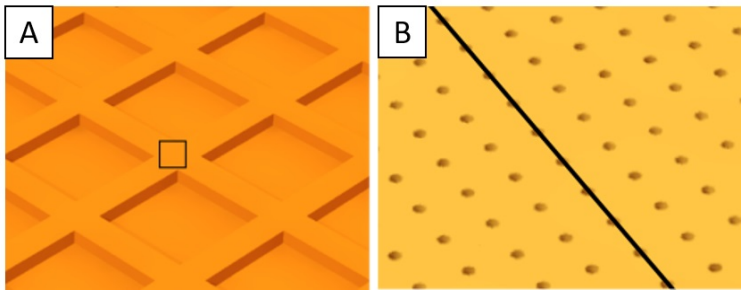

Figure 3.7: Scanned areas of patterned Nafion based membranes by AFM: A) analysis performed on the contour surface (black square) for117 Micro and not inside the wells); B) analysis performed on the black line for 117 Nano)

3.4.2 Influence of surface patterning on the wetting properties

Previous investigation was carried out to examine the potential influence of the imprinting temperature, 135°C, on the surface chemistry and consequently on the surface wettability of samples processed by NIL. It has been reported that thermal treatment of Nafion® membranes may induce conformational changes and spatial reorientation of the hydrophobic an hydrophilic nanodomains leading to a lower water uptake and conductivity [39, 40]. According to the literature, the thermal NIL herein performed would induce minor changes in water content (̃5%) and negligible variations in its crystallinity [39]. In order to confirm such hypotheses, comparative FTIR analyses (see Figure 3.8) were carried out for as received commercial Nafion® 117 membranes, i.e. sample Flat 117, and for thermal imprinted membranes, i.e. sample 117 Nano. As it was expected, the band centered at 3451 cm^{-1}, attributed to the stretching of –OH group, is more intense in the case of 117 Flat sample in accordance to its higher water content (see supporting

information). The remaining part of the two spectra is perfectly overlapping. This observation reinforces the adequacy of the thermal imprinting parameters but highlights the modification of the surface wetting properties of thermal NIL processed samples.

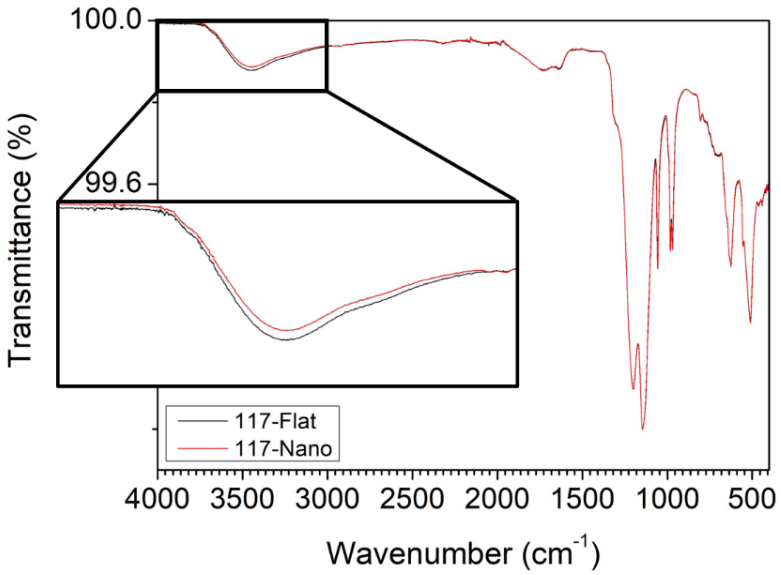

Figure 3.8: Comparative FTIR analyses of Nafion®117 based membranes: commercial 117 Flat (reference) and patterned 117 Nano (NIL).

The determination of the static contact angle, SCA, allowed the establishment of the membranes wettability. The experimental measurements were performed using the same protein solution as the one used for crystallization experiments. The patterning effect on wetting properties is shown in Figure 3.9 for the two Nafion based materials. An apparent opposite behaviour is shown by Nafion® 117 and Nafion™ NR50 samples, respectively. As an example, the SCA registered for 117 Micro and NR50 Micro samples with common features on the surface, are 48±4.2° and 100±4° respectively. Although both starting materials exhibit the same equivalent weight (1100 g/eq) and ion-exchange capacity (0.9meq/g) [33]; the membrane formation process greatly influences the arrangement of the polymer chain conformation and mobility, leading to noticeable variations in macroscopic properties. From structural investigations of the Nafion® ionomer, it is known that the hydrophobic backbone is a continuous semicristalline region, meanwhile the hydrophilic sulfonic groups are organized in clusters that can incorporate water and allow for ions/protons and water transport. Hence, the water uptake is directly related to the size of these clusters [41]. Whereas commercial Nafion® 117 membrane is prepared by extrusion, the Nafion™ NR50 based membranes are herein obtained by casting from

a diluted solution of NR50 superacid resin in DMF. Due to the higher affinity of DMF for the Teflon backbone, the NR50 nanoaggregates in DMF assume a coiled-like shape where the sulfonated groups are buried inside, in order to minimize the interfacial contact with the solvent. Such conformational arrangement, also dependant on the nature of the casting substrate, leads to a random distribution of the hydrophobic and hydrophilic domains that prevents the formation of large clusters. In fact, the lower water uptake properties and the higher SCA values registered for NR50 Flat sample (i.e. 77.7±4.4° when compared to 117 Flat, i.e. 64.7±2.9°) may be attributed to changes in the spatial organization of the Nafion nanoaggregates. From the experimental SCA (θ) values reported in Figure 3.9, it is clearly noticeable the change in wettability of the patterned membranes when compared to the flat counterparts of the same Nafion type. For hydrophobic NR50 based membranes, the patterning on the surface induce larger contact angle. In contrast, a larger wetting tendency (lower SCA values) is observed with patterning on the hydrophilic 117 based membranes.

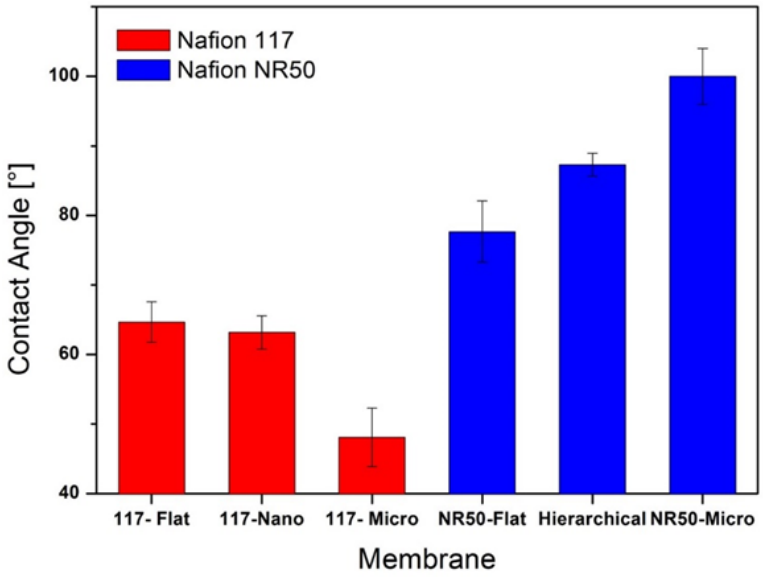

Figure 3.9: Comparison of SCA values for all the Nafion® based membranes studied in this work.

To gain insight the wetting behaviour of the protein solution during crystallization process, the apparent SCA values assuming either homogeneous, i.e. Wenzel equation A.8, or heterogeneous, i.e. Cassie Baxter equation 3.2, equilibrium wetting conditions [42], were also calculated:

$$\tau cos\theta_Y = cos\theta \tag{3.1}$$

Where τ represents the ratio between the actual surface area and the projected surface area and θ_Y represents the ideal Young contact angle (contact angle for 117 flat or NR50 flat samples).

$$cos\theta = f_{solid} cos\theta_Y - f_{air} \tag{3.2}$$

Where f_{solid} is the fraction area of the top surface of the membrane, θ_Y is the ideal Young contact angle and f_{air} is the fraction area of the wells. These values, assuming the topological information provided by SEM images, are comparatively shown with the experimental results in Table 3.2.

Table 3.2: Wettability of the Nafion® based membranes studied in this work.

Type of Membrane	**Ra (nm)**	**Experimental SCA (°)**	**Apparent SCA (Wenzel)**	**Apparent SCA (Cassie-Baxter)**	**CCA (θ_c)**
117-Flat	1.0±0.2	64.7±2.9	n.a.	n.a.	n.a.
117-Nano	14.9±4.9	63.2±2.4	54	80	109
117-Micro	4.0±0.4	48.1±4.2	42	80	101
NR50-Flat	n.a.	77.7±4.4	n.a.	n.a.	n.a.
NR50-Micro	2.8±0.4	100±4	69	90	101
Hierarchical	n.a.	±1.6	70	75	102

It is worthy to mention that the nanoscopic roughness values, Ra, evaluated by AFM and shown in Table 3.1 are not herein considered. In general, the experimental SCA results of patterned 117 membranes are well predicted by the homogeneous Wenzel model. Instead, in the case of the NR50 set, the experimental results are closer to the heterogeneous Cassie-Baxter theory, characteristic of composite solid-air surfaces with heterogeneous wetting, i.e. the drop lying on the top of the patterned surface. In addition, the critical contact angle CCA (θ_c) was calculated as follows:

$$cos\theta_c = -\frac{1 - f_{solid}}{\tau - f_{solid}} \tag{3.3}$$

When $_Y < \theta_c$ the Wenzel state is energetically more favourable; however, a metastable Cassie-Baxter state could still be possible [43]. Based on the CCA calculations, all the Nafion membranes studied in this work fulfilled the Wenzel state condition: $_Y < \theta_c$;

although NR50 set experimentally behaves closer to the heterogeneous Cassie-Baxter model. We attribute this observation to the use of a PDMS mold in the REM (NR50 Micro) or MT (Hierarchical) processes. Owing to the two distinct moieties of the Nafion ionomer: the hydrophobic backbone and hydrophilic sulfonic group; interaction of Nafion with highly hydrophobic PDMS surfaces is possible. Thus, the Nafion nanoaggregates could orientate at the interface in contact with the elastomeric mold to facilitate the interaction between the hydrophobic backbone of the ionomer and the hydrophobic PDMS mold (SCA = 125°±0.6); meanwhile the sulfonic groups would be pointing away from the interfacial layer. In our opinion, such interfacial interaction provokes the modification of the fine structure of Nafion in close vicinity to the replicated features, i.e. altering the distribution of water-filled ionic domains and influences its surface tension properties and wetting regime. On the contrary, the micro and nano hard molds used for the imprinting of Nafion® 117 membranes were hydrophilic.

3.4.3 Impact of surface patterning on protein crystallization

The patterned Nafion® membranes, both 117 and NR50 types, were tested for the crystallization of Trypsin from Bovine Pancreas. The crystallization and precipitant solutions were mixed on the top of the nucleant membranes (0.7 cm x 0.7 cm) and left equilibrating with the stripping solution in a closed system. The experiments were performed in adapted crystallization well plates and followed over time by optical microscopy. Results of nucleation and growth rate are reported in Figure 3.10 and Figure 3.11, respectively. From those data, crystallization parameters such as induction time, nucleation and growth rate were calculated (see Table 3.3). The induction time was extrapolated from the intersection point of the curves in Figure 3.10 with the axis of time, whereas nucleation and growth rate values, were calculated as the first derivative at the time axis intersection of the curves of Figure 3.10 and Figure 3.11, respectively.

In general, all the patterned Nafion® membranes demonstrate an increase in nucleation rate and crystal growth when compared to control sample. When the area of interaction between the solution and substrate is increased, the number of potential nucleation sites available for the same volume of solution increases; and thus, the possibility for successful nucleation. In fact, the probability for a molecule to enter a narrow space (up to 1000 nm) is the same as on a flat surface, however, due to the Brownian motion in

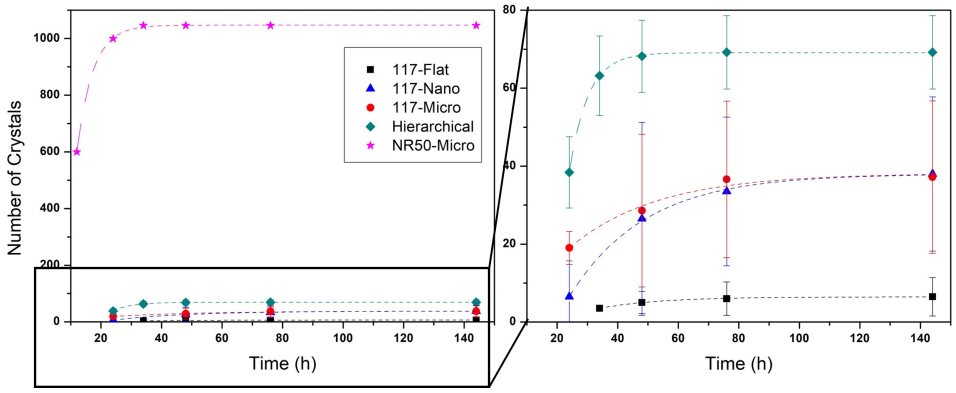

Figure 3.10: Number of crystals observed versus time for the nucleant membranes studied in this work. On the left side it is shown the evolution of the number of crystals as a function of time for all the patterned membranes. On the right side a magnification of the down area of the graph is displayed.

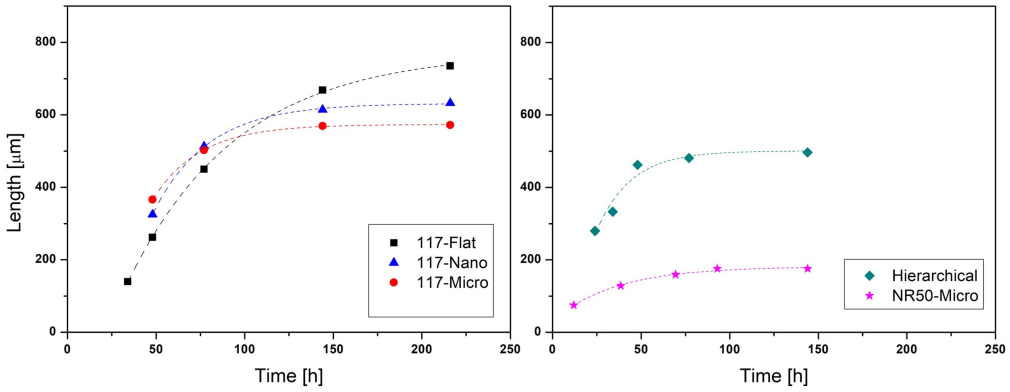

Figure 3.11: Length of crystals observed versus time for the nucleant membranes studied in this work.

all directions, escaping from a narrow space may result much more difficult determining physical entrapment and local accumulation. When this event occurs over time, the concentration of molecules inside the well increases, determining nucleation in the pores and formation of extra nucleation sites (see Figure 3.12) [44].

On the contrary, when looking at the induction time in Table 3.3, there is not a clear apparent correlation with membrane topography It is well reported that not only the surface topography, but also the amount of interactive sites and the enhanced adhesion of the protein solution affect the nucleation phenomena to different extent. In fact, 117 Nano does not show any improvement on induction time compared to 117 Flat, i.e. 19.28 h vs. 18.17 h; whereas 117 Micro displays a significant lower value, i.e. 4.01 h. This observation could be explained by the interfacial surface properties, as the micro-features have a significant effect on the SCA values. For both membranes, i.e. 117 Nano and 117 Micro,

Table 3.3: Estimated values of induction time, nucleation rate and growth rate for the different membranes

Membrane	Ra(nm)	Experimental SCA (°)	**Induction Time (h)**	**Nucleation rate (nuclei/h)**	**Growth rate (μm/h)**
117-Flat	1.0±0.2	64.7±2.9	18.17	0.32±0.04	12.27±0.43
117-Nano	14.9±4.9	63±2.4	19.28	1.51±0.20	20.38±1.24
117-Micro	4.01	4.0±0.4	48±4.2	1.31±0.61	21.38±0.79
NR50-Micro	7.51	2.8±0.4	100±4	198.52±7.96	12.95±0.43
Hierarchical	4.52	87±4.6	19.04	11.30±0.39	25.85±13.90

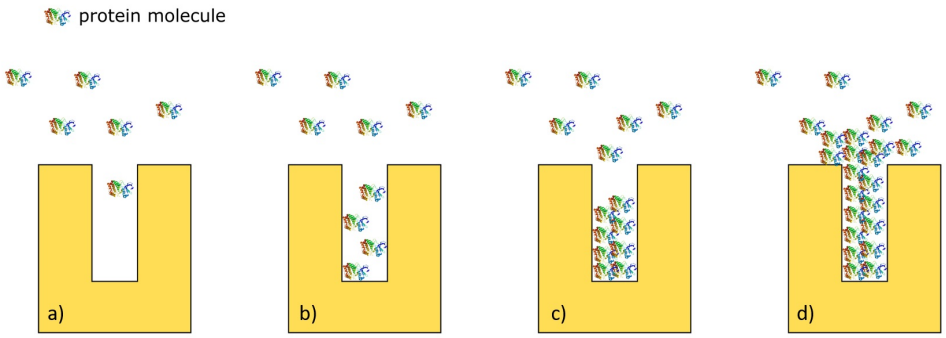

Figure 3.12: Proposed nucleation mechanism in a narrow cavity: a) the probability of a protein molecule of entering in a narrow cavity is the same as on the top of the surface; b) the narrow cavity determines entrapment of the protein molecules that will consequently accumulate over time; c) the increased concentration inside the pore promotes nucleation; d) the top surface of a cavity filled with a nucleus becomes a nucleation point for crystal growth outside the pore.

an increase in the nucleation sites number occurs. However, while in the case of 117 Micro this occurs immediately, due to the spreading of the solution (SCA=48±4.2°) on the nucleant surface and the higher ratio between actual and projected area, in the case of 117 Nano some time is required for accumulation of protein molecules inside the nanowells. Regarding the NR50 Micro membrane, even though the microstructure is the same as the 117 Micro, the two membranes lead to completely different outputs. Indeed, even though the induction time is comparable, i.e. 7.51 h; the nucleation rate and final the number of crystals are the highest among the tested: 198.52±7.96 nuclei/h and 1046±100 crystals per NR50 Micro membrane unit, respectively. Protein adhesion due to the presence of the micro-features is enhanced by the distinctive hydrophobic character of the NR50 surface (SCA=100±4°), motility of the molecules might be reduced and a high number of nuclei

rapidly formed. Due to the formation of this high number of nuclei in a short time, a lower amount of protein is available in the solution determining a slower growth rate compared to the hydrophilic membranes. Finally, the hierarchical membrane (which is a hybrid membrane of NR50-Micro and 117-Nano) has an intermediate behaviour between the 117 Nano and the NR50 Micro membranes.

3.4.4 Modelling the Gibbs free energy of heterogeneous nucleation for the membranes with designed patterns

In order to discuss the effect of surface properties from the point of view of classical nucleation theory, an adaptation of the model developed by Liu et. al [18] including the effect of tailored surface topography in the evaluation of the ratio of heterogeneous to homogeneous nucleation has been developed. Theoretical calculations resulted from this model were compared with experimental results.

The free energy variation for heterogeneous nucleation (ΔG_{Het}) is defined as [45]:

$$\Delta G_{Het} = \phi \Delta G_{Hom} \tag{3.4}$$

Where ϕ is the ratio of Gibbs free energy variation of heterogeneous to homogeneous nucleation and ΔG_{Hom} is the Gibbs' free energy variation for homogeneous nucleation. According to literature [18], for an ideally flat surface (without any patterning), ϕ is defined as:

$$\phi = \frac{(2 - 3cos\theta_Y + 3cos\theta_Y)^3}{4} \tag{3.5}$$

Therefore, the main parameter affecting heterogeneous nucleation is the Young's contact angle θ_Y between the forming nucleus (assumed to be spherical) and the substrate that defines the area of interaction between the nucleus and the surface. In fact, surfaces with lower contact angles lead to lower values of ϕ (ratio of Gibbs free energy variation of heterogeneous to homogeneous nucleation) according to Equation 3.5. In order to include the effect of surface topography in the calculations, Liu et al. [18] developed a model for calculating the ratio of Gibbs free energy variation of heterogeneous to homogeneous nucleation for a rough surface, assuming the surface to be composed by uniform cones and a Wenzel's wetting state.

In this work the model developed by Liu et. al was adapted to the geometry of the topography of the patterned membranes and theoretical values correlated with experimental results. On the top of the substrate, a nucleus with a hypothetical round shape of radius R contacting the substrate with an apparent contact angle θ is considered (Figure 3.13). Details on the derivation of the equations are reported in the Appendix A.

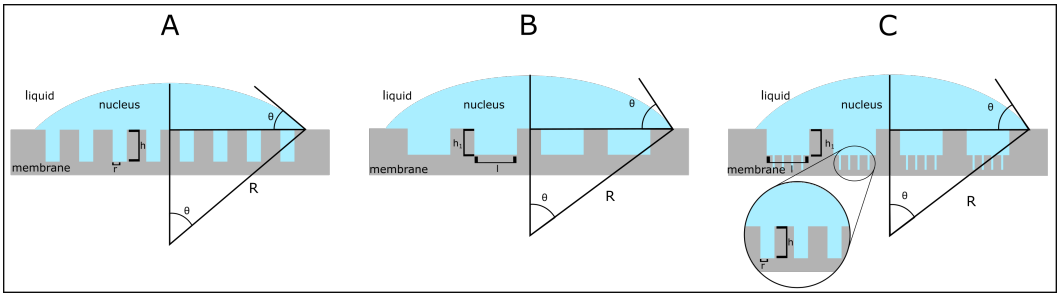

Figure 3.13: Diagram of the geometry parameters of a surface with cylindrical wells

For the 117-Nano membrane the equation used was the following

$$\phi_{117-Nano} = \frac{\Delta G_{het117-Nano}}{\Delta G_{Hom}} = \frac{1}{4}\frac{[2(1-cos\theta)-cos\theta sin^2\theta]^3}{[(1-cos\theta)^2(2+cos\theta)+3n\alpha^2\beta]^2} \tag{3.6}$$

Where $\alpha = r/R$, $\beta = h/R$, r is the radius of the wells, n is the number of wells under the drop area, θ is the apparent contact angle of the protein solution with the surface (Figure 3.13 A).

In the case of 117-Micro and NR50-Micro the same model (replacing the geometric parameters of a cylinder with the ones of a triangular prism) was applied, for a Wenzel surface, resulting in the following equation:

$$\phi_{Micro} = \frac{1}{4}\frac{\pi^2[2(1-cos\theta)-cos\theta sin^2\theta]^3}{[\pi(1-cos\theta)^2(2+cos\theta)+\frac{3}{2}\sqrt{3}n_1\alpha_1^2\beta_1]^2} \tag{3.7}$$

Where $\alpha_1 = l/R$, $\beta_1 = h_1/R$, l is the side of the triangle base of the prisma well, h_1 is the depth, n_1 is the number of wells under the nucleus area θ is the apparent contact angle of nucleus with the surface (Figure 3.13 B).

For the Hierarchical membrane (Triangular prism wells with cylindrical wells inside), both geometries of the cylinder and prisma were included in the model, resulting:

$$\phi_{Hierarchical} = \frac{1}{4}\frac{\pi^2[2(1-cos\theta)-cos\theta sin^2\theta]^2}{[\pi(1-cos\theta)^2](2+cos\theta)+\frac{3}{2}\sqrt{3}n_1\alpha_1^2\beta_1+3n\alpha^2\beta]^2} \tag{3.8}$$

Where $\alpha = r/R$, $\beta = h/R$ $\alpha_1 = l/R$, $\beta_1 = h_1/R$, r is the radius of the nanowells, h is their depth, l is the side of the triangle base of the prisma wells and h_1 is their depth, n is the

number of nanowells inside a microwell, n_1 is the number of wells under the nucleus area, θ is the apparent contact angle of the nucleus with the surface(Figure 3.13 C).

Accordingly, the ratio of the Gibbs free energy of heterogeneous nucleation to homogeneous nucleation, ϕ, has been calculated from Equations 3.5, 3.6, 3.7, 3.8 for each membrane (see Table 3.4).

Table 3.4: Ratio of the Gibbs free energy variation of heterogeneous nucleation to homogeneous nucleation

Membrane	ϕ
117-Flat	0.19
117-Nano	0.18
117-Micro	0.07
NR50-Micro	0.52
Hierarchical	0.45

It is worthy to mention that the nanoscopic roughness values, Ra, evaluated by AFM and shown in Table 1 are not accounted for the model. As expected, the Gibbs free energy of nucleation is always reduced in presence of Nafion type nucleant surface. In addition, 117 Nafion® type membranes induce the highest reduction in ϕ. This decrease is much higher for the 117 Micro compared to 117 Nano in agreement with heterogeneous nucleation theory: surfaces with lower contact angles, hence with high degree of hydrophilicity, favour nucleation of proteins [11, 18]. Indeed, a lower contact angle means a wider spreading of the solution on the top of the surface increasing the contact area for the same volume of solution, and thus the local concentration of solute molecules, lowering the energy barrier for nucleation. The higher value of Gibbs free energy for heterogenous nucleation for NR50 and Hierarchical membrane compared to 117 membrane set can be attributed to their hydrophobic character. Indeed, according to Liu model, the hydrophobic character increases the energy barrier for nucleation due to a lesser area of interaction between the crystallization solution and the surface. This seems to be the case when comparing ϕ for 117 Micro and NR50 Micro samples (0.07 vs. 0.52), which have exactly the same geometry, although with different interfacial properties. When comparing kinetics, a significantly higher number of nuclei per unit time is obtained for NR50 Micro than for 117-Micro: 198.52±7.96 vs. 1.31±0.61. Furthermore, the number of crystals recorded at equilibrium conditions is also superior, although lower in size, for

NR50 Micro nucleant membrane: 175±103 vs. 571±126. We attribute this behaviour to the more predominant role of the surface chemistry and interfacial interactions. Due to ionomeric nature of Nafion and the different fabrication conditions (temperature, solvent, mold nature), 117 and NR50 membranes show different polymer chains organization that leads to different surface properties. In the NR50 membrane the hydrophilic groups are buried inside, enhancing the hydrophobic character of the surface which promotes stronger protein-surface interactions, less motility and consequently higher nucleation rate. Above all, the model developed by Liu et al. does not consider the contribution of interfacial interactions to the Gibbs free energy heterogeneous nucleation. Furthermore, it is based on the simplified assumption that the liquid phase is following the homogeneous Wenzel regime for all the contacting surface and, as previously discussed, metastable Cassie-Baxter state may occur in the case of NR50 membranes.

3.4.5 Guidelines for designing membrane topographies for improved nucleation and crystallization

Nucleation is a probability event, hence different conditions lead to different chances of obtaining crystals. Enhancing the probability for this phenomenon to occur is extremely important for increasing the possibility of obtaining well-diffracting crystals, especially in the case of protein molecules difficult to nucleate. Designing of specific surface topography membranes demonstrated to have an impact on the crystallization process. However, predicting which type of surface topography may promote a more effective nucleation is not obvious and simple. Taking into account the results of this work, we would like to draw guidelines for designing surfaces suitable for nucleation and crystallization of proteins:

- Small features, in the nano size range, lead to higher nucleation due to the creation of extra nucleation sites by physical entrapment. Hence, they might be particularly useful for implementing nucleation on membranes whose surface properties do not favour nucleation.

- Micro-scale features on highly hydrophilic surfaces induce an increase in the wettability and consequently in the surface/volume ratio enhancing the effect of the chemistry of the material. Hence, they can be useful to improve the crystallization output on membranes with surface properties that favour the nucleation process.

- Micro-scale features on hydrophobic surfaces induce a further decrease in the wettability and may lead to higher protein-surface interactions with a much stronger effect on nucleation compared to hydrophilic surfaces carrying the same features.

Hence, depending on the chemistry of the surface and the effect of this surface on nucleation it is possible to decide the best strategy for introducing small or large features, or both, in order to control the number of nuclei and the size of the crystals. Theoretical calculations based on the model developed by Liu et al. help in predicting the effect of a defined geometry on nucleation rate, however, this model presents some obvious limitations. The model relies on the Wenzel equation and the surface/volume ratio (described by the contact angle) is considered the main controlling factor for protein nucleation on the membrane surface. This applies only for hydrophilic surfaces with a high Γ (ratio between actual and projected area). In the case of small surface features, which do not have a strong effect on the contact angle, or more hydrophobic surfaces where the solution does not follow the Wenzel behaviour, other phenomena such as physical entrapment and chemical interactions might occur playing a significant role, that are not taken into consideration by the Liu et al. model. Therefore, a different theoretical approach including the fluid dynamics of the protein solution contacting specific nano cavities and protein-surface interactions should be accounted for a model closer to reality and with a higher prediction capacity.

3.5 Conclusions

Controlling heterogeneous nucleation by surface topography can be regarded as a very effective way to handle the complex process of protein crystallization. So far, modifications of the surface topography were always associated with chemical modifications, making difficult a comparison with a flat surface. What emerged from previous investigations was that an incremented nucleation activity could be observed for surfaces with increased roughness. In this work, Nafion® membranes were processed with low cost and high-throughput soft lithographic techniques in order to create periodic surface topographies with different sizes (micro, nano and a combination of both) in an attempt to minimize the surface chemistry changes and to study in detail the specific effect of topography on the nucleation process. However, the ionomeric nature of Nafion, although

beneficial for fast transport of ions and water, has imposed several constraints when trying to preserve unaltered its interfacial properties whatever the membrane processing strategy used. The results obtained with Trypsin showed, as expected, an increased nucleation activity and crystal grow rate for all the patterned membranes. It was also shown that membranes with the same topography but prepared by following different routes might result in a different crystallization output. This fact is an indication that different nucleation mechanisms might occur, depending not only on the size of the topographical features but also on the surface properties of the membrane and on the contribution of interfacial interactions. All the patterned Nafion® based membranes obey an asymptotic tendency when analysing the dimensions and size of the collected Trypsin crystals: the higher number of crystals the lower in size. Thus, the production of macroscopic Trypsin crystals with tuneable size distribution would be feasible by a proper selection of the nucleant membrane topography. Some obvious limitations arise when the experimental crystallization results were analysed in view of the ratio of the Gibbs free energy variation of heterogeneous nucleation to homogeneous nucleation (ϕ) predicted from the Liu model. Additional phenomena, such as the local accumulation of protein molecules in a restricted space and protein-surface interactions at the interface are playing a key role on heterogeneous nucleation and growth.

References

[1] J. A. Gavira. "Current trends in protein crystallization." In: *Archives of Biochemistry and Biophysics* 602 (2016), pp. 3–11. DOI: 10.1016/j.abb.2015.12.010.

[2] R. Giegé. "A historical perspective on protein crystallization from 1840 to the present day." In: *FEBS Journal* 280.24 (2013), pp. 6456–6497. DOI: 10.1111/febs.12580.

[3] J. M. Garcia. "Nucleation of protein crystals." In: 142 (2003), pp. 22–31. DOI: 10.1016/S1047-8477(03)00035-2.

[4] P. G. Vekilov. "Nucleation of protein crystals." In: *Progress in Crystal Growth and Characterization of Materials* 62.2 (2016), pp. 136–154. DOI: 10.1016/J.PCRYSGROW.2016.04.007.

[5] R.-B. Zhou, H.-L. Cao, C.-Y. Zhang, and D.-C. Yin. "A review on recent advances for nucleants and nucleation in protein crystallization." In: *CrystEngComm* 19.8 (2017), pp. 1143–1155. DOI: 10.1039/C6CE02562E.

[6] A. Mcpherson and P. Shlichta. "Heterogeneous and Epitaxial Nucleation of Protein Crystals on Mineral Surfaces." In: *Science* 239 (1988), pp. 385–387. DOI: 10.1126/science.239.4838.385.

[7] A. Gugliuzza, C Aceto, and E. Drioli. "Interactive functional poly (vinylidene fluoride) membranes with modulated lysozyme affinity : a promising class of new interfaces for contactor crystallizers." In: *Polym Int* 58 (2009), pp. 1452–1464. DOI: 10.1002/pi.2681.

[8] C.-y. Zhang, H.-f. Shen, Q.-j. Wang, Y.-z. Guo, and J. He. "An Investigation of the Effects of Self-Assembled Monolayers on Protein Crystallisation." In: *International Journal of Molecular Sciences* 14 (2013), pp. 12329–12345. DOI: 10.3390/ijms140612329.

[9] D. S. Tsekova, D. R. Williams Nn, and J. Y. Y. Heng. "Effect of surface chemistry of novel templates on crystallization of proteins." In: *Chemical Engineering Science* 77 (2012), pp. 201–206. DOI: 10.1016/j.ces.2012.01.049.

[10] T. Pham, D. Lai, D. Ji, W. Tuntiwechapikul, J. M. Friedman, and T. R. Lee. "Well-ordered self-assembled monolayer surfaces can be used to enhance the growth of protein crystals." In: *Colloids and Surfaces B: Biointerfaces* 34.3 (2004), pp. 191–196. DOI: 10.1016/j.colsurfb.2004.01.003.

[11] E. Curcio, E. Fontananova, G. D. Profio, and E. Drioli. "Influence of the Structural Properties of Poly(vinylidene fluoride) Membranes on the Heterogeneous Nucleation Rate of Protein Crystals." In: *Journal of Physical Chemistry B* 4.1 (2006), pp. 12438–12445. DOI: 10.1021/jp061531y.

[12] U. V. Shah, D. R. Williams, and J. Y. Heng. "Selective crystallization of proteins using engineered nanonucleants." In: *Crystal Growth and Design* 12.3 (2012), pp. 1362–1369. DOI: 10.1021/cg201443s.

[13] U. V. Shah, M. C. Allenby, D. R. Williams, and J. Y. Y. Heng. "Crystallization of proteins at ultralow supersaturations using novel three-dimensional nanotemplates." In: *Crystal Growth and Design* 12.4 (2012), pp. 1772–1777. DOI: 10.1021/cg201190c.

[14] U. V. Shah, C. Amberg, Y. Diao, Z. Yang, and J. Y. Heng. "Heterogeneous nucleants for crystallogenesis and bioseparation." In: 8 (2015), pp. 69–75. DOI: 10.1016/j.coche.2015.03.002.

[15] U. V. Shah, N. H. Jahn, S. Huang, Z. Yang, D. R. Williams, and J. Y. Heng. "Crystallisation via novel 3D nanotemplates as a tool for protein purification and bioseparation." In: *Journal of Crystal Growth* 469 (2017), pp. 42–47. DOI: 10.1016/j.jcrysgro.2016.09.029.

[16] A. S. Ghatak and A. Ghatak. "Precipitantless Crystallization of Protein Molecules Induced by High Surface Potential." In: *Crystal Growth & Design* 16 (2016), pp. 5323–5329. DOI: 10.1021/acs.cgd.6b00833.

[17] A. S. Ghatak, G. Rawal, and A. Ghatak. "Precipitant-Free Crystallization of Protein Molecules Induced by Incision on Substrate." In: *Crystals* 7.8 (2017), p. 245. DOI: 10.3390/cryst7080245.

[18] Y. X. Liu, X. J. Wang, J. Lu, and C. B. Ching. "Influence of the roughness, topography, and physicochemical properties of chemically modified surfaces on the heterogeneous nucleation of protein crystals." In: *Journal of Physical Chemistry B* 111.50 (2007), pp. 13971–13978. DOI: 10.1021/jp0741612.

[19] W. De Poel, J. A. W. Mu, J. A.A. W. Elemans, W. J. P. Van Enckevort, A. E. Rowan, and E. Vlieg. "Surfaces with Controllable Topography and Chemistry Used as a Template for Protein Crystallization." In: *Crystal Growth & Design* 18 (2018), pp. 763–769. DOI: 10.1021/acs.cgd.7b01174.

[20] H. Hou, B. Wang, S.-Y. Hu, M.-Y. Wang, J. Feng, P.-P. Xie, and D.-C. Yin. "An investigation on the effect of surface roughness of crystallization plate on protein crystallization." In: *Journal of Crystal Growth* 468.October 2016 (2017), pp. 290–294. DOI: 10.1016/j.jcrysgro.2016.10.007.

[21] E. Chabanon, D. Mangin, and C. Charcosset. "Membranes and crystallization processes: State of the art and prospects." In: *Journal of Membrane Science* 509 (2016), pp. 57–67. DOI: 10.1016/j.memsci.2016.02.051.

[22] E. Drioli, G. D. Profio, E. Curcio, W. S. W. Ho, and K Li. "Progress in membrane crystallization." In: *Current Opinion in Chemical Engineering* 1 (2012), pp. 178–182. DOI: 10.1016/j.coche.2012.03.005.

[23] X. Zhou, X. Zhu, B. Wang, J. Li, Q. Liu, X. Gao, K. K. Sirkar, and D. Chen. "Continuous production of drug nanocrystals by porous hollow fiber-based anti-solvent crystallization." In: *Journal of Membrane Science* 564 (2018), pp. 682–690. DOI: 10.1016/J.MEMSCI.2018.07.082.

[24] D. L. Chen, C. J. Gerdts, and R. F. Ismagilov. "Using Microfluidics to Observe the Effect of Mixing on Nucleation of Protein Crystals." In: *Journal of the American Chemical Society* 127 (2018), pp. 9672–9673. DOI: 10.1021/ja052279v.

[25] J. Motuzas, C. Yacou, R. S. Madsen, W. Fu, D. K. Wang, A. Julbe, J. Vaughan, and J. C. Diniz da Costa. "Novel inorganic membrane for the percrystallization of mineral, food and pharmaceutical compounds." In: *Journal of Membrane Science* 550 (2018), pp. 407–415. DOI: 10.1016/j.memsci.2017.12.077.

[26] G. D. Profio, M. Polino, F. P. Nicoletta, B. D. Belviso, R. Caliandro, E. Fontananova, G. De Filpo, E. Curcio, and E. Drioli. "Tailored hydrogel membranes for efficient protein crystallization." In: *Advanced Functional Materials* 24.11 (2014), pp. 1582–1590. DOI: 10.1002/adfm.201302240.

[27] S. M. Salehi, A. C. Manjua, B. D. Belviso, C. A. M. Portugal, I. M. Coelhoso, V. Mirabelli, E. Fontananova, R. Caliandro, Joa, G Crespo, E. Curcio, and G. D. Profio. "Hydrogel Composite Membranes Incorporating Iron Oxide Nanoparticles as Topographical Designers for Controlled Heteronucleation of Proteins." In: *Crystal Growth & Design* 18.6 (2018), pp. 3317–3327. DOI: 10.1021/acs.cgd.7b01760.

[28] D. Qin, Y. Xia, and G. M. Whitesides. "Soft lithography for micro- and nanoscale patterning." In: *Nature Protocols* 5.3 (2010), pp. 491–502. DOI: 10.1038/nprot.2009.234.

[29] T. Glinsner and G. Kreindl. "Nanoimprint Lithography." In: *Lithography* 24 (2010), pp. 495–516.

[30] A. Fernandez, J. Medina, C. Benkel, M. Guttmann, B. Bilenberg, L. H. Thamdrup, T. Nielsen, C. M. Sotomayor Torres, and N. Kehagias. "Residual layer-free Reverse Nanoimprint Lithography on silicon and metal-coated substrates." In: *Microelectronic Engineering* 141 (2015), pp. 56–61. DOI: 10.1016/j.mee.2014.11.025.

[31] B. Radha, S. H. Lim, M. S. M. Saifullah, and G. U. Kulkarni. "Metal hierarchical patterning by direct nanoimprint lithography." In: *Scientific Reports* 3.1 (2013), p. 1078. DOI: 10.1038/srep01078.

[32] M. Polino, A. Luísa Carvalho, L. Juknaite, C. A. M Portugal, I. M. Coelhoso, M. J. Romao, and J. G. Crespo. "Ion-Exchange Membranes for Stable Derivatization of Protein Crystals." In: *Crystal Growth & Design* 17 (2017), pp. 4563–4572. DOI: 10.1021/acs.cgd.7b00315.

[33] C.-H. Ma, T. L. Yu, H.-L. Lin, Y.-T. Huang, Y.-L. Chen, U.-S. Jeng, Y.-H. Lai, and Y.-S. Sun. "Morphology and properties of Nafion membranes prepared by solution casting." In: *Polymer* 50 (2009), pp. 1764–1777. DOI: 10.1016/j.polymer.2009.01.060.

[34] H. Le-the, E. Berenschot, R. M. Tiggelaar, N. R. Tas, A. V. D. Berg, and J. C. T. Eijkel. "Shrinkage Control of Photoresist for Large-Area Fabrication of Sub-30 nm Periodic Nanocolumns." In: *Advanced Materials Technologies* (2017). DOI: 10.1002/admt.201600238.

[35] A. Pimpin and W. Srituravanich. "Review on Micro- and Nanolithography Techniques and their Applications." In: *Engineering Journal* 16.1 (2012), pp. 37–55. DOI: 10.4186/ej.2012.16.1.37.

[36] P. K. David Neˇ cas. "Gwyddion : an open-source software for SPM data analysis." In: *Central Euopean Journal of Physics* 10.1 (2012), pp. 181–188. DOI: 10.2478/s11534-011-0096-2.

[37] C. A. Schneider, W. S. Rasband, and K. W. Eliceiri. "NIH Image to ImageJ: 25 years of image analysis." In: *Nature Methods* 9.7 (2012), pp. 671–675. DOI: 10.1038/nmeth.2089.

[38] I. Khan, K. A. Kurnia, F. Mutelet, S. P. Pinho, and J. A. P. Coutinho. "Probing the interactions between ionic liquids and water: Experimental and quantum chemical approach." In: 118.7 (2014), pp. 1848–1860. DOI: 10.1021/jp4113552.

[39] H.-y. Jung and J. Won. "Role of the glass transition temperature of Nafion 117 membrane in the preparation of the membrane electrode assembly in a direct methanol fuel cell (DMFC)." In: *International Journal of Hydrogen Energy* 37.17 (2012), pp. 12580–12585. DOI: 10.1016/j.ijhydene.2012.05.121.

[40] S. H. de Almeida and Y. Kawano. "Thermal Behavior of Nafion Membrane." In: *Journal of Thermal Analysis and Calorimetry* 58 (1999), pp. 569–577. DOI: 10.1023/A:1010196226309.

[41] K. A. Mauritz and R. B. Moore. "State of Understanding of Nafion." In: *Chem. Rev.* 104 (2004), pp. 4535–4585. DOI: 10.1021/cr0207123.

[42] E. Celia, T. Darmanin, E. T. D. Givenchy, S. Amigoni, and F. Guittard. "Recent advances in designing superhydrophobic surfaces." In: *Journal of Colloid and Interface Science* 402 (2013), pp. 1–18. DOI: 10.1016/j.jcis.2013.03.041.

[43] P. Esa, R. Tiina, S. Mika, and A. P. Tapani. "Superhydrophobic Polyolefin Surfaces: Controlled Micro- and Nanostructures." In: *Langmuir* 23.13 (2007), pp. 7263–7268.

[44] C. N. Nanev, E. Saridakis, and N. E. Chayen. "Protein crystal nucleation in pores." In: *Scientific Reports* 7 (2017), pp. 35821–35829. DOI: 10.1038/srep35821.

[45] T. E. Paxton, A. Sambanis, and R. W. Rousseau. "Influence of vessel surfaces on the nucleation of protein crystals." In: *Langmuir* 17.10 (2001), pp. 3076–3079. DOI: 10.1021/la0015841.

Chapter 4

Ion-Exchange Membranes for Stable Derivatization of Protein Crystals

Published as: Mariella Polino, Ana Luısa Carvalho, Lina Juknaite, Carla A. M. Portugal, Isabel M. Coelhoso, Maria João Romão, and João G. Crespo, Ion-Exchange Membranes for Stable Derivatization of Protein Crystals, Cryst. Growth Des., 2017, 17 (9), pp 4563–4572*

4.1 Summary

Ion-exchange membranes were applied in this work to diffuse ions and heavy atoms inside protein crystals in order to gently perform their derivatization. The ion-exchange process rate for three different ions, bromide (Br^-), platinum (Pt^+ through $PtCl_4^{2-}$), and mercury (Hg^{2+}), was evaluated, allowing to determine the concentration of these ions in the crystal solution over time and to evaluate their effect on the crystals. Nafion® and Neosepta AXE01, cation and anion exchange-membranes, respectively, were used for transport of cations and anions to hen egg white lysozyme (HEWL) crystals, selected as model protein. X-ray diffraction analysis of the crystals confirmed the attainment of the derivatives and allowed the *ab initio* building of the bromide derivative model. Derivatization experiments were also conducted by the conventional method, directly soaking the crystals in the heavy atom solution. It was possible to conclude that the controlled diffusion, regulated by the membrane, increases the crystal's stability, avoiding handling procedures (*in-situ* derivatization) and maintaining a safer environment near

the crystals without disturbing the vapor diffusion equilibrium.

4.2 Introduction

Protein crystal derivatization is a modification process required by the multiple isomorphous replacement (MIR) method to solve the unknown structure of macromolecules using single crystal X-ray crystallography [1–4]. Protein crystal derivatization consists of introducing in the crystal heavy atoms like Pt and Hg [4, 5] or halide ions like Br^- and I^- [4, 6–8] without changing the packing of macromolecules in the space group of the native crystal (isomorphism)[9]. In order to diffuse those species into the protein crystals and keep the crystalline lattice isomorphous,[10] the native preformed crystals are soaked in a solution containing low concentrations of these compounds, so they can slowly diffuse into the solvent channels of the crystals [11, 12]. The main problem of this procedure is that the crystals are sensitive to environmental changes, and if they are directly brought in contact with a solution with a different composition from the growing buffer, the crystals very often crack and get damaged. For this reason, soaking has to be performed in several steps involving the use of several solutions with an increasing concentration of the halide or metal ion to be incorporated.

In this work, we propose the use of ion-exchange membranes to gently transport ions by diffusion within the protein drop, avoiding the problems of handling and environmental shock, and the several steps needed to perform this operation in a safer way for the crystals. The use of membranes has been reported in the literature to control supersaturation [13], heterogeneous nucleation rate [13–18], and the formation of polymorphs[19, 20]. However, membranes have not been used before to derivatize protein crystals. Even though ion-exchange membranes, to the best of our knowledge, have never been used to crystallize macromolecules (Nafion® [20] and chitosan [21] were used only for the crystallization of small molecules such as glycine or acetaminophen), they seem to have the ideal properties to achieve protein crystallization and derivatization. Ion-exchange membranes are semipermeable barriers, where fixed charged groups are attached to a hydrophobic backbone (usually made of polystyrene). The presence of charged groups will facilitate the transport of ions with opposite charge and reject those ones carrying the same charge as the groups attached to the membrane (Donnan exclusion)[22–26]. The hydrophobic backbone guarantees that the protein solution remains on the top of

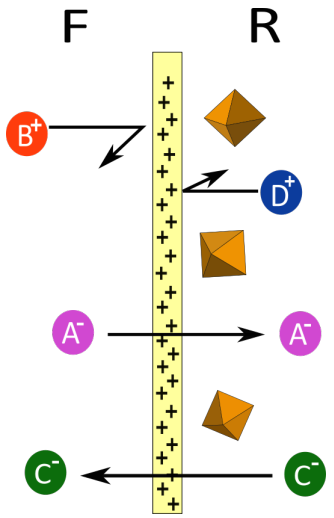

Figure 4.1: Anion exchange membrane to gently exchange the anion A^- in compartment F with the anion C^- in the protein drop. A^- is not initially present in compartment R, so it will diffuse, leading C^- to compartment F. The buffer has the same pH concentration in both compartments. Salt AB is at the same concentration of salt CD. F is the feeding compartment and R is the receiving compartment.

the membrane, and it is not completely adsorbed by the support. At the same time, the presence of charged groups allows the transport of ions across the membrane. In the case of protein crystallization, pH is a key factor with impact on molecule aggregation. Due to the diversity of chemical groups present in the protein amino acids, the total charge of the protein will change, as well as the distribution of charge within the protein molecules, which impacts on the stability of the molecule itself [27]. This determines if the protein molecules will be able to pack together in a well-ordered network (forming a crystal) or if they will just amorphously precipitate when the concentration increases[28–30]. Once the crystals are formed, in order to avoid damages or dissolutions, pH, osmotic pressure, and temperature[31] must be kept stable. Taking into account these considerations, the membrane system for crystal derivatization was designed to prevent the transport of small ions (H^+ and OH^- that could even slightly change the pH) and the leak of water due to a difference in osmotic pressure from the crystal derivatization compartment [32–34]. Figure 4.1 shows the system configuration with an anion exchange membrane separating two compartments. The receiving compartment (**R**) is the crystal growth environment, containing the buffer at a defined pH, the precipitant, and the protein. The feed compartment (**F**), instead, contains a solution of the same composition in terms of buffer type, concentration, and pH, and the same total molar concentration as compartment **R**, just replacing a precise amount of precipitant salt with the salt intended to be used for

derivatization. In this way, the "derivatization" anion of compartment **F** will diffuse into compartment R driving the anion in compartment **R** to compartment **F**. Since the pH is the same in both compartments, there will not be any leakage of H^+ OH^- ions, and since the osmotic pressure is also the same (the contribution of the protein and crystals is negligible), no osmosis will occur and osmotic shock will be prevented. The process is expected to be completely controlled because the only driving force is the difference in species concentration across the membrane. The ionic diffusive transport is what is needed to give the crystals time to adapt to the different ions. Therefore, it is possible to take advantage of the transport properties of ion-exchange membranes to improve the process of derivatization of protein crystals. This concept was implemented for crystals of hen egg white lysozyme (HEWL), as model protein, and using bromide (Br^-), platinum (Pt through $PtCl_4^{2-}$, and mercury (Hg^{2+})as derivatization agents. Conventional crystallization conditions [35–37] were used to obtain HEWL crystals on the top of an anion and a cation exchange membrane. The use of an anion or cation exchange membrane for the derivatization process depends on the charge of the ions used. Therefore, a cation exchange membrane was used for crystal derivatization, when Hg^{2+} was present in the feed solution, and an anion exchange membrane was used for crystal derivatization with $PtCl_4^{2-}$ and Br^-. The kinetics of diffusion of each ion across the membrane may be previously calculated in order to estimate the time of diffusion into the protein solution and predict when the ion-exchange process will be completed. The advantage of crystal derivatization by the ion-exchange process is here evaluated by comparing the quality of the derivatized protein crystals to the ones obtained by conventional soaking, using X-ray diffraction analysis. In a preliminary analysis, indexing of diffraction intensities was sufficient to confirm that crystal isomorphism was maintained. In a more detailed analysis, by collecting complete diffraction data at the appropriate X-ray absorption wavelength, it was also possible to identify the heavy atoms in the calculated anomalous difference electron density maps. Furthermore, in the case of HEWL crystals derivatized with bromide, it was possible to achieve *ab-initio* structure solution by experimental Br-SAD phasing.

4.3 Materials and Methods

4.3.1 Materials

Hen egg white lysozyme (HEWL) purchased from Sigma-Aldrich was used for the crystallization experiments. The protein was solubilized in a 0.1 M $Na(CH_3COO)$ buffer (purchased from Scharlau), pH 4.6, and experiments were carried out with a protein concentration of 25 mg/mL. NaCl (purchased from Applichem Panreac) was added to the protein solution with a final concentration of 0.3 M and used as hypertonic solution to control relative humidity with a concentration of 0.6 M. For crystal derivatization, NaBr (purchased from Applichem Panreac) was solubilized in the protein buffer at a concentration of 0.6 M, while K_2PtCl_4 or $Hg(CH_3COO)_2$ was solubilized in 0.1 M $Na(CH_3COO)$ buffer, pH 4.6 at 5 mM and 10 mM, respectively, together with 0.6 M NaCl and used as solutions for the different derivatization procedures: conventional and within the ion-exchange membrane cell. The design of a membrane based system able to assist consecutive protein crystallization and derivatization processes requires the selection of membranes with ideal transport properties allowing for a suitable diffusion of the derivatizing ions while offering the surface chemistry and topography characteristics needed to promote nucleation. In this regard, it was important to screen several membranes in conventional vapor diffusion plates in order to select the ones allowing nucleation[14–18, 20, 38, 39]. Neosepta Axe 01 (purchased from Tokuyama Soda) and Nafion® (purchased from Sigma-Aldrich) allowed the attainment of crystals (12 hours) under conventional conditions of protein protein and precipitant concentration. Therefore, they were selected to support protein crystallization and derivatization processes. Neosepta Axe 01, an anion exchange membrane, was used to transport Br^- and $PtCl_4^{2-}$, while Nafion®, a cation exchange membrane, was used to diffuse Hg^{2+} to the protein crystals solution.

4.3.2 Contact Angle Measurements

The contact angles of Nafion® and Neosepta AXE01 were measured by the sessile drop method in a contact angle goniometer (CAM 100, KSV Instruments Ltd., Finland). The solution used for the measurement was 25 mg/mL HEWL and 0.3 M NaCl in 0.1 M $Na(CH_3COO)$, pH 4.6. Each measurement has been repeated five times

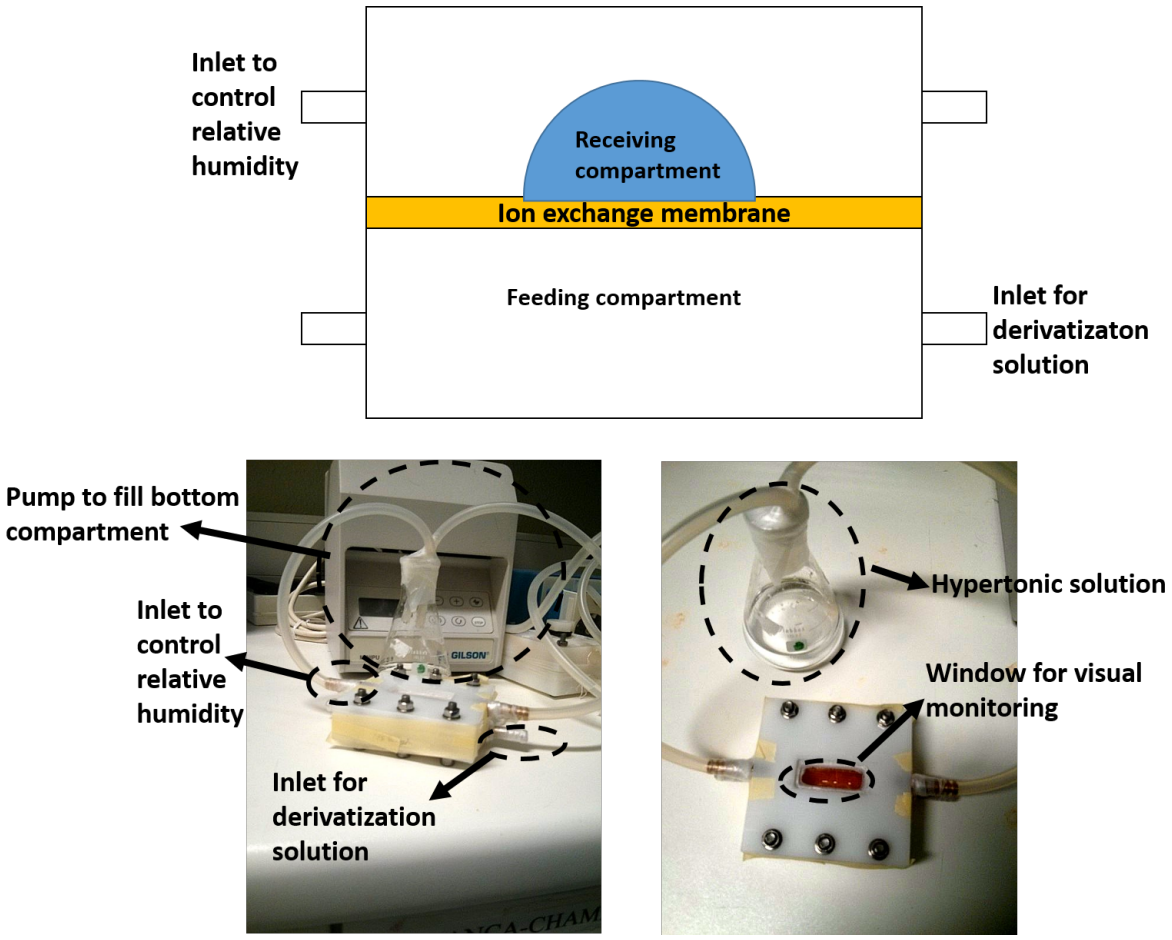

Figure 4.2: Schematic representation and picture of the cell. The feeding compartment is the compartment for heavy atom/halide solution. The receiving compartment is the protein solution. The cell was built by the company IrmaSolda. Details can be provided upon request to the author

4.3.3 Operating Procedure for Crystallization and Derivatization Processes in the Ion-Exchange Membrane Cell

The setup used for crystal derivatization is shown in Figure 4.2. Experiments of crystallization and crystal derivatization in the ionexchange membrane cell were performed using the membrane Neosepta Axe01 to derivatize HEWL crystals with Br^- and Pt^{2+} (through $PtCl_4^{2-}$) that diffuse as anions, and Nafion® to derivatize HEWL crystals with $Hg(CH_3COO)_2$ that diffuse as cations of Hg^{2+}.

In Figure 4.2, the membrane was placed in the middle of the cell, generating two compartments: an upper compartment (receiving compartment) for the protein solution connected to a hypertonic solution to control the air relative humidity and a bottom

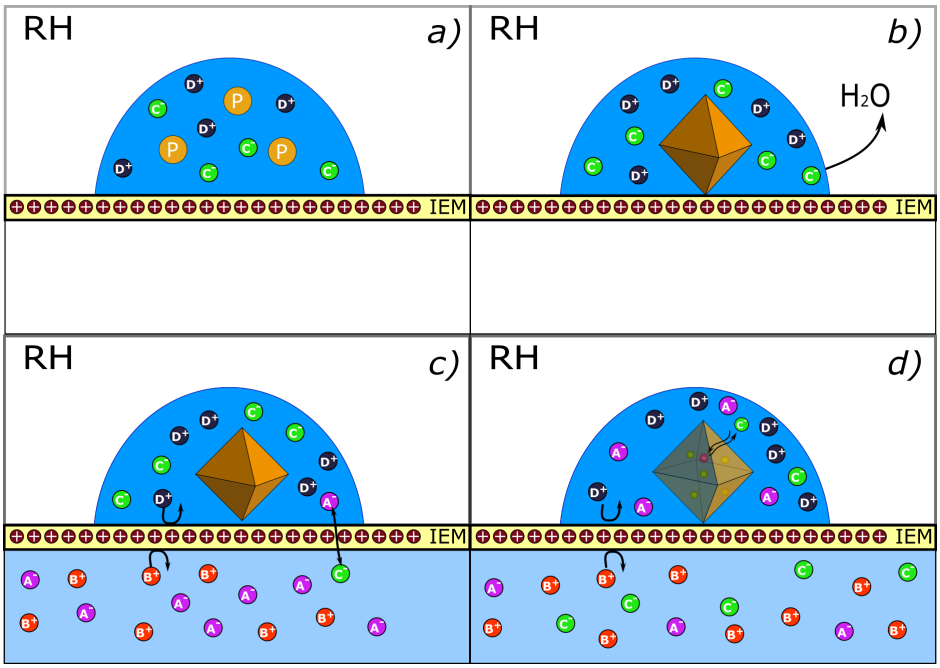

Figure 4.3: Experimental procedure for crystal growth and derivatization: (a) a drop of protein (P) solution and precipitant salt (D^+ and C^- represent the cation and anion of the salt used as precipitant, respectively) is placed onto the ion exchange membrane (IEM) in the cell in equilibrium with a hypertonic solution that controls relative humidity (RH) of the receiving compartment; (b) the solvent evaporates from the protein drop in order to reach equilibrium with the RH of the receiving compartment, supersaturation is generated, and crystals are formed; (c) heavy atom solution (A^- and B^+ represent the anion and cation of the salt used for derivatization, respectively) is brought in contact with the protein drop through the membrane; ion-exchange membranes are made of a hydrophobic backbone containing attached charged groups. The membrane selectivity for anions or cations is defined based on the charge of the groups attached to the backbone. Ions carrying opposite charge (counterions) to the membrane groups are allowed to pass through the membrane; meanwhile, ions carrying the same charge (co-ions) are rejected. In this case, the membrane with positively charged groups allows the transport of anions (A^- and C^-) and prevents the transport of cations (B^+ and D^+); (d) heavy atoms inside the protein drop diffuse inside the crystal's solvent channels.

compartment (feeding compartment) filled with a heavy atomhalide solution using a peristaltic pump (Minipulse, Gilson) (recirculation was not applied in these experiments). In the receiving compartment, 5 μL of protein solution was placed at the membrane surface and then mixed with the same volume of precipitant solution. The cell was sealed, and the relative humidity (RH) was allowed to reach the equilibrium by connecting the receiving compartment with the hypertonic solution (Figure 4.3a). Due to the difference in water activity between the protein and the reservoir solution, supersaturation was reached [28, 30]. The nucleation process was checked under the microscope until crystals appeared (Figure 4.3b). Only at this point the feeding compartment was filled with a solution containing the halide ion or the heavy atom (feeding solution) (Figure 4.3c) and left to equilibrate with the drop containing the protein solution (receiving solution) placed on the surface of the membrane at the receiving compartment (Figure 4.3d). The crystals were monitored everyday under the microscope to check the stability and presence of possible signs of cracking and or degradation. The experiments were conducted at 20 °C in a room with controlled temperature.

4.3.4 Conventional Soaking Experiments

To highlight the potential advantages of the membrane-assisted process, protein crystal derivatization was also carried out by conventional soaking procedures and compared to crystal derivatization using the ion-exchange membrane process. In this case, crystals were produced first in conventional hanging drop plates, and then harvested by a loop and soaked in 5 μL of solution containing 0.1 M Na(CH_3COO) pH 4.6, 0.6 M NaCl, and the same heavy atom concentration expected in the protein solution at the equilibrium [11] (0.6 M NaBr, 5 mM K_2PtCl_4, 10 mM $Hg(CH_3COO)_2$. These values were estimated based on the mass transfer coefficient measurements explained below. The stability of the crystals was monitored everyday under the microscope during 1 week.

4.3.5 Experimental Mass Transfer Coefficient Measurement for Heavy AtomsIons Transport

Measurements of mass transfer coefficients of heavy atoms were performed to estimate the rate of ion-transport in the system (from the feeding solution, through the membrane, to the protein drop). The variation of pH (parameter that can affect crystal stability) was also measured during the ion-exchange process. The measurements were performed

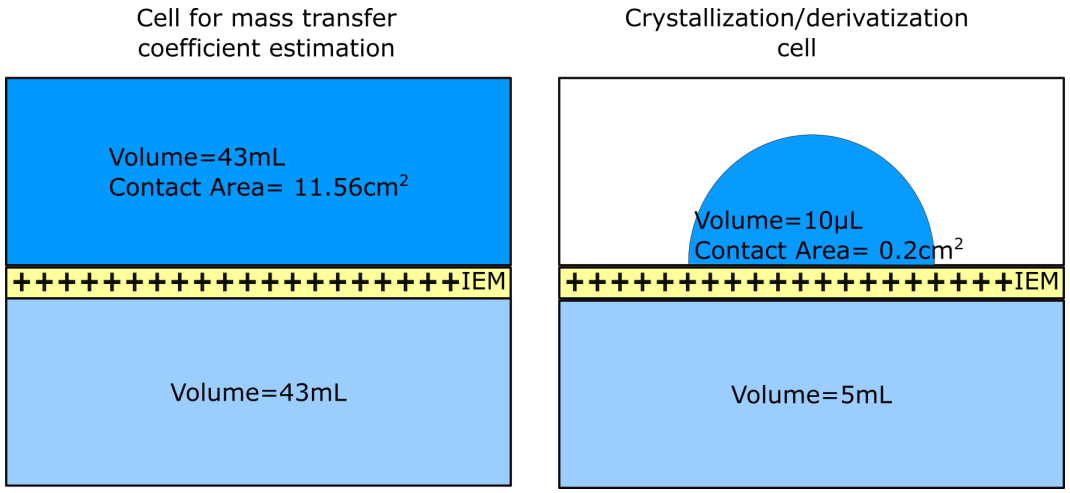

Figure 4.4: Scheme of the cells used to estimate the mass transfer coefficients and to run the crystallization and derivatization experiments. The geometry was flat in both cases, and none of the compartments was stirred. The temperature was the same in both cases.

using a diffusion cell with two compartments (feeding and stripping compartments) with equal volume of solutions [32] and the same geometry and hydrodynamic conditions (flat membrane surface and no stirring of the contacting solutions) as the cell used for derivatization (Figure 4.4). In order to determine the heavy atom and halide mass transfer coefficient under conditions as close as possible to the derivatization process, the compartments were filled with two solutions with equal pH and molar concentration, the feeding compartment containing the heavy atom halide to be diffused and the receiving compartment containing NaCl, both dissolved in the same buffer as the protein solution 0.1 M ($NaCH_3COO$, pH 4.6). The area of the membrane used was 11.56 cm^2, and the volume of each compartment was 43 mL (Figure 4.4). Aliquots (200 μL) were taken regularly from the solutions in the two compartments for 3 days. The values of pH and concentration of halidesmetal salts solutions were monitored using a pH-meter (CRISON BASIC 20 pH) and an Ionic Chromatograph-DIONEX, model ICS3000, for Br^-, and an ICP-AES (Inductively Coupled Plasma-Atomic Emission Spectrometer), Horiba JobinYvon, France, for Hg^{2+} and $PtCl_4^{2-}$. The molar concentration for all the species used for derivatization in both compartments was plotted against time (Figure 4.5).

4.3.6 X-ray Diffraction Analysis

HEWL crystals were equilibrated for a few seconds, first in harvesting buffer (0.1 M $NaCH_3COO$, pH 4.6, and 1 M NaCl) and then in cryo-protectant solution (harvesting

buffer and 30% (v/v) glycerol from Sigma-Aldrich). Preliminary X-ray Article set was collected from this crystal to 1.66 Å resolution at the Swiss Light Source (SLS, beamline X06DA PXIII) using radiation of 0.918 Å wavelength. Diffraction data from the mercury and platinum derivatives were collected at a fixed-wavelength beamline (0.966 Å, at which X-ray anomalous absorption effects for these heavy atoms can be measured) in the European Synchrotron Radiation Facility (ESRF, beamline ID30-A1). All synchrotron data were integrated with program MOSFLM [40] and scaled with AIMLESS [41] from the CCP4 suite. Substructure search, SAD (Single-wavelength Anomalous Dispersion) phasing, density modification, and model building were performed with program AutoSol implemented in Phenix [42]. Data collection, processing, and phasing statistics of the crystals derivatized through the ion-exchange membrane are presented in Table 5.1.

4.4 Results and Discussion

4.4.1 Contact Angle Measurement

The contact angle of the membranes used in this work was measured in order to ensure that the protein solution was stable on the membrane top over the experimental time. Contact angle is approximately 105 ± 14° for Nafion® and 66 ± 7° for Neosepta Axe, and thus, the membranes can be considered slightly hydrophobic and moderately hydrophilic, respectively. These values suggest that the protein drop is stable and that it is not absorbed by the membrane.

4.4.2 Kinetics of Ion-Transport

The mass transfer coefficients for the three ions (K_{Br}, K_{PtCl_4}, and K_{Hg}) were calculated fitting the data obtained from the transport studies (Figure 4.5) with the mass balance equations for each ion and integrating over time [32]. Since no electrical field is applied, the only driving force in the process is the concentration gradient across the membrane of the transported species; therefore, the variation of number of moles of a species can be written as follows:

$$-\frac{dn}{dt} = KA(C - C_{eq}) \tag{4.1}$$

where K is the mass transfer coefficient, A is the area of diffusion, C is the concentration at time t, and C_{eq} is the equilibrium concentration. Since the ion-exchange membranes prevent osmosis, the concentration of the two solutions is approximately the same, and the volumes (V) of the solutions in the two compartments are assumed to be constant when the variation of the concentration of species over time can be derived.

$$-V\frac{dC}{dt} = KA(C - C_{eq}) \tag{4.2}$$

By integrating equation 4.2, equation 4.3 was obtained and used to fit the experimental data. C_0 is the initial ion concentration.

$$C = C_{eq} + (C_0 - C_{eq})e^{-\frac{KA}{V}t} \tag{4.3}$$

Table 4.1: Mass transfer coefficient of the different ions used for derivatization

Ion	**Mass Transfer Coefficient** (m/s)	$\mathbf{R^2}$
Br^-	$1.8*10^{-6}$	0.99
$PtCl_4^{2-}$	$1.9*10^{-7}$	0.99
Hg^{2+}	$1.9*10^{-9}$	0.99

The estimation of ion transport in the derivatization cell was done using equation 4.3 considering the mass transfer coefficients (shown in Table 5.1) calculated from the fitting of ion-transport curves in the receiving compartment (where the ions are diffusing to and the concentration is increasing), area of the membrane in contact with the protein solution (0.2 cm^2) and the volume of the drop, approximated to the initial drop volume (10 μL). Due to the high difference in volume between the protein drop (10 μL) and the Br^- solution (5 mL), the concentration of the exchanging solution was considered constant and used as equilibrium concentration. The ion concentrations estimated over time (Figure 4.6) allow predicting the time needed for the transport process inside the protein drop to be completed, which was found to be 1 hour for Br^-,4 hours for $PtCl_4^{2-}$, and 25 hours for Hg^{2+}.

4.4.3 Stability of the Crystals over Time

The crystals derivatized by conventional soaking and through the ion- exchange membrane process were daily checked under the microscope to monitor possible signs of

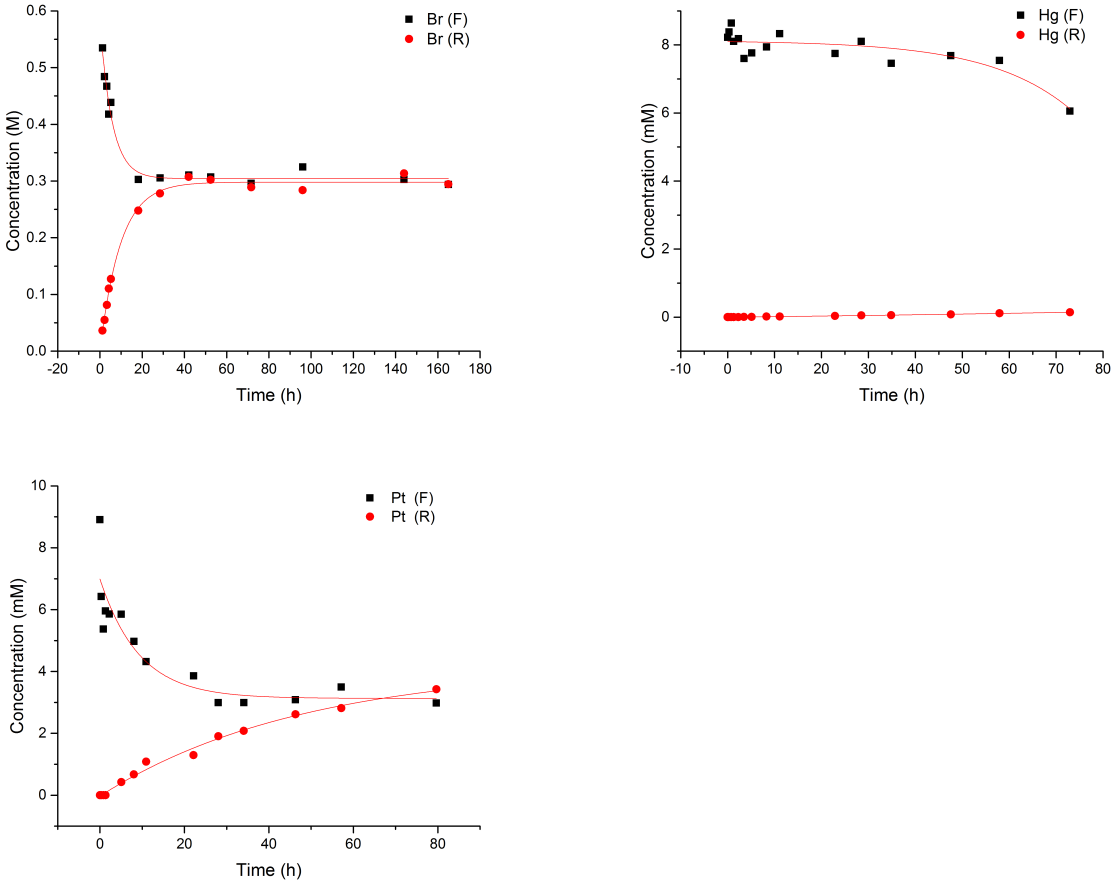

Figure 4.5: Experimental data for the calculation of the mass transfer coefficient for Br^-, $PtCl_4^{2-}$, and Hg^{2+} in the two compartments: **F** (feeding compartment) and **R** (receiving compartment)

cracking and degradation. In Figure 4.7, the morphology of the crystals derivatized with bromide in the cell (Figure 4.7a) was compared to that of the crystals derivatized by soaking (Figure 4.7b). The crystals derivatized in the cell were checked for one month, and their appearance was stable over time. In contrast, after 12 hours,the soaked crystals started showing some defects, and after 3 days, they were clearly degraded (4.7b). In the case of the crystals derivatized with Hg^{2+}, it is clear that when conventional soaking was used, already after 4 hours (Figure 4.8) they revealed signs of degradation. These crystals diffracted to very low resolution (below 10 Å) being useless for X-ray diffraction analysis. In contrast, crystals derivatized in the cell (Figure 4.9) were regularly monitored by visual inspection and were stable over time (114 hours). According to the diffusion studies (Figure 4.6), the concentration of Hg^{2+} in the protein drop placed at the membrane surface reached the concentration of the derivatization solution used for direct soaking

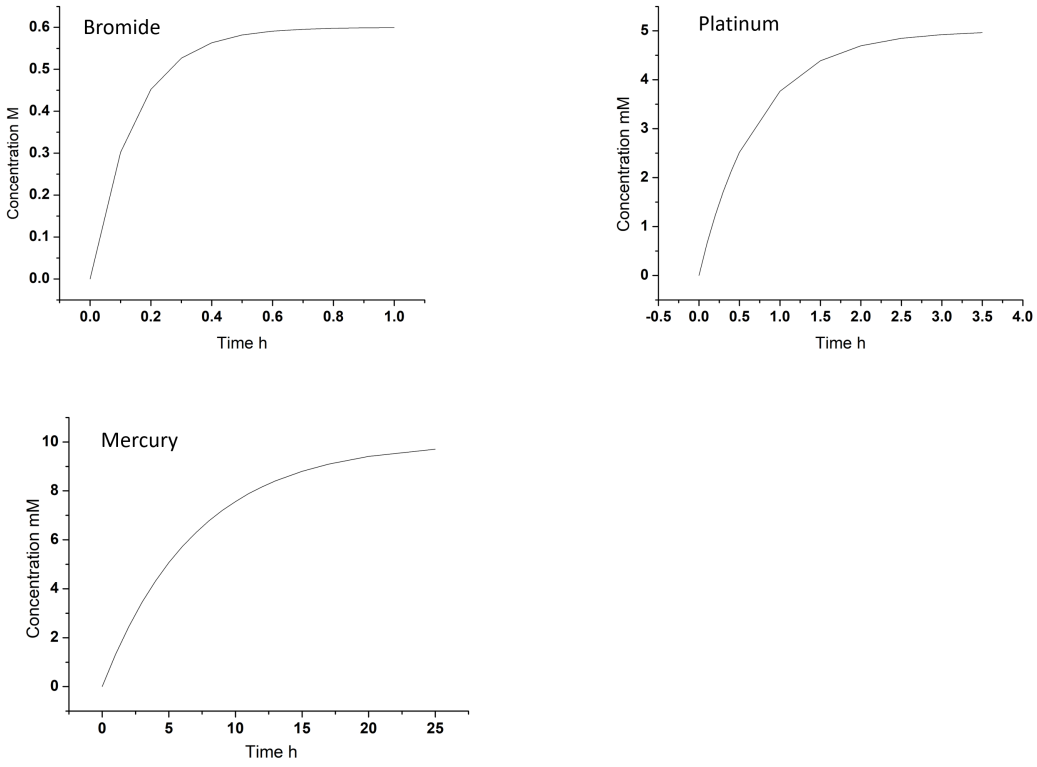

Figure 4.6: Concentration of heavy atoms to estimate time to reach equilibrium in the protein drop, based on the transport studies presented in Figure 4.5.

after 25 hours (Figure 4.6). Nevertheless, the crystals were monitored for about 5 days, a significantly long time after concentration equilibrium was reached inside the drop. The same occurred with the crystals derivatized with platinum (Figures 4.10 and 4.11). Furthermore, in this case, crystals (Figure 4.10) started degrading at the exact moment they were brought in contact with the soaking solution. The edges were degraded, and they did not diffract, as expected. This proves that the damages on the crystals during soaking are due to the abrupt change in the crystal environment [11], and this can be avoided by the gentle and controlled transport of ions by diffusion with ion-exchange membranes.

4.4.4 X-ray Diffraction and Structure Solution

Complete X-ray diffraction data were collected from a crystal derivatized with NaBr using the ion-exchange membrane. Crystals diffracted to 1.66 Å resolution using X-rays from a synchrotron source of 0.918 Å wavelength. This wavelength corresponded to the bromide absorption peak in the crystal, as indicated by the measured X-ray fluorescence scan (not

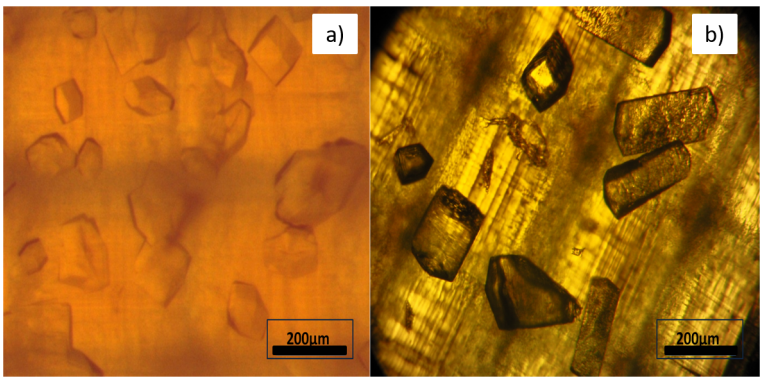

Figure 4.7: HEWL crystals derivatized with Br^- (a) in the cell and (b) by conventional soaking in drops placed on the membrane Neosepta AXE01 (solution of 0.6 M NaBr)

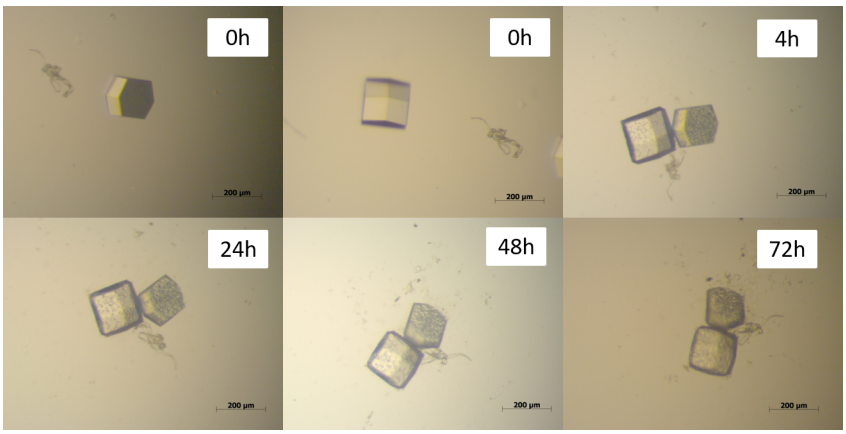

Figure 4.8: Stability of crystals derivatized with 10 mM $Hg(CH_3COO)_2$ by conventional soaking (drop placed on conventional crystallization plates) over time

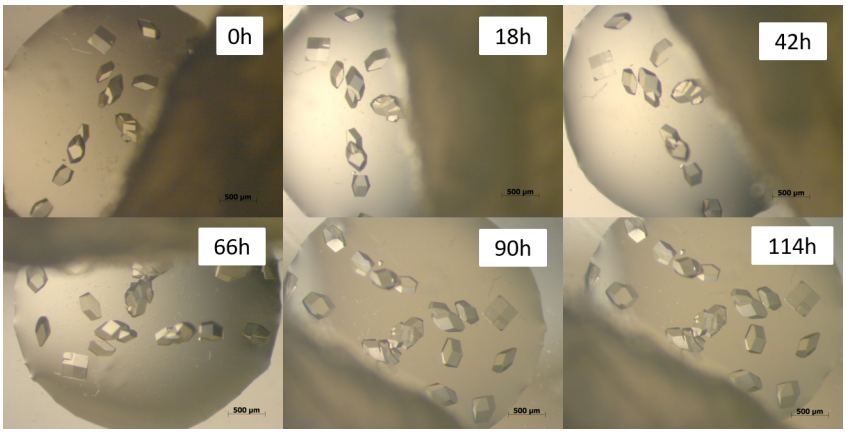

Figure 4.9: Stability of the crystals derivatized with $Hg(CH_3COO)_2$ (10 mM) in the cell (drop placed on Nafion®) over time

Table 4.2: Data Collection, SAD Phasing, and Automated Model Building Statistics of HEWL Crystals Derivatized Using the Ion- Exchange Membrane

	HEWL with NaBr	**HEWL with K_2PtCl_4**	**HEWL with $Hg(CH_3COO)_2$**
wavelenght (Å)	0.918	0.966	0.966
resolution range (Å)	56.62-1.66(1.69-1.66)	79.27-2.37 (2.46-2.37)	39.89-1.79 (1.83-1.79)
space group	80.1, 80.1, 36.2	79.3, 79.3, 37.7	79.8, 79.8, 37.4
unit cell parameters *a*,*b*,*c* (Å)	282531 (13685)	78896 (8270)	136662 (11073)
total reflections	14539 (695)	5239 (520)	11832 (677)
multiplicity	19.4 (19.7)	15.1 (15.9)	11.6 (16.4)
anomalous multiplicity	10.4 (10.2)	8.3 (8.4)	6.1 (8.3)
completeness (%)	100 (100)	100 (100)	100 (100)
anomalous completeness(%)	100 (100)	100 (100)	100 (100)
mean I/σ(I)	13.8 (3.2)	30.1 (18.9)	43.2 (9.0)
Wilson B-factor	13.7	31.1	24.8
R-merge	0.210 (2.110)	0.070(0.134)	0.162 (0.603)
R-pim	0.049 (0.479)	0.019 (0.034)	0.06 (0.153)
$CC_{1/2}$	0.997 (0.861)	0.998 (0.996)	0.987 (0.920)
SAD phasing			
No. of sites found	20	5	2
figure of merit (before/after density modification)	0.41/0.88	0.26/-	0.29/-

Automated model building and refinement from Br-SAD phase	
reflections used in refinement	13471 (1311)
reflections used for R-free	676 (63)
R-work/R-free	0.264/0.312
No. of non-hydrogn atoms	1035
macromolecule	927
heavy atoms	20
No. of protein residues	124
RMS (bonds) (Å)	0.007
RMS (angles) (deg)	0.99
Famachandran favored (%)	96
Ramachandran allowed (%)	4.3
Ramachandran outliers (%)	0
rotamer outliers (%)	2.3
average isotropic thermal parameters ($Å^2$)	17.89
macromolecule	17.60
heavy atoms	15.82
solvent	21.46

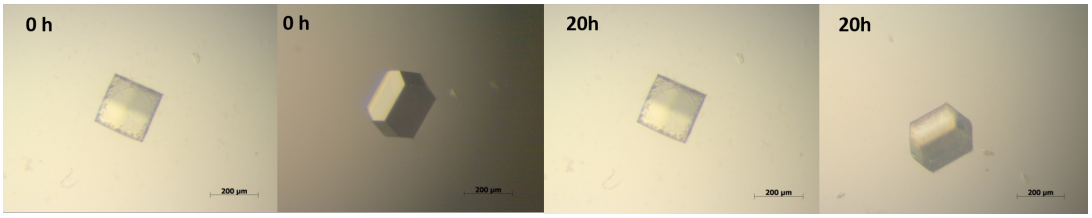

Figure 4.10: Stability of crystals derivatized with $PtCl_4^{2-}$ 5 mM by normal soaking (drop placed on conventional crystallization plate) over time

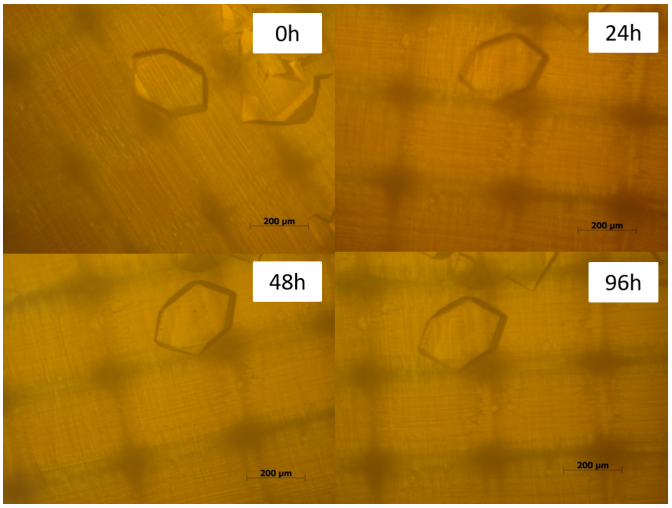

Figure 4.11: Stability of crystals derivatized with $PtCl_4^{2-}$ 5 mM in the cell (drop placed on Neosepta AXE01) over time

shown). The experimental values measured for f and f were -5.07 e and 3.8 e, respectively. A different strategy was adopted to perform SAD phasing from the mercury and platinum derivatives, which were collected at a wavelength of 0.966 Å, at which anomalous signal for these heavy atoms can be experimentally obtained from highly redundant diffraction data sets. A complete SAD data set was collected from the $K2PtCl_4$-derivatized crystal to 2.37 Å resolution, while the $Hg(CH_3COO)_2$ derivatized crystal produced complete data to 1.79 Å resolution. All crystals belonged to space group $P4_32_12$, with unit-cell parameters (reported in Table 4.2) comparable to the parameters known for HEW lysozyme. The asymmetric unit comprises one monomer of HEWL with an approximate solvent content of 35%. A full pipeline of substructure search, SAD phasing, density modification, and model building was performed for the bromide-containing HEWL crystal. Data collection, processing, and phasing statistics are presented in Table 4.2. AutoSol, implemented in Phenix, output 20 possible sites for bromide ions, with occupancies ranging from 0.72 to 0.11, a figure-of-merit of 0.41, and an overall score of 48.9 ± 8.9. After density modification, a figure-of-merit of 0.88 was achieved, followed by successful automated

model building from the obtained Br^- SAD phases. AutoSol could build 124 (out of 145) residues, producing a model with an $R_{work} = 0.26$ and an $R_{free} = 0.31$ and a map-model correlation coefficient of 0.81. Figure 4.12 shows the location of selected bromide atoms at the protein surface. For the research purposes, complete structure refinement was

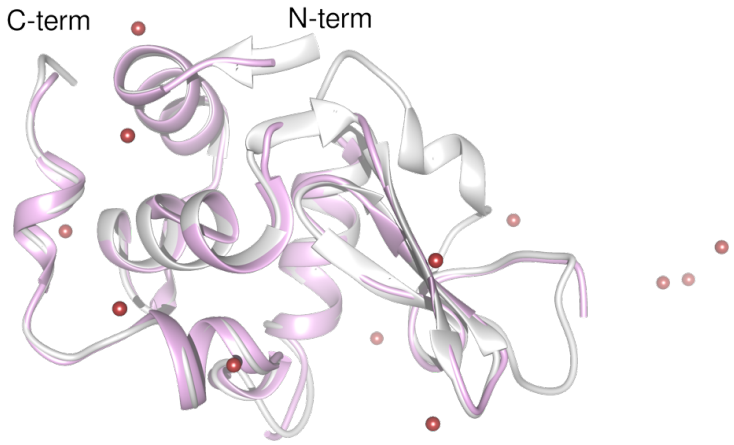

Figure 4.12: Ribbon representation of HEWL showing the surface location of several identified bromide atoms, as revealed by the measured anomalous signal. Bromide atoms are depicted as red spheres. The known structure of HEWL from Gallus gallus (PDB accession code 2LYS) is represented as a gray ribbon, overlaid on the *ab initio* model (in purple ribbon) built by AutoSol from the independent bromide phases. The superposition of both structures generates an rmsd of 0.334 Å for 109 α carbon atoms. Picture was produced with program Chimera [43, 44].

not required. For the platinum derivative, the automated search indicated five potential Pt sites, with a figure-of-merit of 0.26 and an overall score of 18.4 ± 14.3, clearly a weak phasing power for this derivative. A similar result was obtained for the mercury derivative, where AutoSol could detect two sites with respective occupancies of 0.29 and 0.34, a figure-of-merit of 0.18, and an overall score of 11.5 ± 12.6. Not surprisingly, *ab initio* model building was not successful for both Pt and Hg derivatives. The significantly low occupancies for the Hg and Pt atoms in both crystals impaired the automated SAD phasing and subsequent model building. However, in combination with phases from a molecular replacement solution (obtained using a known structure of HEWL), 10 sites

for Hg^{2+} could be identified (with very low occupancies ranging from 0.19 to 0.07) originating a figure-of-merit of 0.74 and an overall score of 75.6 ± 3.3. Similarly, for the phase combination of the platinum derivative with the molecular replacement solution, seven sites could be identified (with very low occupancies ranging from 0.2 to 0.05) originating a figure-of-merit of 0.79 and an overall score of 75.6 ± 3. All structures were analyzed for any differences compared to nonderivatized crystal structures. Calculation of rmsd values confirms that the structures obtained by derivatization were essentially isomorphous without significant differences from the native structures. For some heavy atom sites, clear additional electron density could be observed for the atoms (Br, Pt, and Hg) of which the nature was confirmed by the calculation of anomalous difference maps. The failure to achieve *ab initio* model building from the weak SAD phases obtained for the mercury and platinum derivatives could be overcome with increasing concentrations of the heavy atoms and or longer incubation times. These results prove that, in the designed ion-exchange membrane cell, heavy atoms could be transported through the membrane and diffuse into the crystals. Therefore, this method could be applied to other proteins when heavy atom derivatives are required, since it provides a more gentle way of introducing metal ions or halides in the crystal lattice.

4.5 Conclusions

Protein crystal derivatization is a widely recognized technique used to introduce heavy atoms inside crystals to solve the threedimensional structure of proteins using the Multiple Isomorphous Replacement method. Soaking is a laborious and uncertain procedure, working on a trial-and-error basis, currently used to derivatize protein crystals. This technique requires the removal of the crystals from their growth environment and their slow immersion in a different solution containing the heavy atom salt for derivatization. In this work, an alternative crystal derivatization method is proposed, consisting of the smooth increase of the target ionic species concentration (derivatizing agents) in the protein environment (protein drop) achieved by controlling the diffusion of these species using an ion-exchange membrane. The ion-exchange membrane system designed in this work allowed not only a controlled transport of the ionic species from the feeding to the receiving solution (protein drop located at the membrane surface) but also the control of other factors that influence the growth and stability of protein crystals, such as pH,

temperature, and osmotic pressure. The rate of ion transport through the membrane was estimated in order to know the concentration of heavy atom in the protein solution along the derivatization time, allowing to define the concentration of the derivatizing agent in the feeding compartment, needed to reach the desirable concentration of this ionic species in the protein drop (receiving compartment). This allowed a fair comparison of the derivatization process with the conventional direct soaking, showing how a controlled diffusion leads to a better stability of the crystals during the derivatization process, with the three ions tested. X-ray diffraction analysis of the derivatives showed that the heavy atom incorporation was successful and that isomorphism was maintained in all cases. Bromide derivatives also allowed determining the protein structure using the SAD phasing technique. Although it was not possible to complete the solution process for the mercury and platinum derivatives due to the lower occupancies of the diffused atoms in the crystal lattice, this could probably be overcome by using higher concentrations of the heavy atoms. Besides the increased control on the process, the ion-exchange membrane allowed to overcome problems due to the disturbance of the vapour diffusion equilibrium and handling of the crystals, performing the process in a gentle and continuous way, avoiding several steps normally required in conventional soaking. This method, which does not intend to completely replace the traditional procedures, should be considered in difficult cases: e.g., extreme frailty of crystals, presence of volatile compounds in mother liquor, or low availability of protein. Furthermore, the system is easy to be used and highly versatile: no particular manual skills are required for preparing and conducting experiments, and it allows to play with solution composition and concentration to regulate the ion transport rate. Further studies involving the tailoring of the membrane features such as thickness, ion-exchange capacity, and area of exchange may lead to a greater level of control on the process. These results pave the way to the development of designer membranes capable of transporting other ligands of interest and, in a non-invasive procedure, diffuse these ligands in the crystals of protein of interest.

References

[1] G. L. Taylor. "Introduction to phasing." In: *Acta Crystallographica Section D: Biological Crystallography* 66.4 (2010), pp. 325–338. DOI: 10.1107/S0907444910006694.

[2] I Usón and G. M. Sheldrick. "Advances in direct methods for protein crystallography." In: *Current opinion in structural biology* 9.5 (1999), pp. 643–648. DOI: 10.1016/S0959-440X(99)00020-2.

[3] J. P. Rose and B. C. Wang. "SAD phasing: History, current impact and future opportunities." In: *Archives of Biochemistry and Biophysics* 602 (2016), pp. 80–94. DOI: 10.1016/j.abb.2016.03.018.

[4] T. J. Boggon and L. Shapiro. "Screening for phasing atoms in protein crystallography." In: *Structure* 8.7 (2000), pp. 143–149. DOI: 10.1016/S0969-2126(00)00168-4.

[5] J. Agniswamy, M. G. Joyce, C. H. Hammer, and P. D. Sun. "Towards a rational approach for heavy-atom derivative screening in protein crystallography." In: *Acta Crystallographica Section D: Biological Crystallography* 64.4 (2008), pp. 354–367. DOI: 10.1107/S0907444907068849.

[6] S. Panjikar and P. A. Tucker. "Xenon derivatization of halide-soaked protein crystals." In: *Acta Crystallographica Section D: Biological Crystallography* 58.9 (2002), pp. 1413–1420. DOI: 10.1107/S0907444902011010.

[7] M. Dauter and Z. Dauter. "Phase determination using halide ions." In: *Methods in molecular biology (Clifton, N.J.)* 364.9 (2007), pp. 149–158. DOI: 10.1385/1-59745-266-1:149.

[8] Z. Dauter, M. Dauter, and K. R. Rajashankar. "Novel approach to phasing proteins: Derivatization by short cryo-soaking with halides." In: *Acta Crystallographica Section D: Biological Crystallography* 56.2 (2000), pp. 232–237. DOI: 10.1107/S0907444999016352.

[9] B. Heras and J. L. Martin. "Post-crystallization treatments for improving diffraction quality of protein crystals." In: *Acta Crystallographica Section D: Biological Crystallography* 61.9 (2005), pp. 1173–1180. DOI: 10.1107/S0907444905019451.

[10] J. Newman. "A review of techniques for maximizing diffraction from a protein crystal in stilla." In: *Acta Crystallographica Section D: Biological Crystallography* 62.1 (2006), pp. 27–31. DOI: 10.1107/S0907444905032130.

[11] A. C. W. Pike, E. F. Garman, T. Krojer, F. von Delft, and E. P. Carpenter. "An overview of heavy-atom derivatization of protein crystals." In: *Acta crystallographica. Section D, Structural biology* 72.Pt 3 (2016), pp. 303–318. DOI: 10.1107/S2059798316000401.

[12] A. M. Hassell, G. An, R. K. Bledsoe, J. M. Bynum, H. L. Carter, S. J. J. Deng, R. T. Gampe, T. E. Grisard, K. P. Madauss, R. T. Nolte, W. J. Rocque, L. Wang, K. L. Weaver, S. P. Williams, G. B. Wisely, R. Xu, and L. M. Shewchuk. "Crystallization of protein-ligand complexes." In: *Acta Crystallographica Section D: Biological Crystallography* 63.1 (2006), pp. 72–79. DOI: 10.1107/S0907444906047020.

[13] G. Di Profio, A. Caridi, R. Caliandro, A. Guagliardi, E. Curcio, and E. Drioli. "Fine dosage of antisolvent in the crystallization of L-histidine: Effect on polymorphism." In: *Crystal Growth and Design* 10.1 (2010), pp. 449–455. DOI: 10.1021/cg901038g.

[14] E. Curcio, E. Fontananova, G. D. Profio, and E. Drioli. "Influence of the Structural Properties of Poly(vinylidene fluoride) Membranes on the Heterogeneous Nucleation Rate of Protein Crystals." In: *Journal of Physical Chemistry B* 4.1 (2006), pp. 12438–12445. DOI: 10.1021/jp061531y.

[15] F. Kertis, S. Khurshid, O. Okman, J. W. Kysar, L. Govada, N. Chayen, and J. Erlebacher. "Heterogeneous nucleation of protein crystals using nanoporous gold nucleants." In: *Journal of Materials Chemistry* 22.41 (2012), pp. 21928–21934. DOI: 10.1039/c2jm34527g.

[16] K Ino, I Udagawa, K Iwabata, Y Takakusagi, and M Kubota. "Heterogeneous Nucleation of Protein Crystals on Fluorinated Layered Silicate." In: *PLoS ONE* 6.7 (2011), p. 22582. DOI: 10.1371/journal.pone.0022582.

[17] Y. X. Liu, X. J. Wang, J. Lu, and C. B. Ching. "Influence of the roughness, topography, and physicochemical properties of chemically modified surfaces on the heterogeneous nucleation of protein crystals." In: *Journal of Physical Chemistry B* 111.50 (2007), pp. 13971–13978. DOI: 10.1021/jp0741612.

[18] G. D. Profio, M. Polino, F. P. Nicoletta, B. D. Belviso, R. Caliandro, E. Fontananova, G. De Filpo, E. Curcio, and E. Drioli. "Tailored hydrogel membranes for efficient protein crystallization." In: *Advanced Functional Materials* 24.11 (2014), pp. 1582–1590. DOI: 10.1002/adfm.201302240.

[19] G. Di Profio, S. Tucci, E. Curcio, and E. Drioli. "Selective glycine polymorph crystallization by using microporous membranes." In: *Crystal Growth and Design* 7.3 (2007), pp. 526–530. DOI: 10.1021/cg0605990.

[20] G. Di Profio, E. Fontananova, E. Curcio, and E. Drioli. "From tailored supports to controlled nucleation: Exploring material chemistry, surface nanostructure, and wetting regime effects in heterogeneous nucleation of organic molecules." In: *Crystal Growth and Design* 12.7 (2012), pp. 3749–3757. DOI: 10.1021/cg3005568.

[21] H. Hsu, O. O. Adigun, L. S. Taylor, S. Murad, and M. T. Harris. "Crystallization of acetaminophen on chitosan films blended with different acids." In: *Chemical Engineering Science* 126 (2015), pp. 1–9. DOI: 10.1016/j.ces.2014.10.046.

[22] N. P. Berezina, N. A. Kononenko, O. A. Dyomina, and N. P. Gnusin. "Characterization of ion-exchange membrane materials: Properties vs structure." In: *Advances in Colloid and Interface Science* 139.1-2 (2008), pp. 3–28. DOI: 10.1016/j.cis.2008.01.002.

[23] T. Xu. "Ion exchange membranes: State of their development and perspective." In: *Journal of Membrane Science* 263.1-2 (2005), pp. 1–29. DOI: 10.1016/j.memsci.2005.05.002.

[24] R. K. Nagarale, G. S. Gohil, and V. K. Shahi. "Recent developments on ion-exchange membranes and electro-membrane processes." In: *Advances in Colloid and Interface Science* 119.2-3 (2006), pp. 97–130. DOI: 10.1016/j.cis.2005.09.005.

[25] C. Klaysom, S. H. Moon, B. P. Ladewig, G. Q. M. Lu, and L. Wang. "Preparation of porous ion-exchange membranes (IEMs) and their characterizations." In: 371.1-2 (2011), pp. 37–44. DOI: 10.1016/j.memsci.2011.01.008.

[26] T. Mohammadi, S. Chieng, and M. Skyllas Kazacos. "Water transport study across commercial ion exchange membranes in the vanadium redox flow battery." In: *Journal of Membrane Science* 133.2 (1997), pp. 151–159. DOI: 10.1016/S0376-7388(97)00092-6.

[27] D. E. Otzen. "Protein unfolding in detergents: effect of micelle structure, ionic strength, pH, and temperature." In: *Biophysical journal* 83.4 (2002), pp. 2219–30. DOI: 10.1016/S0006-3495(02)73982-9.

[28] N. E. Chayen. "Turning protein crystallisation from an art into a science." In: *Current Opinion in Structural Biology* 14.5 (2004), pp. 577–583. DOI: 10.1016/j.sbi.2004.08.002.

[29] S. Sugiyama, M. Maruyama, G. Sazaki, M. Hirose, H. Adachi, K. Takano, S. Murakami, T. Inoue, Y. Mori, and H. Matsumura. "Growth of protein crystals in hydrogels prevents osmotic shock." In: *Journal of the American Chemical Society* 134.13 (2012), pp. 5786–5789. DOI: 10.1021/ja301584y.

[30] A. McPherson and J. A. Gavira. "Introduction to protein crystallization." In: *Acta Crystallographica Section F:Structural Biology Communications* 70.1 (2014), pp. 2–20. DOI: 10.1107/S2053230X13033141.

[31] N. Asherie. "Protein crystallization and phase diagrams." In: *Methods* 34.3 (2004), pp. 266–272. DOI: 10.1016/j.ymeth.2004.03.028.

[32] J. Luo, C. Wu, T. Xu, and Y. Wu. "Diffusion dialysis-concept, principle and applications." In: *Journal of Membrane Science* 366.1-2 (2011), pp. 1–16. DOI: 10.1016/j.memsci.2010.10.028.

[33] J. Luo, C. Wu, Y. Wu, and T. Xu. "Diffusion dialysis of hydrochloride acid at different temperatures using PPO-SiO2 hybrid anion exchange membranes." In: *Journal of Membrane Science* 347.1-2 (2010), pp. 240–249. DOI: 10.1016/j.memsci.2009.10.029.

[34] J. Luo, C. Wu, Y. Wu, and T. Xu. "Diffusion dialysis processes of inorganic acids and their salts: The permeability of different acidic anions." In: *Separation and Purification Technology* 78.1 (2011), pp. 97–102. DOI: 10.1016/j.seppur.2011.01.028.

[35] C. Y. Zhang, D. C. Yin, Q. Q. Lu, Y. Z. Guo, W. H. Guo, X. K. Wang, H. S. Li, H. M. Lu, and Y. J. Ye. "Cycling temperature strategy: A method to improve the efficiency of crystallization condition screening of proteins." In: *Crystal Growth and Design* 8.12 (2008), pp. 4227–4232. DOI: 10.1021/cg800689j.

[36] "Lysozyme User Guide, Hampton Research." In: (2014), pp. 1–2.

[37] Y. Liu, X. Wang, and C. B. Ching. "Toward further understanding of lysozyme crystallization: Phase diagram, protein-protein interaction, nucleation kinetics,

and growth kinetics." In: *Crystal Growth and Design* 10.2 (2010), pp. 548–558. DOI: 10.1021/cg900919w.

[38] a. Kimble, W.L.; Paxton, T. E.; Rousseau, R. W.; Sambanis. "The effect of mineral substrates on the crystallization of lysozyme." In: *Journal of Crystal Growth* 187 (1998), pp. 268–276. DOI: 10.1016/S0022-0248(97)00838-5.

[39] G. Tosi, S. Fermani, G. Falini, J. A. Gavira Gallardo, and J. M. Garcia Ruiz. "Crystallization of proteins on functionalized surfaces." In: *Acta Crystallographica Section D: Biological Crystallography* 64.10 (2008), pp. 1054–1061. DOI: 10.1107/S0907444908025079.

[40] T. G. G. Battye, L. Kontogiannis, O. Johnson, H. R. Powell, and A. G. W. Leslie. "iMOSFLM: A new graphical interface for diffraction-image processing with MOSFLM." In: *Acta Crystallographica Section D: Biological Crystallography* 67.4 (2011), pp. 271–281. DOI: 10.1107/S0907444910048675.

[41] P. R. Evans and G. N. Murshudov. "How good are my data and what is the resolution?" In: *Acta Crystallographica Section D: Biological Crystallography* 69.7 (2013), pp. 1204–1214. DOI: 10.1107/S0907444913000061.

[42] P. D. Adams, P. V. Afonine, G. Bunkóczi, V. B. Chen, I. W. Davis, N. Echols, J. J. Headd, L. W. Hung, G. J. Kapral, R. W. Grosse-Kunstleve, A. J. McCoy, N. W. Moriarty, R. Oeffner, R. J. Read, D. C. Richardson, J. S. Richardson, T. C. Terwilliger, and P. H. Zwart. "PHENIX: A comprehensive Python-based system for macromolecular structure solution." In: *Acta Crystallographica Section D: Biological Crystallography* 66.2 (2010), pp. 213–221. DOI: 10.1107/S0907444909052925.

[43] E. F. Pettersen, T. D. Goddard, C. C. Huang, G. S. Couch, D. M. Greenblatt, E. C. Meng, and T. E. Ferrin. "UCSF Chimera visualization system for exploratory research and analysis." In: *Journal of Computational Chemistry* 25.13 (2004), pp. 1605–1612. DOI: 10.1002/jcc.20084.

[44] T. D. Goddard, C. C. Huang, and T. E. Ferrin. "Visualizing density maps with UCSF Chimera." In: *Journal of Structural Biology* 157.1 (2007), pp. 281–287. DOI: 10.1016/j.jsb.2006.06.010.

CHAPTER 5

MICROFLUIDIC CRYSTALLIZATION OF PROTEINS WITH NAFION® MEMBRANES

5.1 Summary

Protein crystallization and protein crystals derivatization are rather empirical sciences. Several conditions need to be tested to obtain crystals with enough quality for X-ray analysis. In this work, the advantages of microfluidics technology for protein crystallization (high throughput, low budget) were combined with the fine control that membranes can provide to the crystallization and derivatization process. Hence, a commercial 117 Nafion® membrane, that allows a controlled transport of water and ions, was sandwiched between a channels layer and a wells layer of PDMS, in order to build a microdevice with 75 micro-contactors in which nano to micro volumes of protein solution can be used to optimize protein crystallization. Hen Egg White Lysozyme (HEWL) was used in the crystallization experiments in order to test reproducibility and the functionality of the device. Number and size of crystals were modulated by changing the volume of solution in the microdevice wells for the same area of transport through the membrane. Crystals obtained in the microdevice were stable over time and demonstrated a high diffraction quality during X-ray diffraction analysis.

5.2 Introduction

The attainment of high quality diffracting crystals is still the main limitation in protein crystallography applied for the solution of the three-dimensional molecular structure of proteins. The diffraction quality may depend on several crystallization parameters: pH, temperature, solvent removal rate, additives, among others. Therefore, when the structure of a new protein has to be unraveled, an enormous number of conditions have to be tested, before an adequate recipe is found that leads to an accurate crystallographic analysis [1]. Microfluidic technology has been revolutionary for protein crystallization. The creativity of scientists has led to the development of several intricate chip designs (valve-based [2], droplet-based[3], slip chips [4], or centrifugal designs [5]) that allowed for the fast screening of hundreds of process conditions, using only very low amounts of protein [6]. On the other hand, advances in membrane technology have contributed to excellent control of the solvent removal rate, required for regulation of the crystallization process, by modulating the porosity of hydrophobic microporous membranes and by controlling the difference in water activity between the protein solution and the stripping solution [7]. This allowed to control the crystal growth rate [8], shape [9], polymorphism [10] and, consequently, the diffraction quality [11]. In some cases, such as for completely unknown structures, routine diffraction analysis (Molecular Replacement Techniques) is not able to solve the structure. In these cases, the introduction of heavy atoms into the crystal (derivatization) is routinely carried out to use Isomorphous Replacement Techniques [12–16]. Similar to crystallization, derivatization is also a challenging procedure. Finding the adequate heavy atom and concentration for a specific protein requires persistence. Crystals may easily crack and get damaged due to the use of a wrong heavy atom or due to abrupt changes in the local growth environment and the handling of crystals. Attempts were made to predict the interaction between the protein and the heavy atoms [17, 18], but for most protein cases, a previous screening of different heavy atoms and concentrations becomes essential. We have recently described how ion-exchange membranes can be used to facilitate the derivatization of protein crystals with heavy atoms [19]. Ion-exchange membranes are typically made of a hydrophobic backbone with attached charged groups [20]. Such membranes are able to mediate the selective diffusion of ions (cations or anions depending on the type of fixed charged groups attached to the polymer backbone) inside the protein crystal solution determining a smooth and

controlled increase of the target ion-concentration, reducing the risks of cracking due to abrupt changes of the crystal environment and handling [19]. Besides the selective ion transport, ion-exchange membranes promote water transport when a difference in water activity occurs between the two sides of the membrane: water spontaneously moves from the least to the most concentrated compartment [21]. Hence, controlled diffusion of water by osmosis can be exploited to generate supersaturation and promote nucleation. Herein, a commercial ion-exchange membrane (117 Nafion®) is integrated into a PDMS microdevice to form 75 microcontactors. The microdevice consists of two independent chambers (the wells layer dedicated to the crystallization solution and the channels layer filled with stripping/derivatization solution) and an ion-exchange flat membrane between them. In particular, each well of the crystallization chamber can accommodate nano or microliter volumes of protein solution, defining the area/volume ratio for water transport or ion-exchange for crystallization or derivatization processes. Due to miniaturization, the volume of protein crystallization/derivatization solutions required in the well/channel chambers is notably reduced while providing high throughput for the preliminary screening of different crystallization/derivation operational conditions. Thus, the final aim of this work is the demonstration of ion-exchange membrane-driven crystallization process with a Nafion® based microfluidic device. The crystallization performance, i.e. growth rate, size and diffraction quality of crystals, is evaluated using Hen Egg White Lysozyme (HEWL) as protein model.

5.3 Materials and Methods

5.3.1 Crystallization solutions

Hen Egg White Lysozyme (HEWL) from Sigma Aldrich was dissolved in $NaCH_3COO$ buffer 0.1M (pH 4.6) at a concentration of 50mg/mL (protein solution). NaCl (Applichem Panreac, Barcelona, Spain) was dissolved in $NaCH_3COO$ 0.1M buffer (pH 4.6) at a concentration of 3.5% (precipitant solution). The protein and the precipitant solution were mixed in equal volumes in order to obtain a starting crystallization solution composed of HEWL 25mg/mL, NaCl 1.75% and $NaCH_3COO$ 0.1M at pH 4.6. NaCl 3.5% in $NaCH_3COO$ 0.1M pH 4.6 was used as stripping agent in the channels. In order to perform measurements of the mass transfer coefficient of Hg^{2+} to be eventually used for derivatization, $Hg(CH_3COO)_2$ was dissolved in a solution containing $NaCH_3COO$ 0.1M

at pH 4.6 and NaCl 0.59M.

5.3.2 Design and fabrication of the microdevice

The microdevice was fabricated by soft lithography [22–24]. Two photomasks, one for a microwell layer and another one for a channel layer, were designed using CleWin software (WieWeb software, Hengelo, the Netherlands). Master molds were fabricated by standard photolithography (Figure 5.1 A)[25]. A negative photoresist resin (SU-8 2150, MicroChemicals GmbH, Ulm, Germany) was spun onto 4 Si wafers, baked and exposed to UV light in order to transfer the pattern from the mask to the photoresist layers on the wafers. The subsequent use of an SU-8 developer allowed to remove the soluble (non-exposed) parts of the resin. The final thickness of photoresist structures was measured with a micrometer, and it was found to be 300 ± 15 μm for both moulds. PDMS mixture (Sylgard 184, Dow Corning, prepolymer: curing agent = 10:1) was casted onto the master molds and baked at 80°C for 1 hour (Figure 5.1B). For the channel layer, an amount of PDMS was casted to cover the mold completely (Figure 5.1B). Instead, in the case of the wells layer, the volume of PDMS casted was calculated in order to give a thickness lower than the height of the pillars, determining the formation of holes, instead of cavities (Figure 5.1B). In order to flow the solutions inside the channels, an inlet and an outlet were created by punching. Each device has 5 lines of 15 wells for a total of 75 wells. The wells have a circular shape with 1 mm diameter (this diameter was chosen to allow the harvesting of crystals with conventional crystallography loops) and 250 μm depth. The channel part comprises 5 channels (with a width of 2mm and a depth of 300 μm), matching with the 5 lines of wells; therefore, 5 different solutions can be used simultaneously as stripping solutions (1 per channel) for crystallization. The driving force in each channel will be dependent on the solution inside the wells. The same channels may be used later to circulate the solutions selected for crystal derivatization. An AutoCAD (Autodesk, San Rafael, USA) rendering of the three layers of the device is shown in Figure 5.1C; photos of the fabricated device are shown in Figure 5.1D (cross-section) and 5.1E (top-view).

A 117 Nafion® membrane (Sigma-Aldrich, 1100EW) was sandwiched between the channel and the well layers. Nafion® is a material with a high degree of swelling. Therefore the bonding with PDMS was quite challenging. Several attempts are described in the literature [26–29] but, eventually, the protocol developed by Pham et al., for the commercial 117 Nafion® membrane , was optimized and used in this work [30]. Briefly,

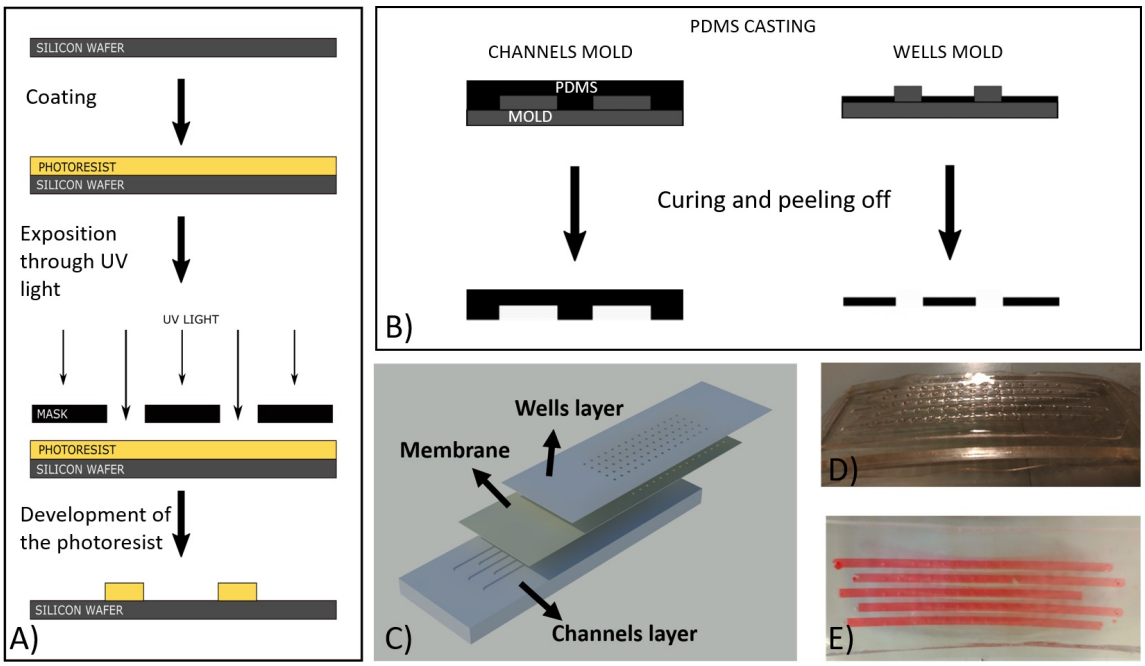

Figure 5.1: A) Photolithography process: SU8 photoresist deposition on Si wafer; exposition to UV light through the designed mask; development of the SU8 photoresist to attain the final mold. B) The SU8 molds were used for the fabrication of both PDMS compartments by Casting. C) AutoCAD rendering of the microdevice. D) and E) pictures of the fabricated device. The scale bar in figure E) corresponds to 1 cm.

the Nafion® membrane was cleaned in H_2O_2 3% at 80°C for 1 hour, H_2O at 80°C for 1 hour, H_2SO_4 1M at 80°C for 1 hour and H_2O at 80°C for 1 hour. The membrane was dried at 80°C for 24 hours and then treated for 15 minutes at 150°C in order to reduce the swelling behavior. It has been reported that thermal treatment of Nafion® membranes may induce conformational changes and spatial reorientation of the hydrophobic an hydrophilic nanodomains leading to a lower water uptake and conductivity [31]. The washed and thermally treated 117 Nafion® was modified with a corona discharge (BD-20AC Laboratory Corona Treater) for 10 minutes in order to generate hydroperoxide groups. Previous trials were made with plasma oxygen equipment; however the strong vacuum determined a severe shrinkage of the membrane that turned to be too wavy to create a good contact with the modified PDMS surface. The PDMS layers were treated with oxygen plasma for 60 seconds, in order to form hydroxide groups, then immersed in 4 % triethoxyvinylsilane (VTES), (purchased from Sigma-Aldrich, 97%) in Ethanol (Honeywell, purity 98.8%) with 10% of water for 2 minutes and baked at 100°C for 15 minutes to allow the grafting to occur. Afterwards, the treated 117 Nafion® membrane was contacted with the grafted PDMS and baked at 100°C for 2 hours to promote the

formation of radical groups on the membrane, which would attach to the vinyl group in PDMS-VTES and form the bonding. After the bonding, the microdevice was soaked in NaCl 2M, in order to exchange acidic groups with Na^+ and avoid pH changes in the crystallization solution that may induce crystals' dissolution. The NaCl solution was replaced until pH of solution maintained neutral to ensure that all protons were exchanged for Na^+.

5.3.3 Crystallization experiments

Crystallization experiments were performed in order to confirm the ability of the device to produce the crystals. For the crystallization experiments, firstly, the channels of the device were filled with the stripping solution (3.5 % w/v NaCl dissolved in 0.1M $NaCH_3COO$) using a syringe pump and later, the wells were filled with the protein solution using a micropipette (Figure 5.2). Mainly, three different volumes of solution were used: 500nL, 1μL, and 2μL; for the same membrane area. Each condition was repeated at least 9 times for reproducibility assessment. Finally, the chip was placed in a sealed box to prevent evaporation, in a room with controlled temperature (20°C).

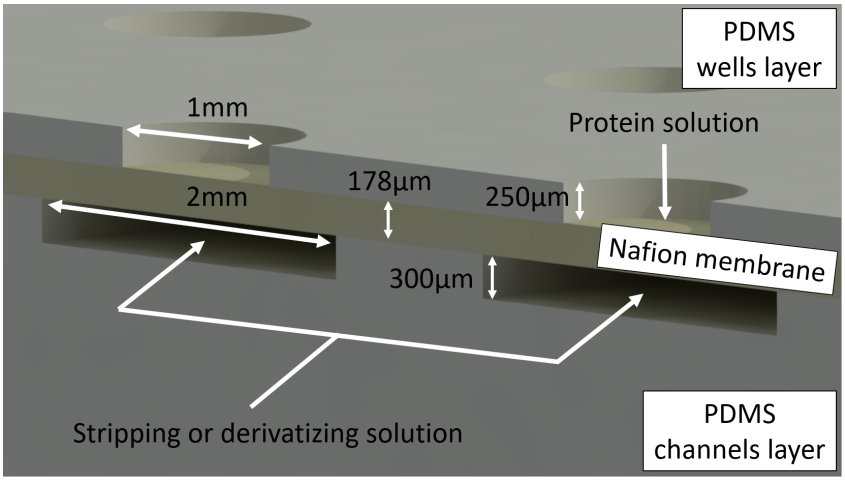

Figure 5.2: Cross-section schematics of the microdevice

5.3.4 Modelling of water and mercury acetate transport through the Nafion® membrane.

From structural investigations of the Nafion® ionomer, it is well-known that the hydrophilic sulfonic groups organized in clusters can incorporate water and allow for ions/protons and water transport. Accordingly, we tried to exploit these properties for the

water removal from the protein solution in order to achieve local supersaturation and facilitate nucleation. The driving force for water transport in the microdevice is established when filling the channels with a stripping solution with a lower water activity compared to the protein solution placed in the wells (more details are reported in the 'Crystallization experiments' section). Furthermore, the hydrophobic polytetrafluoroethylene (PTFE) backbone of Nafion® contains negatively fixed charged groups that enables the selective transport of cations. In order to evaluate the transport of water through the 117 Nafion® membrane and estimate the variation of NaCl concentration, a diffusion cell was set-up to mimic the conditions of the crystallization environment in the micro-device. The diffusion cell, sandwiching 117 Nafion® membrane (previously hydrated) between two compartments, is shown in Figure 5.3a. Compartment A was filled with distilled water, and compartment B was filled with NaCl 0.55M in order to create a driving force. Two graduated pipettes were connected to the extremities of the cell to record changes in volume as a function of time. In this situation, no ion-exchange process occurs due to the absence of a cation to be exchanged in compartment A with the Na^+ available in compartment B.

However, a leak of NaCl due to the high osmotic pressure might still be possible [32]. In order to assess the entity of the leak and the variation of driving force within the monitoring time, conductivity of the solutions was evaluated and results are reported in the Appendix (B) file. The selective transport of cations promoted by the membrane might instead be exploited for promoting a controlled diffusion of ions to/from the protein crystals solution and perform gentle derivatization. Protein crystals derivatization is normally performed after the crystals are formed in order to maintain the isomorphism [12]. Hence, when derivatization is performed, the protein crystal solution composition is already equilibrated with the stripping solution because they have the same osmotic pressure. Therefore, in order to investigate the transport of cations for derivatization in the microdevice a second diffusion cell (shown in Figure 5.3b) was set up, in which conditions for derivatization were simulated. The diffusion cell was used to calculate the mass transfer coefficient of Hg^{2+} (a cation commonly used for the derivatization of protein crystals) across the membrane (previously equilibrated in a NaCl solution). Two solutions with the same osmotic pressure were used. Compartment A was filled with a solution containing NaCl 0.59M and $Hg(CH_3COO)_2$ 0.01M; whereas Compartment B was

filled with a solution of NaCl 0.6M. Na^+ and Hg^{2+} will exchange until they reach equilibrium. Samples were taken over time, and the concentration of Hg^{2+} in Compartment B was measured by ICPAES (Inductively Coupled PlasmaAtomic Emission Spectrometer, Horiba Jobin-Yvon, France).

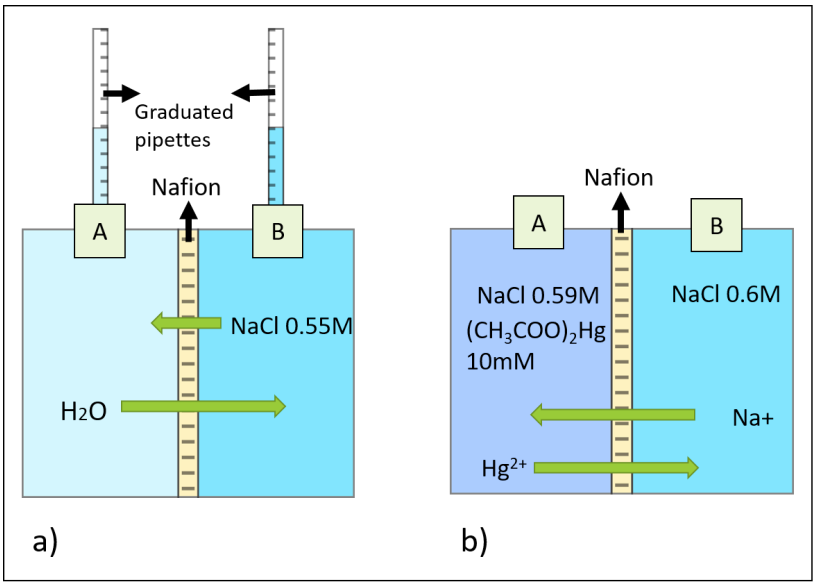

Figure 5.3: Diffusion cell used to measure water and NaCl mass transfer coefficients in Nafion®; b) Diffusion cell used to measure Hg^2+ mass transfer coefficient in Nafion®

5.3.5 X-ray diffraction analysis

HEWL crystals were equilibrated for a few seconds, first in harvesting buffer (CH_3COONa 0.1M, pH 4.6, and NaCl 1M) and then in cryo-protectant solution (harvesting buffer with 30% (v/v) glycerol from Sigma-Aldrich). X-ray diffraction analysis, to evaluate diffraction quality was performed using an in-house X-ray diffractometer (IμS 3.0 microfocus D8 Venture from Bruker, with CuKα radiation), coupled to a CMOS Photon 100 detector, at 110 K. Indexing, integration and scaling were done using PROTEUM3 software pipeline (Bruker AXS 2015). Scaled and merged intensities were converted to amplitudes using program COMBAT from the CCP4i suite [33]. Phases were calculated using Expert MR-PHASER from CCP4ii suite. The pdb model from the pdb database used for phase calculation was the 3a8z. Model building and refinement were done, iteratively, using COOT [34] and REFMAC5 [35]. A final model was built using BUCCANEER [36] and viewed in CCP4mg [37] . Program MOLPROBITY [38] was used for the validation of the final model.

5.4 Results and Discussion

5.4.1 Estimation of water and Hg^2+ permeation across Nafion® membrane

Water mass transfer coefficient was used to estimate the variation of concentration of salt in the protein solution due to osmosis. The mass transfer coefficient of Hg^2+ was used to estimate the Hg^2+ concentration profile over time in the protein crystals solution during the derivatization process. When a cation-exchange membrane (as Nafion®) contacts a pure water solution on one side and a salt solution on the other side, water will move from the water compartment to the salt solution compartment until the osmotic pressure is equilibrated. In order to calculate the mass transfer coefficient of water, a previously hydrated Nafion® membrane was placed in the diffusion cell (Figure 5.3a) and the variation of volume was followed over time in the two compartments (Figure 5.4); At the beginning of the osmosis process, the volume decreases linearly with time in compartment A (with a slope of 0.125mL/min). Hence, the volumetric flow rate of water across the membrane (Q_w) corresponds to the slope of the line of compartment A in Figure 5.4.

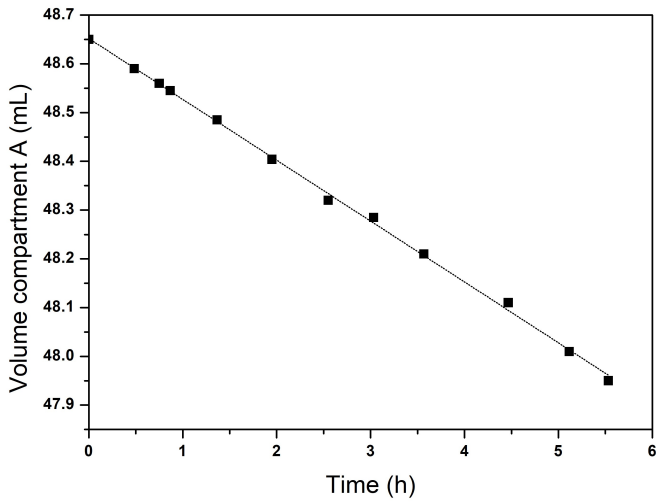

Figure 5.4: Volume of water over time in compartment A of the diffusion cell in Figure 5.3a).

From Q_w, considering the values of density (d), molecular weight (M_w) of water and the membrane area (A) (7.54cm^2), it is possible to calculate the molar flux of water J_w as follows:

$$J_w = \frac{Q_w d}{A M_w} \tag{5.1}$$

From J_w the mass transfer coefficient K_w was calculated as follows:

$$J_w = \frac{K_w(\Delta p - \Delta\pi)}{l} \tag{5.2}$$

$$K_w = \frac{J_w l}{\Delta p - \Delta\pi} \tag{5.3}$$

Where Δp is the hydrostatic pressure difference, $\Delta\pi$ is the osmotic pressure difference, l is the membrane thickness (178μm). The hydrostatic pressure was considered negligible, instead the $\Delta\pi$ was calculated as $\Delta\pi = \Delta CRT$, where ΔC is the concentration difference of NaCl in the two compartments (the short time of measurement ensured a very small variation of driving force, i.e. 4%, details are reported in the Supporting Information), hence an average value between the concentrations within the measurement interval was used for this calculation (0.52M), R is the ideal gas constant ($0.08206\frac{Latm}{molK}$) and T is the temperature ($298.15K$).

In order to calculate the mass transfer coefficient for Hg^{2+}, the concentration of Hg^{2+} over time was measured in the cell shown in Figure 5.3b for a membrane already equilibrated in a NaCl solution. In this case, the osmotic pressure on the two sides at the beginning of the experiment is the same. However, the charge difference between Hg^{2}+ and Na^{+} leads to the exchange of $2Na^{+}$ for each Hg^{2+}, changing the osmotic equilibrium between the two solutions. In order to reinstate the osmotic equilibrium, some water might cross the membrane. However, since the amount of Hg^{2+} used here is very low (10 mM) compared to the concentration that is responsible for the total osmotic pressure (0.7 M) the water transport has been considered negligible, and the volume of the solutions on the two sides of the membrane was considered constant (confirmed experimentally). Keeping this into account, the molar flux (J_{Hg}) was calculated by dividing the slope of the curve (0.00192mM/h) in Figure 5.5 by the area of the membrane (A) and multiplying by the Volume (V) (eq.5.4):

$$J_{Hg} = \frac{mol_{Hg}}{tA} \tag{5.4}$$

J_{Hg} can be also defined as:

$$J_{Hg} = K_{Hg}\Delta C \tag{5.5}$$

Where K_{Hg} is the mass transfer coefficient and ΔC is the Hg^{2+} concentration difference between the two sides of the membrane (10 mM). Hence, K_{Hg} was calculated as:

$$K_{Hg} = \frac{J_{Hg}}{\Delta C} \tag{5.6}$$

The mass transfer coefficients of water and Hg2+ through the Nafion® membrane are compared in Table 5.1. The low mass transfer coefficient of Hg2+ indicates a slow diffusion of this cation through the membrane, which is an excellent characteristic regarding the need to promote a gentle derivatization process.

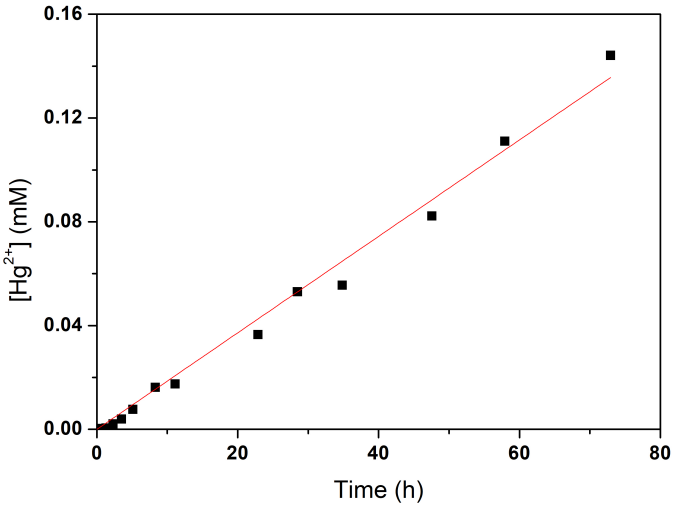

Figure 5.5: Hg^{2+} concentration over time in compartment A of the diffusion cell

Table 5.1: Mass transfer coefficient for water, NaCl, and Hg^2+

Substance	**Mass Transfer Coefficient** (m/s)
water	$4.1*10^{-6}$
NaCl	$2.7*10^{-8}$
Hg^{2+}	$1.9*10^{-9}$

5.4.2 Simulation of transport in the microdevice

Crystallization experiments in the microdevice were performed using a widely investigated protein, Hen Egg White Lysozyme (HEWL). Crystallization conditions for HEWL can be found in the phase diagram of the protein [39]. The phase diagram of HEWL combined with simulations of the evolution of the salt concentration in the micro-device was used to predict when conditions for nucleation were reached. The evolution of the

initial protein solution composition (Protein concentration: 25mg/mL and NaCl concentration: 1.75%) to the final concentration equilibrated with the stripping solution (Protein concentration: 50mg/mL and NaCl: 3.5%) was overlaid to the phase diagram in Figure 5.6. It is possible to notice that when the salt concentration is about 2.9%, the solution is supersaturated at a level where nucleation is likely to occur. By using the calculated mass transfer coefficient of water (Table 5.1) and the geometry dimensions of the device it is possible to simulate the variation of NaCl concentration in the protein well over time, when a stripping solution of 3.5% NaCl is used in the channels to promote osmosis. Results of the simulation are reported in Figure 5.7.

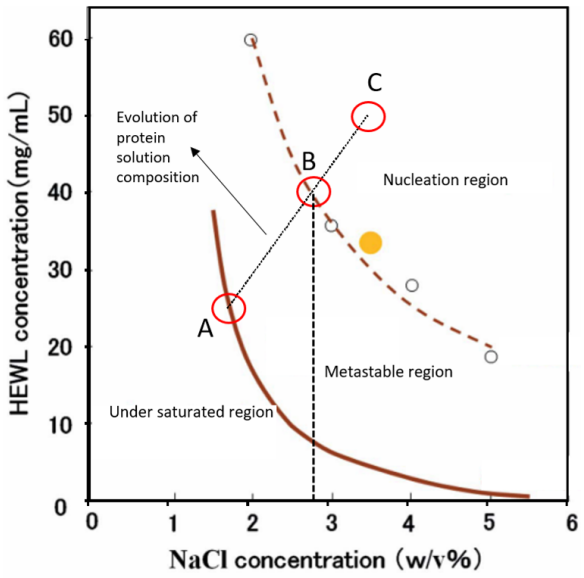

Figure 5.6: Solubility diagram of Lysozyme extracted from [36]. A) corresponds to the composition of the crystallizing solution in the beginning of the experiment (25mg/mL HEWL and 1.75% NaCl); B) corresponds to the composition of the crystallizing solution when crossing the boundary for nucleation to occur (41mg/mL HEWL , 2.9% NaCl); C) corresponds to the equilibrium point with the stripping solution (50mg/mL HEWL, %3.5 NaCl).

The experimental simulation was run for three different volumes (V_1=0.5μL, V_2=1μL, V_3=2μL) of solution for the same area (A_{wells} = 7.85cm^2) of transport. The time at which nucleation may start was highlighted, and for the 3 different volumes, the nucleation condition is reached in a short fraction of an hour, meaning that the kinetics of nucleation is very fast.

In order to investigate the impact of Hg^{2+} on the crystals, a simulation was run for calculating the increase of Hg^{2+} in the wells (Figure 5.8). The protein solution deposited in the wells in the beginning of the experiments has a NaCl concentration of 1.75%.

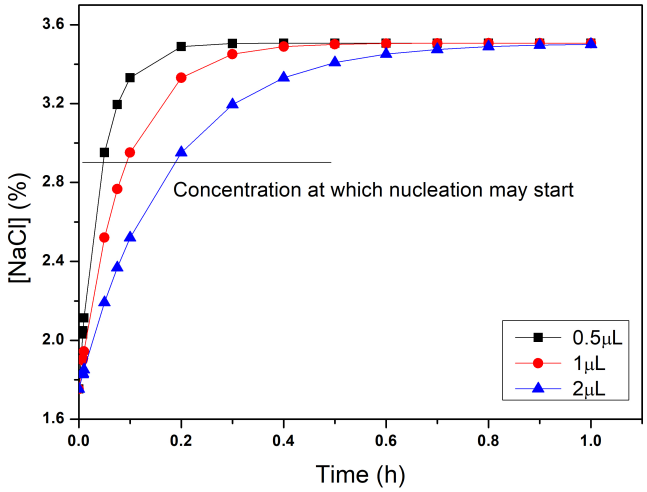

Figure 5.7: NaCl concentration in the wells of the micro-device over time for different volumes of protein solution

Instead, the solution used as stripping in the channels has a NaCl concentration of 3.5%.

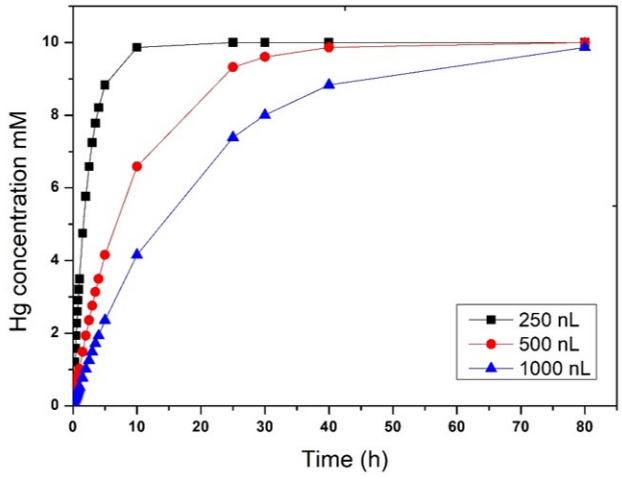

Figure 5.8: Evolution of Hg^{2+} concentration in the protein solution

Taking into consideration that the buffer type, concentration, and pH (CH_3COONa 0.1 M at pH 4.6) are the same for both solutions and that the contribution of the protein molecules to the osmotic pressure is negligible, the protein solution presents an osmotic pressure that is half of the stripping solution. The channels volume ($\tilde{3}3\mu$L) is significantly higher than the volume of the solution placed in the wells (0.5-2μL). Therefore, during the osmosis process, the change of concentration in the channels will be minimal, and the solution in the well will tend to equal the concentration in the channel. Since equilibrium

will be reached mainly by water transport, the volume at equilibrium in the wells will be half of the initial volume. The derivatization with Hg^{2+} would be performed only when crystallization is completed (in order to keep isomorphism [17]). For this reason, the volumes used for the calculation of the increase of Hg^{2+} concentration in the wells are the half of the initial volumes placed. In this case, the maximum cation concentration is reached in about 20 hours for 250 nL, 40 hours for 500 nL and about 80 hours for 1 μL of the solution. These long diffusion times will allow a gentle transport of the derivatized ions, reducing the risk of crystal cracking, and damage during the process. Furthermore, the different ion concentration-time dependence between the three volumes is useful for controlling the stability of the crystals and the efficiency of derivatization.

5.4.3 Microfluidic Crystallization of HEWL

The first crystallization experiments in the microdevice revealed the formation of HEWL crystals after a short time (2 hours), in accordance with the simulation results presented in Figure 5.7. However, they quickly degraded and completely disappeared (Figure 5.9). This empirical observation is attributed to the H^+/Na^+ exchange process between the protonated 117 Nafion® membrane and the protein solution. As a consequence, the pH gradually decreases to an extreme condition unbearable for the crystals provoking its degradation.

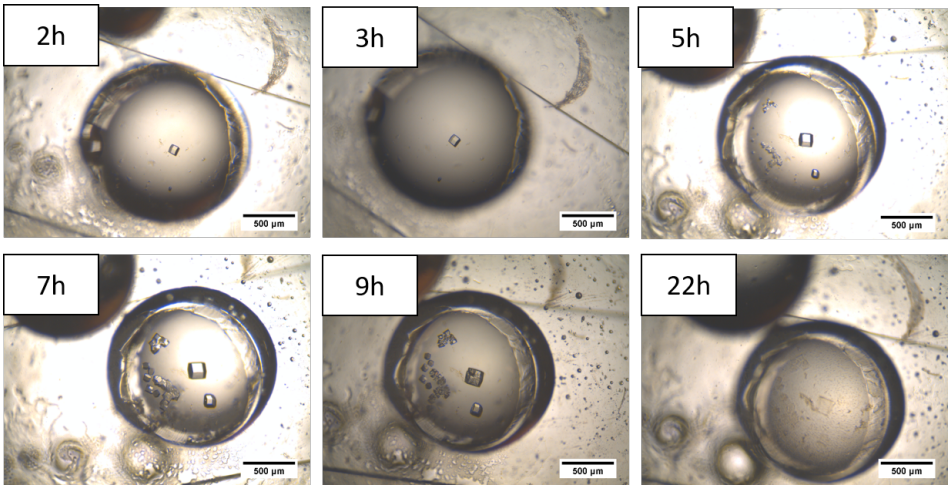

Figure 5.9: Crystals degradation in the microdevice due to acidic pH of the membrane

In order to avoid this inconvenience, after the PDMS-Nafion® assembly (described in the section Design and fabrication of the microdevice) the resulting microdevice was soaked in 2 M NaCl solution to obtain the 117 Nafion® membrane in its sodium form.

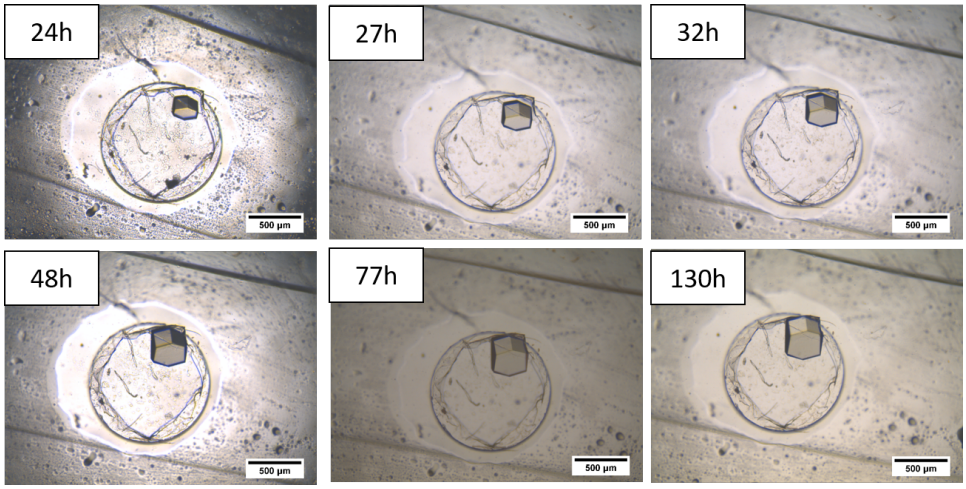

Figure 5.10: Crystallization experiments after the microdevice was soaked in 2M NaCl

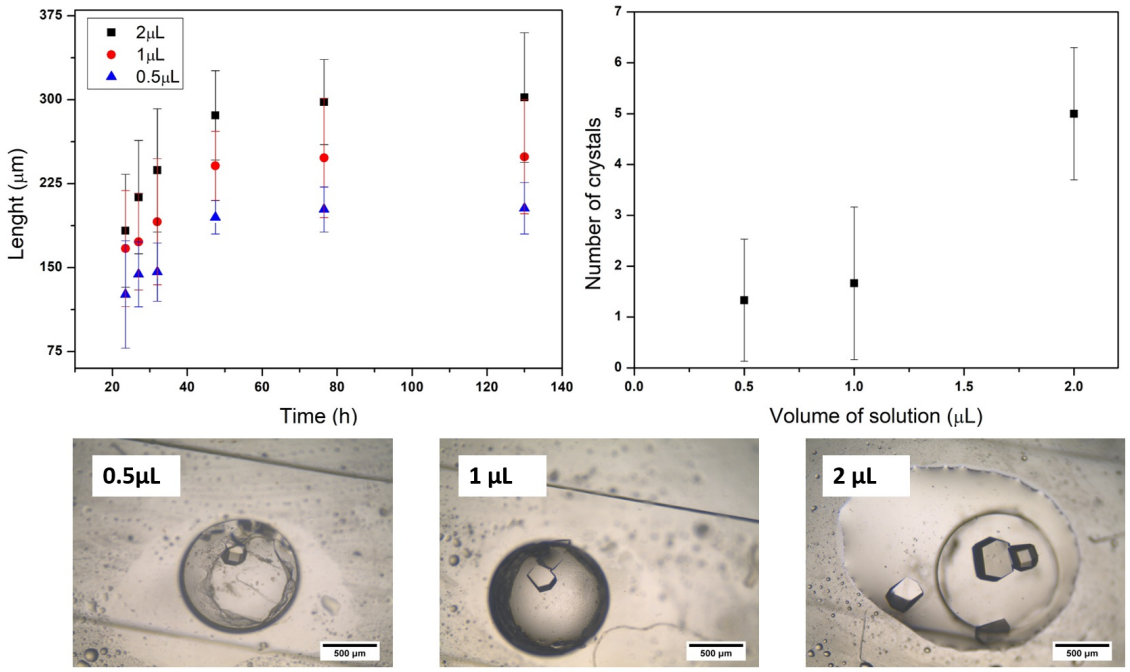

Figure 5.11: Crystal growth kinetics (top left), and number of crystals per volume of solution (top right). On the bottom: crystals grown in different volumes of solution, observed after 130 hours

Preliminary results, not shown here, demonstrated unsuccessful chip bonding when the Na-exchanged 117 Nafion® membrane was used. During the H^+/Na^+ exchange process, the pH of the solution was monitored over time, and the NaCl solution periodically replaced until the pH stayed neutral and constant. Once equilibrated the microfluidic device, HEWL crystallization experiments were similarly performed. Pictures of the crystals at different time points are shown in Figure 5.10. In this case, it is possible to notice that crystals continue growing for several days and do not show any sign of degradation. This makes clear that, in order to use a Nafion® 117 membrane as nucleant support for HEWL crystallization, previous proton exchange becomes essential to avoid pH-driven degradation of protein crystals. Reproducibility of the crystallization outcomes was assessed for different volumes of protein solution in the well-type microcontactor. Each condition was repeated 9 times. Figure 5.11 displays the results related to the length and the number of crystals obtained, using different volumes of the crystallization solution: varying from 0.5μL to 2.0μL but keeping the same membrane contact area. Even though the final equilibrium condition and the water transport rate through the membrane are the same, the number and size of crystals increase with the volume of the solution dispensed in well-type microcontactor. The higher number of crystals may be attributed to the higher amount of protein available for nucleation and crystal growth. In fact, no differences were found in the time required for the first crystals to appear. This behaviour is probably due to the low time shift for reaching nucleation conditions between the different volumes tested. In general, it is possible to conclude that the designed micro-device allows controlling crystal number and size, by changing the volume of the protein solution dispensed in the well-type micro-contactor. The crystals obtained were extremely stable over a long time.

5.4.4 X-ray diffraction analysis

In order to assess the diffraction quality of the crystals grown on the Nafion® membrane in the micro-device, a diffraction analysis was performed using a in-house diffractometer at a wavelength of 1.5418Å. Data collection, processing and phasing are reported in Table 5.2. The crystals diffracted to a maximum resolution of 1.6Å. The collected, indexed and integrated data were scaled and merged using the software pipeline in PROTEUM3 (Bruker AXS 2015). The analysed crystals belongs to space group $P4_32_12$. The diffraction data of the crystals are characterized by a low R_{merge} value, high signal-to-noise ratio.

Table 5.2: Statistics of X-ray diffraction data collection and automated model building and refinement (values for the last resolution shell are in parenthesis)

X-ray diffraction	
space group	P $4_3 2_1 2$
wavelength (Å)	1.5418
resolution range (Å)	21.50-1.60 (1.63-1.60)
unit cell parameters (Å) a, b, c	77.5, 77.5, 37.2
total reflections	26912 (1142)
unique reflections	15197 (706)
multiplicity	1.8 (1.6)
completeness (%)	98.0 (93.5)
mean I / σ (I)	8.7 (4.4)
Wilson B factor	1.77
R_{merge}	0.068 (0.337)
R_{meas}	0.097 (0.447)
R_{pim}	0.068 (0.337)
CC1/2	0.988 (0.78)
Refinement	
R_{work}/R_{free}	0.238/0.266
N of non-hydrogen atoms	1121
macromolecules atoms	1007
N of protein residues	129
ligands atoms	23
water molecules	91
RMSD (bonds) (Å)	0.0092
RMSD (angles) (deg)	1.629
Ramachandran favoured (%)	98.43
Ramachandran allowed (%)	1.56
Ramachandran outliers (%)	0.00
rotamers outliers (%)	0.01
all-atom clashscore	9
Molprobity score	1.48
Average B-factor molecules	9.4
Average B-factor macromolecules	8.7
Average B-factor ligands	23.3
Average B-factor waters	12.9

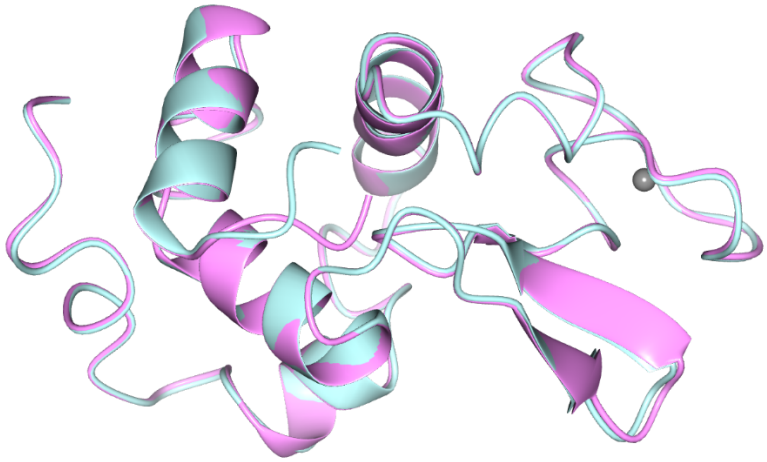

Figure 5.12: Ribbon representation of HEWL. The model obtained by molecular replacement using the in-house collected data (pink) is superposed on the known structure of HEWL (light blue) (PDB code: 3a8z). The superposition of the pdb model and the calculated structure generate and rmsd of 0.22 Å for 126 α carbon atoms. The picture was produced by using the program CCP4mg.

Multiplicity is 98%. The electron density map was generated after structure solution by molecular replacement (MR) using 3a8z as a reference structure. The R_{work}/R_{free} ratio after refinement was lowered to 0.238/0.266. According to Ramachandran statistics analysis the 98.4% of the residues were found in favoured regions, 1.6% were found in allowed regions, no outlier residues were found. A ribbon representation of the HEWL molecule is displayed in Figure 5.12. Summarizing, all the parameters evaluated in Table 5.2 and described in this section are indicators of high diffraction quality. Additionally, for situations where the crystals obtained diffract poorly or for completely unknown structures, derivatization of the crystals might be performed using the same microdevice. In these cases, the derivatization process can be controlled by the selective diffusion of ions across the membrane, avoiding abrupt changes of the local environment and handling of the crystals [19]. Indeed, simulation of Hg2+transport in the microdevice showed how it is possible to control the rate of ion diffusion by changing the volume of protein solution.

5.5 Conclusions

Trial and error is still the leading strategy for finding conditions for protein crystallization and for crystals derivatization. Microfluidics technology provides advantages to the

crystallization field with several designs that allow a lower consumption of reagents for a higher number of trials. Also, membrane technology concurred to the control of supersaturation and ligand diffusion helps to obtain a high diffraction quality of the crystals. In this work, a Nafion® membrane was integrated with a PDMS microdevice for protein crystallization. Functionality of the device was tested for the crystallization of HEWL. Stability tests showed that Nafion® should be used in the sodium form in order to avoid exchange of H^+ with the protein solution that lowers the pH to extreme conditions, with consequent degradation of the crystals. Furthermore, size and number of crystals were tuned by changing the volume of solution in the microdevice wells. Finally, the crystals grown in the micro-device were picked up and analyzed by X-rays showing a high diffraction quality. The presence of the 75 wells might allow a parallel screening of 75 different conditions were it is possible to play with concentration and volume of solution, furthermore the presence of the ion-exchange transport mediated by Nafion® membrane may be exploited for performing an in-situ gentle derivatization, avoiding abrupt changes of the local environment and handling of the crystals [19].

References

[1] J. A. Gavira. "Current trends in protein crystallization." In: *Archives of Biochemistry and Biophysics* 602 (2016), pp. 3–11. DOI: 10.1016/j.abb.2015.12.010.

[2] L. Li and R. F. Ismagilov. "Protein Crystallization Using Microfluidic Technologies Based on Valves, Droplets, and SlipChip." In: *Annu. Rev. Biophys* 39 (2010), pp. 139–58. DOI: 10.1146/annurev.biophys.050708.133630.

[3] B. G. Abdallah, S. Roy-Chowdhury, R. Fromme, P. Fromme, and A. Ros. "Protein Crystallization in an Actuated Microfluidic Nanowell Device." In: *Crystal Growth and Design* 16.4 (2016), pp. 2074–2082. DOI: 10.1021/acs.cgd.5b01748.

[4] W. Du, L. Li, K. P. Nichols, and R. F. Ismagilov. "SlipChip." In: *Lab on a Chip* 9.16 (2009), p. 2286. DOI: 10.1039/b908978k.

[5] L. Wang, K. Sun, X. Hu, G. Li, Q. Jin, and J. Zhao. "A centrifugal microfluidic device for screening protein crystallization conditions by vapor diffusion." In: *Sensors and Actuators B: Chemical* 219 (2015), pp. 105–111. DOI: 10.1016/J.SNB.2015.04.105.

[6] Y. Yu, X. Wang, D. Oberthür, A. Meyer, M. Perbandt, L. Duan, and Q. Kang. "Design and application of a microfluidic device for protein crystallization using an evaporation-based crystallization technique." In: *Journal of Applied Crystallography* 45.1 (2012), pp. 53–60. DOI: 10.1107/S0021889811048047.

[7] E. Curcio, A. Criscuoli, and E. Drioli. "Membrane crystallizers." In: *Industrial and Engineering Chemistry Research* 40.12 (2001), pp. 2679–2684. DOI: 10.1021/ie000906d.

[8] G. D. Di Profio, E. Curcio, A. Cassetta, D. Lamba, and E. Drioli. "Membrane crystallization of lysozyme: Kinetic aspects." In: *Journal of Crystal Growth* 257.3-4 (2003), pp. 359–369. DOI: 10.1016/S0022-0248(03)01462-3.

[9] G. Di Profio, E. Curcio, and E. Drioli. "Trypsin crystallization by membrane-based techniques." In: *Journal of Structural Biology* 150.1 (2005), pp. 41–49. DOI: 10.1016/j.jsb.2004.12.006.

[10] S. Simone, E. Curcio, G. Di, M. Ferraroni, and E. Drioli. "Polymeric hydrophobic membranes as a tool to control polymorphism and protein – ligand interactions." In: *Jornal of Membrane Science* 283 (2006), pp. 123–132. DOI: 10.1016/j.memsci.2006.06.028.

[11] G. D. Profio, M. Polino, F. P. Nicoletta, B. D. Belviso, R. Caliandro, E. Fontananova, G. De Filpo, E. Curcio, and E. Drioli. "Tailored hydrogel membranes for efficient protein crystallization." In: *Advanced Functional Materials* 24.11 (2014), pp. 1582–1590. DOI: 10.1002/adfm.201302240.

[12] A. C. W. Pike, E. F. Garman, T. Krojer, F. von Delft, and E. P. Carpenter. "An overview of heavy-atom derivatization of protein crystals." In: *Acta crystallographica. Section D, Structural biology* 72.Pt 3 (2016), pp. 303–318. DOI: 10.1107/S2059798316000401.

[13] G. L. Taylor. "Introduction to phasing." In: *Acta Crystallographica Section D: Biological Crystallography* 66.4 (2010), pp. 325–338. DOI: 10.1107/S0907444910006694.

[14] M. Dauter and Z. Dauter. "Phase determination using halide ions." In: *Methods in molecular biology (Clifton, N.J.)* 364.9 (2007), pp. 149–158. DOI: 10.1385/1-59745-266-1:149.

[15] J. P. Morth, T. L. M. Sørensen, and P. Nissen. "Membrane's eleven: Heavy-atom derivatives of membrane-protein crystals." In: *Acta Crystallographica Section D: Biological Crystallography* 62.8 (2006), pp. 877–882. DOI: 10.1107/S0907444906023547.

[16] C. Giacovazzo, M. Ladisa, and D. Siliqi. "The approach of the joint probability distribution functions: the SIR-MIR, SAD-MAD and SIRAS-MIRAS, cases." In: *Zeitschrift für Kristallographie - Crystalline Materials* 217.12 (2002), pp. 703–709. DOI: 10.1524/zkri.217.12.703.20660.

[17] M. G. Joyce, S. Radaev, and P. D. Sun. "A rational approach to heavy-atom derivative screening." In: *Acta Crystallographica Section D: Biological Crystallography* 66.4 (2010), pp. 358–365. DOI: 10.1107/S0907444909053074.

[18] J. Agniswamy, M. G. Joyce, C. H. Hammer, and P. D. Sun. "Towards a rational approach for heavy-atom derivative screening in protein crystallography." In: *Acta Crystallographica Section D: Biological Crystallography* 64.4 (2008), pp. 354–367. DOI: 10.1107/S0907444907068849.

[19] M. Polino, A. Luísa Carvalho, L. Juknaite, C. A. M Portugal, I. M. Coelhoso, M. J. Romao, and J. G. Crespo. "Ion-Exchange Membranes for Stable Derivatization of Protein Crystals." In: *Crystal Growth & Design* 17 (2017), pp. 4563–4572. DOI: 10.1021/acs.cgd.7b00315.

[20] T. Xu. "Ion exchange membranes: State of their development and perspective." In: *Journal of Membrane Science* 263.1-2 (2005), pp. 1–29. DOI: 10.1016/j.memsci.2005.05.002.

[21] C. F. Galinha, G. Carvalho, C. A. M. Portugal, G. Guglielmi, M. A. M. Reis, and J. G. Crespo. "Multivariate statistically-based modelling of a membrane bioreactor for wastewater treatment using 2D fluorescence monitoring data." In: *Water Research* 46.11 (2012), pp. 3623–3636. DOI: 10.1016/j.watres.2012.04.010.

[22] D. Qin, Y. Xia, and G. M. Whitesides. "Soft lithography for micro- and nanoscale patterning." In: *Nature Protocols* 5.3 (2010), pp. 491–502. DOI: 10.1038/nprot.2009.234.

[23] X. Li, F. Feng, K. Zhang, S. Ye, D. Y. Kwok, and V. Birss. "Wettability of Nafion and Nafion/ Vulcan Carbon Composite Films." In: *Langmuir* 28 (2012), pp. 6698–6705. DOI: 10.1021/la300388x.

[24] Y. Xia and G. M. Whitesides. "Soft-lithography." In: *Angewandte Chemie International Edition* 37.0 (1998), pp. 550–575. DOI: 10.1039/c1lc20189a.

[25] A. Pimpin and W. Srituravanich. "Review on Micro- and Nanolithography Techniques and their Applications." In: *Engineering Journal* 16.1 (2012), pp. 37–55. DOI: 10.4186/ej.2012.16.1.37.

[26] D.-T. Phan, C. Yang, and N.-T. Nguyen. "A sugar-template manufacturing method for microsystem ion-exchange membranes Characterization of C-PDMS electrodes for electrokinetic applications in microfluidic systems A-L Deman, M Brun, M Quatresous et al. - Fabrication of nanoporous junctions using o." In: *Journal of Micromechanics and Microengineering* 27 (2017), pp. 1–9.

[27] P. K. Yuen, H. Su, V. N. Goral, and K. A. Fink. "Three-dimensional interconnected microporous poly(dimethylsiloxane) microfluidic devices." In: 11 (2011), pp. 1541–1544. DOI: 10.1039/c01c00660b.

[28] D.-T. Phan, C. Yang, and N.-T. Nguyen. "Fabrication of nanoporous junctions using off-the- shelf Nafion membrane." In: *Journal of Micromechanics and Microengineering* 25 (2015), pp. 1–7. DOI: 10.1088/0960-1317/25/11/115019.

[29] Z. Slouka, S. Senapati, and H.-C. Chang. "Microfluidic Systems with Ion-Selective Membranes." In: 7 (2014), pp. 317–355. DOI: 10.1146/annurev-anchem-071213-020155.

[30] M. H. Pham and D. P. Barz. "Bonding Nafion® with polydimethysiloxane: A versatile approach towards ion-exchange membrane microfluidic devices." In: *Journal of Membrane Science* 537.May (2017), pp. 310–314. DOI: 10.1016/j.memsci.2017.05.020.

[31] H.-y. Jung and J. Won. "Role of the glass transition temperature of Nafion 117 membrane in the preparation of the membrane electrode assembly in a direct methanol fuel cell (DMFC)." In: *International Journal of Hydrogen Energy* 37.17 (2012), pp. 12580–12585. DOI: 10.1016/j.ijhydene.2012.05.121.

[32] M. Pessoa-Lopes, J. G. Crespo, and S. Velizarov. "Arsenate removal from sulphate-containing water streams by an ion-exchange membrane process." In: *Separation and Purification Technology* 166 (2016), pp. 125–134. DOI: 10.1016/j.seppur.2016.04.032.

[33] P. R. Evans, H. T. Jenkins, R. Keegan, E. Krissinel, K. Stevenson, A. Lebedev, S. J. Mcnicholas, R. A. Nicholls, M. Noble, N. S. Pannu, C. Roth, G. Sheldrick, and P. Skubak. "CCP 4 i 2 : the new graphical user interface to the CCP 4 program suite research papers." In: *acta crystallographica section D: Structural biology* (2018), pp. 68–84. DOI: 10.1107/S2059798317016035.

[34] P. Emsley and K. Cowtan. "Coot : model-building tools for molecular graphics research papers." In: *Acta Crystallographica Section D: Biological Crystallography* D60 (2004), pp. 2126–2132. DOI: 10.1107/S0907444904019158.

[35] G. N. Murshudov, P. Skubák, A. A. Lebedev, N. S. Pannu, R. A. Steiner, R. A. Nicholls, M. D. Winn, F. Long, and A. A. Vagin. "REFMAC5 for the refinement of macromolecular crystal structures." In: *Acta Crystallographica Section D: Biological Crystallography* 67.4 (2011), pp. 355–367. DOI: 10.1107/S0907444911001314.

[36] K. Cowtan. "The Buccaneer software for automated model building. 1. Tracing protein chains." In: *Acta Crystallographica Section D: Biological Crystallography* 62.9 (2006), pp. 1002–1011. DOI: 10.1107/S0907444906022116.

[37] S. McNicholas, E. Potterton, K. S. Wilson, and M. E. Noble. "Presenting your structures: The CCP4mg molecular-graphics software." In: *Acta Crystallographica Section D: Biological Crystallography* 67.4 (2011), pp. 386–394. DOI: 10.1107/S0907444911007281.

[38] V. B. Chen, W. B. Arendall, J. J. Headd, D. A. Keedy, R. M. Immormino, G. J. Kapral, L. W. Murray, J. S. Richardson, and D. C. Richardson. "MolProbity: All-atom structure validation for macromolecular crystallography." In: *Acta Crystallographica Section D: Biological Crystallography* 66.1 (2010), pp. 12–21. DOI: 10.1107/S0907444909042073.

[39] W. Iwai, D. Yagi, T. Ishikawa, Y. Ohnishi, I. Tanaka, and N. Niimura. "Crystallization and evaluation of hen egg-white lysozyme crystals for protein pH titration in the crystalline state." In: *J. Synchrotron Rad* 15 (2008), pp. 312–315. ISSN: 0909-0495. DOI: 10.1107/S0909049507059559.

CHAPTER 6

Outlook and Future work

6.1 Outlook

In this PhD thesis the use of ion-exchange membranes has been investigated for the production and derivatization of protein crystals in order to determine their structure by X-ray crystallography. The work was divided in three parts, hence, the general outlook for each part of the work will be here drawn. The aim of the first part of the work was to investigate the topographical effect on nucleation avoiding membrane's surface chemistry changes. In order to achieve this objective, 117 Nafion® and NR50 Nafion® membranes' topography was modified by soft lithographic techniques. Three surface topographic patterns with different scales were designed with CleWin software: cylindrical wells with nano sized diameter, triangular prism wells with micro sized dimensions and a hierarchical surface patterning composed by micro sized triangular prism wells with nano sized cylindrical wells inside. Moulds with the designed topographies were produced by photolithography and soft lithography and used for patterning the commercial membranes by thermal nanoimprint lithography or casting of the polymer solution. The effect of the membrane surface pattern on its roughness was investigated by Atomic Force Microscopy (AFM). The analysis of AFM images showed that the nanostructure affected the roughness at nanoscopic level, but no significant change in the roughness value compared to the plain membrane was observed for the microstructure since the size of the imprinted topographical features was larger than the size range of analysis. Instead, microscopical

topographical features (with a high actual/projected area ratio) had a stronger impact on the apparent contact angle compared to nano structures (with actual/projected area ratio closer to 1). Calculations of the theoretical Wenzel and Cassie-Baxter contact angles were also performed in order to establish the predominant wetting regime on the membranes. According to the results of these calculations the Wenzel model is predominant in the case of the 117-Nafion® based membranes, meanwhile Cassie-Baxter state may or may not occur in the case of NR50-Nafion® based membranes. A theoretical model for calculating the ratio between Gibbs free energy variation of heterogeneous to homogeneous nucleation that takes into account the impact of surface topography has been already presented in the literature. This model was adapted to the specific geometry and dimensions of the designed membranes (evaluated by Scanning Electron Microscopy (SEM) and optical microscopy) and used to calculate the effect of the patterned membranes on nucleation. Theoretical calculations were compared with experimental results of nucleation and crystal growth rate of Trypsin from Bovine Pancreas on the patterned membranes. An enhancement of crystals number in all the patterned membranes compared to the same membrane without patterning was observed. Different mechanisms of nucleation were proposed, according to the scale of the topographical features: large surface features that determine a significant decrease of contact angle may induce an enhancement in nucleation rate due to the higher contact area between protein solution and membrane surface; instead, small topographical features may promote local accumulation of protein molecules. Finally, this first part of the work provides a methodology for designing surfaces with specific characteristics and topographies for protein crystallization, which helps for a better control of protein nucleation and crystallization, through the understanding of local supersaturation phenomena due to the specific features created at the membrane surface. The second part of this PhD thesis was focused on the development of a membrane-based method for a controlled and stable derivatization of protein crystals. Post-crystallization treatments for resolution purposes imply the handling and removal of the crystals from their native environment with consequent shock and high risk of crystals damage. In this part of the work, two ion-exchange membranes, Nafion® (anion-exchange membrane) and Neosepta01 (cation-exchange membrane) were used to gently and selectively diffuse heavy atoms in ionic form into the crystals solution avoiding handling, breaking of vapour diffusion equilibrium and any other abrupt change of environmental conditions, guaranteeing the stability of the crystals over time.

The transport kinetics of ions commonly used for derivatization (Br^-, $PtCl_4^{2-}$, Hg^{2+}) was studied by monitoring the variation of concentration of the ions over time and used for modelling the transport in the experimental crystallization set-up. The crystallization and derivatization experiments were performed in a membrane contactor where two compartments were separated by the ion-exchange membrane. In the first compartment an unsaturated protein solution was crystallized by controlling the relative humidity with a hypertonic solution. The second compartment was filled (after crystallization) with a solution containing the ion for derivatization. Stability of the crystals derivatized by ion-exchange membranes was monitored over time by optical microscopy analysis and compared with the stability of crystals derivatized with conventional soaking. Crystals derivatized with conventional soaking started degrading after few hours, while crystals derivatized by the ion-exchange membrane were stable for over 1 month after the end of the diffusion process (hence after reaching the same ion concentration used during conventional soaking). Synchrotron analysis of the derivatized crystals allowed to confirm the presence of the three heavy atoms tested in the crystal lattice and resolve the structure of the protein by Isomorphous Replacement. Hence, in the second part of the work a new concept for performing in-situ derivatization of protein crystals has been developed avoiding the main drawbacks of the conventional technique. In the third part of this PhD thesis, the concept of derivatization by ion-exchange membrane was integrated in a polydimethylsiloxane (PDMS) microfluidic device in order to improve the throughput. A microdevice was designed by CleWin software and fabricated by soft lithography. An ion-exchange membrane was sandwiched in between two layers of PDMS by grafting. In this case, crystallization experiments were carried out by controlling the removal of water from the protein solution by osmosis through the membrane. Hence, experiments to measure the water and salt diffusion kinetics through Nafion® were performed in order to model their transport inside the microdevice. Crystallization experiments were performed for testing reproducibility, functionality of the device and crystals stability. Increasing the volume of solution for the same area of transport it was possible to obtain larger size and higher number of crystals due to a higher availability of protein molecules. The crystals grown in the microdevice showed a high diffraction quality after processing of the x-ray diffraction collected data. Finally, in this last part of this work a micro-device was developed where, with a low consumption of protein solution, it was possible to perform protein crystallization controlled by ion-exchange membranes. The same device

may be exploited for screening ions for the derivatization of protein crystals.

6.2 Future work

This PhD thesis investigated the application of ion-exchange membranes for enhanced protein crystallization and protein crystals derivatization. This work made a step towards the possibility of understanding better the topographical effect of the membrane on protein crystallization and suggested guidelines for broader experimental studies that can help the development of a more accurate model for predicting the topographical effect. Hence, a more extensive work can be done for experimenting a wider number of conditions in terms of shapes and size for different types of proteins, also comparing the effect of the same topography on different types of materials and to attempt the development of a model that can comprehend a wider number of occurring phenomena. This work also allowed the development of an *in-situ* method for the derivatization of protein crystals. The *in-situ* transport concept might be extended to other types of ligands (also using different types of membranes) such as drugs or carbohydrates in order to facilitate the study of protein-ligand interactions. Furthermore, , the use of other types of membranes also for the transport of glycerol in order to membrane-regulate the cryoprotection process and further reduce the handling of crystals by operators, is recommended. The microdevice developed in this thesis is made of PDMS in order to simplify the sealing process with the membrane. However, some efforts should be devoted to the investigation of X-ray transparent and not gas permeable materials and in finding a method for an easier bonding of these materials with the membrane. When a new method is developed, in order to test it, the first step cannot be different than using it for the crystallization of a model protein. This gives insights on where this method stands in terms of advantages and disadvantages compared to what already exists in the literature. For this reason, all the experiments reported in this PhD thesis were performed with model proteins. However, once advancements of this work are performed, it would be useful to finally test the developed concept and micro-device for the crystallization of proteins that are usually difficult to crystallize such as membrane proteins.

Conclusões e trabalho futuro

Conclusões

Nesta tese de doutoramento, foi investigada a utilização de membranas de permuta iónica para produção e derivatização de cristais de proteínas, a fim de determinar a sua estrutura por cristalografia de raios-X. O trabalho foi dividido em três partes, encontrando-se aqui as conclusões gerais para cada parte do trabalho. O objetivo da primeira parte do trabalho foi investigar o efeito topográfico na nucleação, evitando alterações químicas na superfície da membrana. Para alcançar este objetivo, a topografia das membranas Nafion® 117 e Nafion® NR50 foi modificada por *soft*- litografia. Foram desenhados três padrões topográficos de superfície diferentes com diferentes escalas, utilizando o software CleWin: poços cilíndricos com nano diâmetros, poços de prisma triangulares com dimensões micro e um padrão de superfície hierarquizado composto por micro-poços de prisma triangulares e nano-poços cilíndricos. Foram produzidos moldes, por fotolitografia e *soft*-litografia com as topografias descritas e utilizados para padronizar as membranas comerciais por litografia térmica de nano-impressão ou por casting da solução polimérica. O efeito do padrão da superfície na rugosidade da membrana foi investigado por Microscopia de Força Atómica (AFM). A análise das imagens por AFM revelou que a nanoestrutura afectou a rugosidade ao nível nanoscópico, mas não foram observadas alterações significativas no valor da rugosidade da microestrutura, comparativamente com a membrana simples, uma vez que o tamanho das características topográficas impressas é superior ao intervalo da análise. Por outro lado, o ângulo de contato das superfícies com padrões foi afetado pela relação entre a área real e a área projetada, mais do que a rugosidade no nível nanoscópico. Assim, as características topográficas microscópicas (com uma elevada rázão entre área real/área projetada) tiveram um impacto superior no ângulo de contato, em comparação com as nanoestruturas (com uma razão de área real/área projetada próximo de 1). Foram efectuados cálculos dos ângulos de contato teóricos através

das equações de Wenzel e de Cassie-Baxter para estabelecer o regime de humedecimento predominante nas membranas. De acordo com os resultados destes cálculos, o modelo de Wenzel é predominante no caso das membranas derivadas do 117-Nafion®; por outro lado o estado de Cassie-Baxter pode ocorrer ou não nas membranas derivadas do NR50-Nafion®. Encontra-se descrito na literatura um modelo teórico que considera o impacto da topografia da superfície, através do cálculo da razão da variação da energia livre de Gibbs entre a nucleação heterogénea e homogénea. Este modelo foi adaptado à geometria e dimensões específicas (obtidas por Microscopia Eletrónica de Varrimento (SEM) e microscopia óptica) das membranas desenhadas e utilizado para calcular o efeito dos padrões das membranas na nucleação. Os resultados experimentais obtidos, para as membranas com padrões, na nucleação e na velocidade do crescimento dos cristais da tripsina do pâncreas de bovinos, foram comparados com os cálculos teóricos. Observou-se um aumento do número de cristais em todas as membranas com padrões em comparação com a mesma membrana sem padronização. Foram propostos diferentes mecanismos de nucleação, de acordo com a escala dos detalhes topográficos: grandes detalhes na superfície que determinam uma diminuição significativa do ângulo de contato podem induzir um aumento na velocidade de nucleação devido à maior área de contato entre a solução proteica e a superfície da membrana; por outro lado, pequenos detalhes topográficos podem promover uma acumulação local de moléculas de proteína. Finalmente, esta primeira parte do trabalho fornece uma metodologia para desenhar superfícies com características e topografias específicas para a cristalização de proteínas, o que ajuda a um melhor controlo da nucleação e cristalização das proteínas, através da compreensão dos fenómenos de supersaturação locais devido aos detalhes específicos criados na superfície das membranas. A segunda parte desta tese de doutoramento teve como foco o desenvolvimento de um método baseado em membranas para a derivatização controlada e estável de cristais de proteína. Tratamentos de pós-cristalização para fins de resolução implicam o manuseio e remoção dos cristais do seu ambiente nativo com consequente choque e alto risco de danos nos cristais. Nesta parte do trabalho, duas membranas de permuta iónica, Nafion® (membrana de permuta catiónica) e Neosepta01 (membrana de permuta aniónica) foram usadas para difundir suavemente e seletivamente átomos pesados na forma iónica para a solução de cristais, evitando o manuseio, quebra do equilíbrio de difusão de vapor e qualquer outra alteração abrupta das condições ambientais, garantindo a estabilidade dos cristais ao longo do tempo. A cinética do transporte de iões habitualmente utilizados

para derivatização (Br^-, $PtCl_4^{2-}$, Hg^{2+}) foi estudada através da monitorização da variação de concentração dos iões ao longo do tempo e utilizada para modelar o transporte na configuração experimental de cristalização. Os ensaios de cristalização e derivatização foram realizados num contactor de membranas, onde dois compartimentos foram separados pela membrana de permuta iónica. No primeiro compartimento, uma solução proteica insaturada foi cristalizada controlando a humidade relativa com uma solução hipertónica. O segundo compartimento foi preenchido (após a cristalização) com uma solução contendo o ião para a derivatização. A estabilidade dos cristais derivatizados das membranas de permuta iónica foi monitorizada ao longo do tempo, por análise de microscopia óptica e comparada com a estabilidade dos cristais derivatizados por imersão. Os cristais derivatizados por imerção começaram a degradar após algumas horas, enquanto que os cristais derivatizados com a membrana de permuta iónica permaneceram estáveis por mais de 1 mês após o término do processo de difusão (portanto, após alcançar a mesma concentração de iões utilizada na imersão convencional). A análise por Synchrotron dos cristais derivatizados permitiu confirmar a presença dos três átomos pesados testados na rede cristalina e resolver a estrutura da proteína por substituição isomórfica. Assim, na segunda parte do trabalho, foi desenvolvido um novo conceito para a derivatização *in-situ* de cristais de proteínas, evitando-se as principais desvantagens da técnica convencional. Na terceira parte desta tese de doutoramento, foi integrado o conceito de derivatização por membrana de permuta iónica num dispositivo microfluídico de polidimetilsiloxano (PDMS) para melhorar o rendimento. Foi desenhado um microdispositivo através do software CleWin e fabricado por *soft*-litografia. Uma membrana de permuta iónica foi prensada entre duas camadas de PDMS por grafting. Neste caso, as experiências de cristalização foram realizadas controlando a remoção de água da solução de proteína por osmose através da membrana. Assim, foram realizados ensaios para medir a cinética de difusão de água e do sal através de membrana de Nafion®,para modelar o transporte dentro do microdispositivo. Foram realizados ensaios de cristalização para testar a reprodutibilidade, funcionalidade do dispositivo e estabilidade dos cristais. Foi possível obter maior número e tamanho de cristais aumentando o volume de solução para a mesma área de transporte, devido à maior disponibilidade de moléculas de proteína. Os cristais formados no microdispositivo, apresentaram elevada qualidade de difração após o processamento dos dados recolhidos por difração de raios-X. Finalmente, nesta última parte do trabalho, foi desenvolvido um micro-dispositivo onde, com um baixo consumo

de solução proteica, foi possível realizar a cristalização de proteínas controlada por membranas de permuta iónica. O mesmo dispositivo pode ser explorado para a derivatização de cristais de proteína.

Trabalho futuro

Nesta tese de doutoramento foi investigada a utilização de membranas de permuta iónica, para cristalização de proteínas e derivatização dos cristais de proteínas. Este trabalho deu um passo na direção de um melhor entendimento do efeito topográfico da membrana, na cristalização de proteínas e sugeriu diretrizes para estudos experimentais mais amplos, que possam auxiliar no desenvolvimento de um modelo mais preciso para a previsão do efeito topográfico. Assim, pode ser realizado um trabalho mais extenso considerando um maior número de condições, em termos de forma e tamanho para diferentes tipos de proteínas, comparando também o efeito da mesma topografia em diferentes tipos de materiais e tentar o desenvolvimento de um modelo, que pode compreender um número maior de fenómenos que ocorrem. Esta tese também possibilitou o desenvolvimento de um método para a derivatização *in-situ* de cristais de proteínas. O conceito de transporte in situ pode ser estendido a outros tipos de ligantes (utilizando também diferentes tipos de membranas), tais como drogas ou carboidratos, a fim de facilitar o estudo das interações proteína-ligante. Além disso, é recomendada a utilização de outros tipos de membranas, também para o transporte de glicerol, a fim de regular o processo de crioproteção com uma membrana e reduzir ainda mais o manuseio de cristais pelos operadores. O microdispositivo desenvolvido nesta tese é feito de PDMS, a fim de simplificar o processo de vedação com a membrana. No entanto, devem ser direccionados alguns esforços para a investigação de materiais transparentes e impermeáveis a gases e encontrar um método para uma ligação mais fácil destes materiais com a membrana. Quando um novo método é desenvolvido, para testá-lo, o primeiro passo deve ser a sua implementação na cristalização de uma proteína modelo. Assim, alcançamos a compreensão sobre as o vantagens e desvantagens do método, em comparação com o que se encontra na literatura. Por esta razão, todos os ensaios descritos nesta tese de doutoramento foram realizados com proteínas modelo. No entanto, uma vez que sejam realizados avanços sobre este trabalho, seria útil testar finalmente o conceito desenvolvido e o microdispositivo para a cristalização de proteínas que são geralmente difíceis de cristalizar, tais como proteínas

de membrana.

Conclusiones y trabajo futuro

Conclusiones

En esta tesis doctoral, se ha investigado el uso de membranas de intercambio iónico para la producción y derivación de cristales de proteínas con el fin de determinar su estructura mediante cristalografía de rayos X. El trabajo se dividió en tres partes, por lo tanto, aquí se dibujarán las perspectivas generales para cada parte del trabajo. El objetivo de la primera parte del trabajo fue investigar el efecto topográfico en la nucleación evitando cambios en la química de la superficie. Para lograr este objetivo, se modificó la topografía de las membranas 117 Nafion® y NR50 Nafion® mediante técnicas de *soft*-litografía. Se diseñaron tres patrones topográficos de superficie diferentes con diferentes escalas con el software CleWin: pozos cilíndricos con diámetros de tamaño nanométrico, pozos de prisma triangular con dimensiones de tamaño micro y un patrón de superficie jerárquico compuesto por pozos de prisma triangular de tamaño micro con pocillos cilíndricos de tamaño nanométrico en el interior. Los moldes con las topografías diseñadas se produjeron mediante fotolitografía y *soft*-litografía y se utilizaron para modelar las membranas comerciales mediante litografía por nanoimpresión térmica o colada de la solución de polímero. El efecto del patrón de la superficie de la membrana sobre su rugosidad se investigó mediante un microscopio de fuerza atómica (AFM). El análisis de las imágenes de AFM mostró que la nanoestructura afectó la rugosidad a nivel nanoscópico, pero no se observó ningún cambio significativo en el valor de la rugosidad en comparación con la membrana plana para la microestructura, ya que el tamaño de las características topográficas impresas fue mayor que el rango de tamaño del análisis. En cambio, el ángulo de contacto de las superficies modeladas resultó afectado por la relación entre el área de superficie real y proyectada más que la rugosidad a nivel nanoscópico. Por lo tanto, las características topográficas microscópicas (con una alta relación de área real / proyectada) tuvieron un mayor impacto en el ángulo de contacto final en comparación con las nano

estructuras (con una relación de área real / proyectada más cercana a 1). También se realizaron cálculos del ángulo de contacto teórico de Wenzel y Cassie-Baxter para establecer el régimen de humectación predominante en las membranas. De acuerdo con los resultados de estos cálculos, el modelo de Wenzel es predominante en el caso de las membranas basadas en 117-Nafion®, mientras que el estado de Cassie-Baxter puede ocurrir en el caso de las membranas basadas en NR50-Nafion®. En la literatura ya se ha presentado un modelo teórico para calcular la relación entre la energía libre de Gibbs de nucleación heterogénea a homogénea que tiene en cuenta el impacto de la topografía de superficie. Este modelo se adaptó a la geometría y dimensiones específicas de las membranas diseñadas (evaluadas mediante microscopía electrónica de barrido (SEM) y microscopía óptica) y se utilizó para calcular el efecto de las membranas modeladas en la nucleación. Los cálculos teóricos se compararon con los resultados experimentales de la nucleación y la tasa de crecimiento cristalino de la tripsina del páncreas bovino en las membranas con dibujos. Se observó un aumento del número de cristales en todas las membranas con patrón en comparación con la misma membrana sin patrón. Se propusieron diferentes mecanismos de nucleación, según la escala de las características topográficas: las grandes características de la superficie que determinan una disminución significativa del ángulo de contacto pueden inducir un aumento en la velocidad de nucleación debido a la mayor área de contacto entre la solución de proteínas y la superficie de la membrana; en cambio, las pequeñas características topográficas pueden promover la acumulación local de moléculas de proteína. Finalmente, esta primera parte del trabajo proporciona una metodología para diseñar superficies con características específicas y topografías para la cristalización de proteínas, que ayuda a un mejor control de la nucleación y la cristalización de proteínas, a través de la comprensión de los fenómenos de sobresaturación locales debido a las características específicas creadas en el superficie de la membrana. La segunda parte de esta tesis doctoral se centró en el desarrollo de un método basado en membrana para una derivatización controlada y estable de cristales de proteínas. Los tratamientos posteriores a la cristalización con fines de resolución implican el manejo y la eliminación de los cristales de su entorno nativo con el consiguiente shock y el alto riesgo de daño de los cristales. En este trabajo, se utilizaron dos membranas de intercambio iónico, Nafion® (membrana de intercambio de aniones) y Neosepta01 (membrana de intercambio de cationes) para difundir de forma suave y selectiva átomos pesados en forma iónica en la solución de cristales, evitando el manejo y la ruptura del equilibrio de difusión de

vapor. y cualquier otro cambio brusco de las condiciones ambientales, que garantice la estabilidad de los cristales a lo largo del tiempo. La cinética de transporte de los iones comúnmente utilizados para la derivación (Br-, PtCl42-, Hg2 +) se estudió al monitorear la variación de la concentración de los iones a lo largo del tiempo y se utilizó para modelar el transporte en la configuración de cristalización experimental. Los experimentos de cristalización y derivatización se realizaron en un contactor de membrana en el que dos compartimentos estaban separados por la membrana de intercambio iónico. En el primer compartimento se cristalizó una solución de proteína insaturada controlando la humedad relativa con una solución hipertónica. El segundo compartimento se llenó (después de la cristalización) con una solución que contenía el ion para la derivatización. La estabilidad de los cristales derivatizados por membranas de intercambio iónico se monitorizó a lo largo del tiempo mediante análisis de microscopía óptica y se comparó con la estabilidad de los cristales derivatizados con remojo convencional. Los cristales derivados con remojo convencional comenzaron a degradarse después de unas pocas horas, mientras que los cristales derivados por la membrana de intercambio iónico se mantuvieron estables durante más de 1 mes después del final del proceso de difusión (por lo tanto, después de alcanzar la misma concentración de iones utilizada durante el remojo convencional). El análisis sincrotrón de los cristales derivados permitió confirmar la presencia de los tres átomos pesados probados en la red cristalina y resolver la estructura de la proteína por *Isomorphous Replacement*. Por lo tanto, en la segunda parte del trabajo, se ha desarrollado un nuevo concepto para realizar la derivación in situ de cristales de proteínas, evitando los principales inconvenientes de la técnica convencional. En la tercera parte de esta tesis doctoral, el concepto de derivatización por membrana de intercambio iónico se integró en un dispositivo microfluídico de polidimetilsiloxano (PDMS) para mejorar el rendimiento. El software CleWin diseñó un microdispositivo y se fabricó mediante *soft*-litografía. Una membrana de intercambio iónico se emparedó entre dos capas de PDMS mediante injerto. En este caso, los experimentos de cristalización se llevaron a cabo controlando la eliminación del agua de la solución proteica mediante ósmosis a través de la membrana. Por lo tanto, se realizaron experimentos para medir la cinética de difusión del agua y la cinética de la sal a través de Nafion® para modelar su transporte dentro del microdispositivo. Se realizaron experimentos de cristalización para probar la reproducibilidad, la funcionalidad del dispositivo y la estabilidad de los cristales. Al aumentar el volumen de solución para la misma área de transporte, fue posible obtener un tamaño más grande y un mayor

número de cristales debido a una mayor disponibilidad de moléculas de proteína. Los cristales crecidos en el microdispositivo mostraron una alta calidad de difracción después del procesamiento de los datos recolectados por difracción de rayos X. Finalmente, en la última parte de este trabajo se desarrolló un microdispositivo en el que, con un bajo consumo de solución proteica, fue posible realizar una cristalización de proteínas controlada por membranas de intercambio iónico. El mismo dispositivo puede ser explotado para seleccionar iones para la derivatización de cristales de proteínas.

Trabajo Futuro

Esta tesis doctoral investigó la aplicación de membranas de intercambio iónico para la cristalización de proteínas y la derivatización de cristales de proteínas. Este trabajo dio un paso hacia la posibilidad de comprender mejor el efecto topográfico de la membrana en la cristalización de proteínas y sugirió pautas para estudios experimentales más amplios que pueden ayudar al desarrollo de un modelo más preciso para predecir el efecto topográfico. Por lo tanto, se puede realizar un trabajo más extenso para experimentar un número más amplio de condiciones en términos de formas y tamaños para diferentes tipos de proteínas, comparando también el efecto de la misma topografía en diferentes tipos de materiales y para intentar el desarrollo de un modelo que Puede comprender un número más amplio de fenómenos que ocurren. Esta tesis también trabajó en el desarrollo de un método para la derivación in-situ de cristales de proteínas. El concepto de transporte insitu podría extenderse a otros tipos de ligandos (también utilizando diferentes tipos de membranas) como medicamentos o carbohidratos para facilitar el estudio de las interacciones proteína-ligando. Además, sugeriría explorar la posibilidad de usar otros tipos de membranas también para el transporte de glicerol con el fin de regular también el proceso de crioprotección por membrana y reducir aún más el manejo de los cristales por parte de los operadores. El microdispositivo desarrollado en esta tesis está hecho de PDMS para simplificar el proceso de sellado con la membrana. Sin embargo, se deben dedicar algunos esfuerzos a la investigación de materiales transparentes a los rayos X y no permeables a los gases, y a encontrar un método para unir más fácilmente estos materiales con la membrana. Cuando se desarrolla un nuevo método, para probarlo, el primer paso no puede ser diferente a usarlo para la cristalización de una proteína modelo. Esto da una idea de dónde se encuentra este método en términos de ventajas y desventajas en

comparación con lo que ya existe en la literatura. Por este motivo, todos los experimentos en esta tesis doctoral se realizaron con proteínas modelo. Sin embargo, una vez que se realicen avances en este trabajo, sería útil probar finalmente el concepto desarrollado y el microdispositivo para la cristalización de proteínas que generalmente son difíciles de cristalizar, como las proteínas de membrana.

Vooruitblik en toekomstig werk

Vooruitblik

In dit PhD proefschrift is het gebruik van ionuitwisselingsmembranen voor de productie en derivatie van proteïnekristallen onderzocht, om zo hun structuur te kunnen bepalen via röntgen kristallografie. Het onderzoek was verdeeld in drie delen, voor elk deel zal hier beschreven worden. Het doel van het eerste onderzoeksdeel was het onderzoeken van het topografische effect van nucleatie, waarbij verandering van de oppervlaktechemie worden vermeden. Om dit doel te behalen, is de topografie van 117-Nafion® en NR50 Nafion® membranen gemodificeerd door middel van zachte lithografie technieken. Drie verschillende oppervlak-topografische patronen met verschillende groottes werden ontworpen met CleWin-software: cilindrische putjes met een diameter van nanoformaat, driehoekige prisma putjes met micro afmetingen en een hiërarchisch oppervlaktepatroon, van binnen samengesteld door driehoekige driehoekige prisma putjes met cilindrische putjes van nano-afmetingen aan de binnenkant. Matrijzen met de ontworpen topografieën werden geproduceerd door fotolithografie en zachte lithografie en gebruikt voor het bewerken van de commerciële membranen via thermische nano-opdruk lithografie of gieten van de polymeeroplossing. Het effect van het membraanoppervlaktepatroon op de ruwheid werd onderzocht door Atomic Force Microscope (AFM). Analyse van de AFM-afbeeldingen toonde aan dat de nanostructuur de ruwheid op nanoscopisch niveau beïnvloedde, maar er werd geen significante verandering in de ruwheidswaarde in vergelijking met het gewone membraan waargenomen voor de microstructuur, omdat de grootte van de bedrukte topografische kenmerken groter was dan de grootte van het analysegebie. In plaats daarvan bleek de contacthoek van de patroonoppervlakken meer te worden beïnvloed door de verhouding tussen het werkelijke en het geprojecteerde oppervlak dan de ruwheid op nanoscopisch niveau. Hieruit bleek dat microscopische topografische kenmerken (met een hoge werkelijke / geprojecteerde oppervlakverhouding)

een sterkere invloed hadden op de uiteindelijke contacthoek dan nanostructuren (met een werkelijke / geprojecteerde oppervlakteverhouding dichter bij 1). Berekeningen met de theoretische Wenzel en Cassie-Baxter contacthoek werden ook uitgevoerd om het overheersende bevochtigingsregime op de membranen vast te stellen. Volgens de resultaten van deze berekeningen is het Wenzel-model het predominante model in het geval van de op 117-Nafion® gebaseerde membranen, terwijl de Cassie-Baxter-toestand zich kan voordoen in het geval van op NR50-Nafion® gebaseerde membranen. Een theoretisch model voor het berekenen van de verhouding tussen Gibbs vrije energie van heterogene tot homogene nucleatie, die rekening houdt met de impact van oppervlaktetopografie, is al in de literatuur gepresenteerd. Dit model werd aangepast aan de specifieke geometrie en dimensies van de ontworpen membranen (zoals geëvalueerd door Scanning Electron Microscope (SEM) en optische microscopie) en gebruikt om het effect van de patroonmembranen op nucleatie te berekenen. De theoretische berekeningen werden vergeleken met experimentele resultaten van nucleatie en kristalgroeisnelheid van rundertrypsine op de patroonmembranen. Een verhoging van het aantal kristallen in alle patroonmembranen vergeleken met hetzelfde membraan zonder patroontoevoeging werd waargenomen. Verschillende mechanismen van nucleatie werden voorgesteld, volgens de schaal van de topografische kenmerken: grote oppervlaktekenmerken, die een significante afname van de contacthoek bepalen, kunnen een verhoging in nucleatiesnelheid creëren vanwege het hogere contactoppervlak tussen de eiwitoplossing en het membraanoppervlak; terwijl kleine topografische kenmerken de lokale accumulatie van eiwitmoleculen bevorderen. Ten slotte biedt dit eerste deel van het werk een methodologie voor het ontwerpen van oppervlakken met specifieke kenmerken en topografieën voor eiwitkristallisatie, die helpt bij een betere controle van de nucleatie en kristallisatie van eiwitten, door het in acht nemen van lokale oververzadigingsverschijnselen door de specifieke kenmerken die zijn gecreëerd bij de membraan oppervlak. Het tweede deel van dit proefschrift was gericht op de ontwikkeling van een membraan-gebaseerde methode voor een gecontroleerde en stabiele derivatisering van eiwitkristallen. Post-kristallisatiebehandelingen voor resolutiedoeleinden impliceren de hantering en verwijdering van de kristallen uit hun natieve omgeving, wat kan relatering in shock en een hoog risico op beschadigingen aan de kristallen. In dit onderzoek werden twee ionuitwisselingsmembranen, Nafion® (anionuitwisselingsmembraan) en Neosepta01 (kationenuitwisselingsmembraan) gebruikt om voorzichtig en selectief zware atomen in ionvorm in de kristallenoplossing te diffunderen

terwijl hantering, het breken van het dampdiffusie-evenwicht en elke andere abrupte verandering van omgevingsomstandigheden die de stabiliteit van de kristallen in de loop van de tijd garandeert werd gemeden. De transportkinetiek van ionen die gewoonlijk worden gebruikt voor derivatisering (Br^-, $PtCl_4^{2-}$, Hg^{2+}) werd bestudeerd door het volgen van de variatie in concentratie van de ionen in de tijd en gebruikt voor het modelleren van het transport in de experimentele kristallisatie-opzet. De kristallisatie- en derivatisatie-experimenten werden uitgevoerd in een membraan contactor waarbij twee compartimenten werden gescheiden door het ionuitwisselingsmembraan. In het eerste compartiment werd een onverzadigde eiwitoplossing gekristalliseerd door de relatieve vochtigheid te regelen met een hypertone oplossing. Het tweede compartiment werd (na kristallisatie) gevuld met een oplossing die het ion voor derivatisering bevat. Stabiliteit van de door ionenuitwisselingsmembranen gederivatiseerde kristallen werd over tijd gevolgd via optische microscopieanalyse en vergeleken met de stabiliteit van met conventioneel onderdompelen gederivatiseerde kristallen. Kristallen die waren gederivatiseerd met conventioneel weken begonnen na enkele uren te degraderen, terwijl kristallen gederivatiseerd door het ionuitwisselingsmembraan gedurende meer dan 1 maand na het einde van het diffusieproces (dus na het bereiken van dezelfde ionconcentratie die werd gebruikt tijdens conventioneel onderdompelen) stabiel waren. Synchrotron-analyse van de gederivatiseerde kristallen maakte het mogelijk de aanwezigheid van de drie zware atomen die in het kristalrooster waren getest te bevestigen en de structuur van het eiwit door isomorfe vervanging te analyseren. Dat wil zeggen dat in het tweede deel van het werk een nieuw concept is ontwikkeld voor het uitvoeren van in-situ derivatisering van eiwitkristallen, waarbij de belangrijkste nadelen van de conventionele techniek worden vermeden. In het derde deel van dit proefschrift werd het concept van derivatisering door ionuitwisselingsmembraan geïntegreerd in een microfluïdisch polydimethylsiloxaan (PDMS) apparaat om de doorvoer te verbeteren. Een micro-apparaat werd ontworpen door CleWin-software en gefabriceerd door zachte lithografie. Een ionuitwisselingsmembraan werd ingeklemd tussen twee lagen PDMS via enten. In dit geval werden kristallisatie-experimenten uitgevoerd door het controleren van de verwijdering van water uit de eiwitoplossing via osmose door het membraan. Hierom werden experimenten om de waterdiffusiekinetiek en zoutkinetiek door Nafion® te meten uitgevoerd, om hun transport in het micro apparaat te modelleren. Kristallisatie-experimenten werden uitgevoerd voor het testen van de reproduceerbaarheid, de functionaliteit van het apparaat

en de stabiliteit van de kristallen. Door het volume van de oplossing over hetzelfde transportgebied te vergroten, was het mogelijk om een grotere afmeting en een groter aantal kristallen te verkrijgen vanwege een hogere beschikbaarheid van eiwitmoleculen. De kristallen gekweekt in het micro apparaat vertoonden een hoge diffractiekwaliteit na verwerking van de door röntgendiffractie verzamelde gegevens. Ten slotte werd in het laatste deel van dit werk een micro apparaat ontwikkeld waarbij, met een laag eiwitverbruik, het mogelijk was om eiwitkristallisatie uit te voeren die werd gecontroleerd door ionuitwisselingsmembranen. Hetzelfde apparaat kan worden gebruikt voor het screenen van ionen voor de derivatisering van eiwitkristallen.

Aanbevelingen voor toekomstig werk

Dit proefschrift onderzocht de toepassing van ionuitwisselingsmembranen voor verbeterde eiwitkristallisatie en derivaatvorming van eiwitkristallen. Dit werk maakte een stap in de richting van de mogelijkheid om het topografische effect van het membraan op eiwitkristallisatie beter te begrijpen en stelde richtlijnen voor bredere experimentele studies voor die kunnen helpen bij de ontwikkeling van een nauwkeuriger model voor het voorspellen van het topografische effect. Vandaar dat er uitgebreider werk kan worden gedaan op het gebied van experimenteren met een groter aantal variaties in vormen en afmetingen voor verschillende soorten eiwitten, ook kan het vergelijken van het effect van dezelfde topografie op verschillende soorten materialen en het ontwikkelen van een model voor groter aantal voorkomende fenomenen worden ondernomen. Dit proefschrift heeft ook gewerkt aan de ontwikkeling van een in-situ methode voor de derivatisering van eiwitkristallen. Het in-situ transportconcept kan worden uitgebreid naar andere soorten liganden (ook met behulp van verschillende soorten membranen), zoals geneesmiddelen of koolhydraten, om de studie van eiwit-ligand-interacties te vereenvoudigen. Verder zou ik willen voorstellen om de mogelijkheid te onderzoeken om andere soorten membranen ook te gebruiken voor het transport van glycerol om het cryoprotectieproces membraangereguleerd te maken en de hantering van kristallen door operators verder te verminderen. Het micro apparaat dat in dit proefschrift is ontwikkeld, is gemaakt van PDMS om het afdichtproces met het membraan te vereenvoudigen. Er moet echter enige moeite worden gestoken in het onderzoeken van röntgenstralingsdoorzichtige en niet gasdoorlatende materialen en om een methode te vinden voor een gemakkelijkere binding van deze

materialen aan het membraan. Wanneer een nieuwe methode wordt ontwikkeld kan, om deze te testen, de eerste stap niet anders zijn dan deze te gebruiken voor de kristallisatie van een standaard eiwit. Dit geeft inzicht in waar deze methode staat in termen van voor- en nadelen in vergelijking met wat al bestaat in de literatuur. Om deze reden zijn alle experimenten die in dit proefschrift zijn beschreven, uitgevoerd met standaard eiwitten. Echter, zodra verbeteringen van dit werk worden uitgevoerd, zou het nuttig zijn om eindelijk het ontwikkelde concept en het micro apparaat te testen voor de kristallisatie van eiwitten die gewoonlijk moeilijk te kristalliseren zijn, zoals membraaneiwitten.

APPENDIX A

APPENDIX

A.1 Nafion® structure

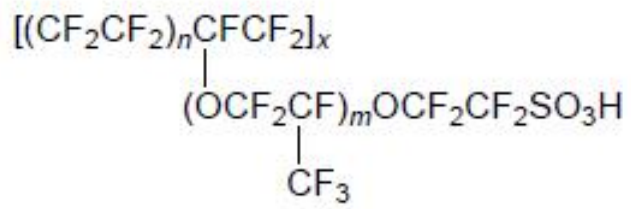

Figure A.1: Nafion structure: where m) 1, 2, or 3, and n typically has a value of about 6-7. For EW=1100g/eq m=1.

A.2 Definition of Imprinting Temperature by Differential Scanning Calorimetry

Thermal Nanoimprint Lithography (or hot embossing) transfers a pattern from a mould to a thermoplastic substrate. The process is commonly performed by heating the material to be imprinted at a temperature 20-50 °C higher than the glass transition temperature (Tg) of the substrate and afterwards high pressure is applied to improve the contact between the mould and the substrate. Therefore, in order to assess the conditions for a successful imprinting, the Tg of Nafion® was determined by DSC analysis. The measurements

were performed within a temperature interval of 35-250 °C, with a heating rate of 10 °C/min. Since, according to the literature [1, 2], the water content of the polymer might affect the Tg because of plasticization effects, and Nafion® membranes easily change the water content according to environmental humidity variations, measurements were carried out for a range (from 0% to 24%) of water content of Nafion®. In order to control the membrane water content, membranes were left equilibrating in closed vessels with different saturated salt solutions (all conditions are reported in Table A.1), and weight measured over time until no variation was recorded.

Table A.1: Nafion® at different water contents

Membrane	**Water content(%)**
Nafion® dried at 80 °C	0
Untreated Nafion®	4.5
Nafion® equilibrated with K2CO3 saturated solution RH=43%	9.8
Nafion® equilibrated with KCl saturated solution RH=85%	18.4
Hydrated Nafion®	24.0

The results reported in Figure A.2 show a Tg value of 114 ± 2 °C and no significant differences were found for different water content of Nafion®. The Tg measured for this work is in agreement with the values reported in the literature (115 °C) [1, 2]. In light of this result it was decided to perform the imprinting process at 135 °C.

A.3 Fabrication of the SU8 micromold

The design (triangles with side 165 *mu*m and repeating unit of 350 *mu*m x 185 *mu*m) has been made using the CleWin software (WieWeb software, Hengelo, NL) and transferred to a photolithography mask. A negative photoresist (SU-8 50 DE MicroChem) was spin-coated onto a Silicon wafer and exposed to UV light through the mask design in order to transfer the pattern onto the SU-8 layer. The SU-8 wafer was baked and developed with SU-8 developer, in order to remove the non-cross-linked photoresist.(Figure A.3).

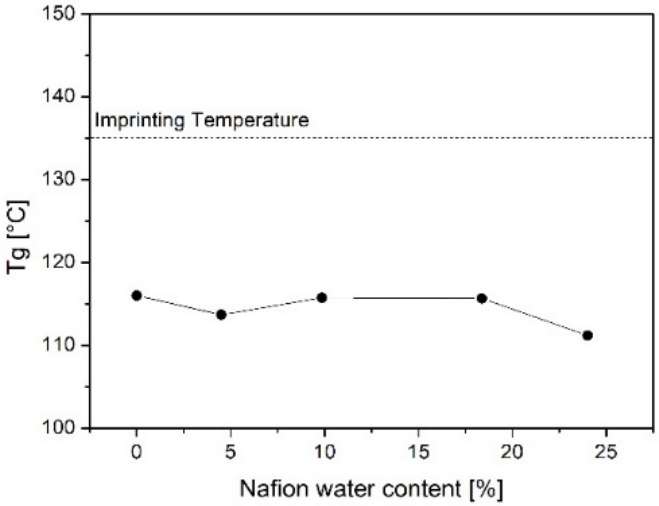

Figure A.2: DSC results for Nafion® at different water contents

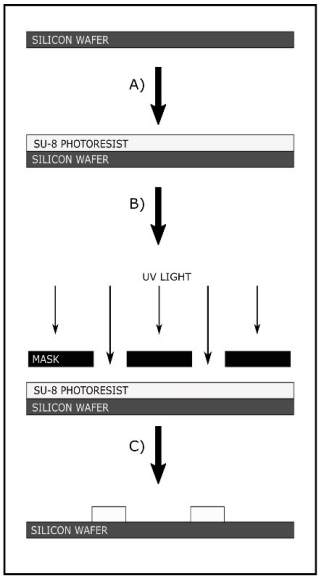

Figure A.3: Photolithography process: A) Spin-coating of the photoresist onto the silicon wafer; B) UV light exposure trough the designed mask; C) Development of the photoresist and attainment of the final mould

A.4 Calculation of Gibbs free energy variation ratio of heterogeneous to homogeneous nucleation

According to the Classical Nucleation Theory (CNT) ΔG_{Het} is defined as:

$$\Delta G_{Het} = -\frac{\Delta\mu}{\Omega} V_N + A_{NL}\gamma_{NL} - A_{NS}(\gamma_{SL} - \gamma_{NS}) \tag{A.1}$$

where μ is the chemical potential, Ω is the molar Volume, V_N is the Volume of the nucleus, A_{NL} is the area of the interface between liquid and nucleus, γ_{NL} is the interfacial energy between the nucleus and the liquid, A_{NS} is the interfacial area between the nucleus and the surface, γ_{SL} and γ_{NS} are the interfacial energy between the substrate and the liquid and between the nucleus and the substrate, respectively. We can define geometrical relations:

$$\alpha = \frac{r}{R} \tag{A.2}$$

$$\beta = \frac{h}{R} \tag{A.3}$$

If the topography is applied to a Wenzel's surface [3], where the protein solution is able to follow the geometry filling the cavities, V_N will be given by the sum of the volume of the spherical cap and the volume of the wells on the surface covered by the cap.

$$V_N = \frac{1}{3}\pi R^3[(1 - cos\theta)^2(2 + cos\theta) + \pi R^3 n\alpha^2\beta] \tag{A.4}$$

A_{NS} (the surface between the nucleus and the surface) will be given by the surface of contact between the nucleus and the surface, including the walls of the wells.

$$A_{NS} = \pi R^2(sin^2\theta + sn\alpha\beta) \tag{A.5}$$

A_{NL} (the surface between the liquid and the nucleus) will be given by the surface of the spherical cap

$$A_{NL} = 2\pi R^2(1 - cos\theta) \tag{A.6}$$

The Young Equation states:

$$\gamma_{SL} - \gamma_{NS} = \gamma_{NL} cos\theta_Y \tag{A.7}$$

where θ_Y is the Young's contact angle (contact angle for an ideally flat surface) of the solution on the substrate. When the solution is following the geometry of the surface, θ_Y

can be related to the apparent contact angle θ by the Wenzel's equation[4] :

$$cos\theta_Y = \frac{cos\theta}{\Gamma} = \frac{cos^2\theta}{sin^2\theta + 2n\alpha\beta} \tag{A.8}$$

Replacing equations A.8 in equation A.7 and later equations A.4, A.5, A.6, A.7 in equation A.1, we obtain:

$$\Delta G_{Het} = -\frac{\Delta\mu}{\Omega}\frac{1}{3}\pi R^3[(1-cos^2\theta)(2+cos\theta)+3n\alpha^2\beta]+\pi\gamma_{SL}R^2[2(1-cos\theta)-cos\theta sin^2\theta] \tag{A.9}$$

As it is evident from equation A.9 , ΔG_{Het} is given by a combination of the free energy variation of two events:

- the formation of a new phase (a spontaneous process that gives a negative contribution to the total variation of free energy, increasing as the volume of the nucleus increases);
- the formation of a new interface between nucleus and surface and nucleus and liquid (an energetically disfavoured process that has a positive contribution to the total variation of free energy, increasing as the surface of the nucleus increases).

The nucleus size (the radius) determines which of the two energy contributions is prevailing on the total value of Gibbs free energy variation of nucleation. Indeed, small nuclei exhibit high surface to volume ratio, therefore, the interface free energy component has predominance on the new-phase free energy component causing stabilization of the nuclei by their dissolution. Instead, for nuclei of larger size, the surface of the nuclei is associated with a much larger volume, hence, the new-phase free energy dominates the total free energy determining the stabilization of the nuclei by growth. Therefore, the critical nucleus radius (R^*) can be calculated as follows [5]:

$$\frac{\delta\Delta G_{Het}}{\delta R} = 0 \tag{A.10}$$

$$R^* = \frac{2\gamma_L[2(1-cos\theta)-cos\theta sin^2\theta]}{\left(\frac{\Delta\mu}{\Omega}\right)^2[(1-cos\theta)^2(2+cos\theta)+3n\alpha^2\beta]} \tag{A.11}$$

Replacing R^* in Equation A.9 we obtain ΔG^*_{Het}:

$$\Delta G^*_{Het} = \frac{16}{3}\pi\left(\frac{\Delta\mu}{\Omega}\right)^2\gamma_{L^3}\frac{[2(1-cos\theta)-cos^2\theta]^3}{[(1-cos\theta)^2(2+cos\theta)+3n\alpha^2\beta]^2} \tag{A.12}$$

From CNT we can define the variation of free energy for homogeneous nucleation for the formation of a nucleus of critical size ΔG_{Hom} as:

$$\Delta G^*_{Hom} = \frac{16}{3}\pi\gamma_L^3\left(\frac{\Delta\mu}{\Omega}\right)^2 \tag{A.13}$$

Therefore, finally we can obtain $\phi_{117Nano}$:

$$\Phi_{117Nano} = \frac{\Delta G^*_{Het}}{\Delta G^*_{Hom}} = \frac{1}{4}\frac{[2(1-cos\theta)-cos\theta sin\theta^2]^3}{[(1-cos\theta)^2(2+cos\theta)+3n\alpha^2\beta]^2} \tag{A.14}$$

In the case of 117-Micro and NR50-Micro the same model (replacing the geometric parameters of a cylinder with the ones of a triangular prism) was applied, for a Wenzel surface. Therefore, the following geometrical relationships were defined:

$$\alpha_1 = \frac{l}{R} \tag{A.15}$$

$$\beta_1 = \frac{h_1}{R} \tag{A.16}$$

Where l is the side of the triangle base of the prisma well and h_1 is the depth.

$$\Phi_{Micro} = \frac{\Delta G^*_{Het}}{\Delta G^*_{Hom}} = \frac{1}{4}\frac{[\pi^2 2(1-cos\theta)-cos\theta sin\theta^2]^3}{[\pi(1-cos\theta)^2(2+cos\theta)+\frac{3}{2}\sqrt{3}3n_1\alpha_1^2\beta_1]^2} \tag{A.17}$$

Where n_1 is the number of wells on the contact area between the nucleus and the surface. For the Hierarchical membrane (Triangular prism wells with cylindrical wells inside), both geometries of the cylinder and prisma were included in the model, resulting:

$$\Phi_{Hierarchical} = \frac{\Delta G^*_{Het}}{\Delta G^*_{Hom}} = \frac{1}{4}\frac{[\pi^2 2(1-cos\theta)-cos\theta sin\theta^2]^3}{[\pi(1-cos\theta)^2(2+cos\theta)+\frac{3}{2}\sqrt{3}3n_1\alpha_1^2\beta_1^2+3n\alpha^2\beta]2} \tag{A.18}$$

References

[1] S. H. de Almeida and Y. Kawano. "Thermal Behavior of Nafion Membrane." In: *Journal of Thermal Analysis and Calorimetry* 58 (1999), pp. 569–577. DOI: 10.1023/A:1010196226309.

[2] H.-y. Jung and J. Won. "Role of the glass transition temperature of Nafion 117 membrane in the preparation of the membrane electrode assembly in a direct methanol fuel cell (DMFC)." In: *International Journal of Hydrogen Energy* 37.17 (2012), pp. 12580–12585. DOI: 10.1016/j.ijhydene.2012.05.121.

[3] T. S. Meiron, A. Marmur, and I. S. Saguy. "Contact angle measurement on rough surfaces." In: *Image (Rochester, N.Y.)* 274 (2004), pp. 637–644. DOI: 10.1016/j.jcis.2004.02.036.

[4] E. Celia, T. Darmanin, E. T. D. Givenchy, S. Amigoni, and F. Guittard. "Recent advances in designing superhydrophobic surfaces." In: *Journal of Colloid and Interface Science* 402 (2013), pp. 1–18. DOI: 10.1016/j.jcis.2013.03.041.

[5] Y. X. Liu, X. J. Wang, J. Lu, and C. B. Ching. "Influence of the roughness, topography, and physicochemical properties of chemically modified surfaces on the heterogeneous nucleation of protein crystals." In: *Journal of Physical Chemistry B* 111.50 (2007), pp. 13971–13978. DOI: 10.1021/jp0741612.

APPENDIX B

APPENDIX

B.1 NaCl transport across Nafion®

When a cation-exchange membrane (as Nafion®) contacts a pure water solution on one side and a salt solution on the other side, water will move from the water compartment to the salt solution compartment until the osmotic pressure is equilibrated. However, due to the high osmotic pressure difference and the absence of a cation in the water compartment to be exchanged with Na^+, a leak of NaCl is expected (electrolyte leakage) [1].

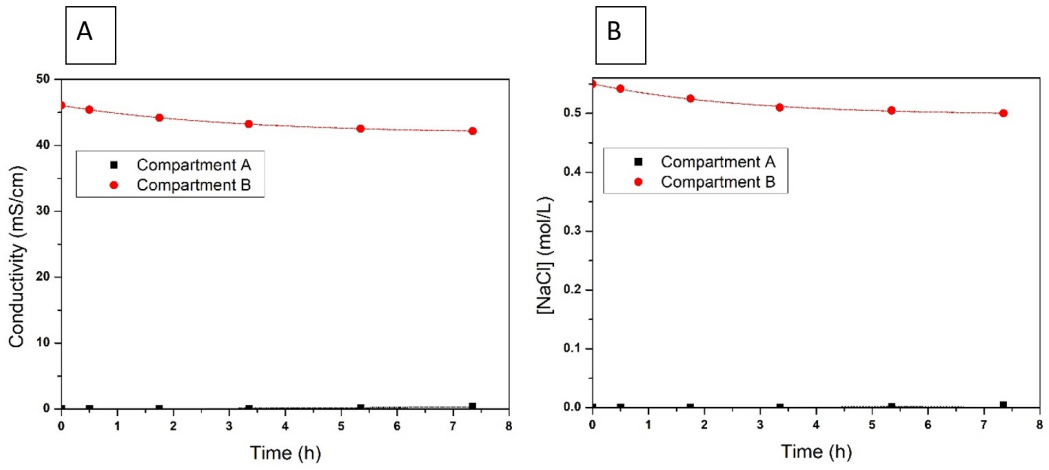

Figure B.1: A) Conductivity over time in the diffusion cell; B): NaCl concentration over time in compartment A and B of the diffusion cell

In order to assess the entity of the leak, conductivity of the solutions in the compartment A and B of the diffusion cell in Figure B.1a of the main text was followed over time (Figure B.1) By means of equipment calibration, the conductivity values were converted

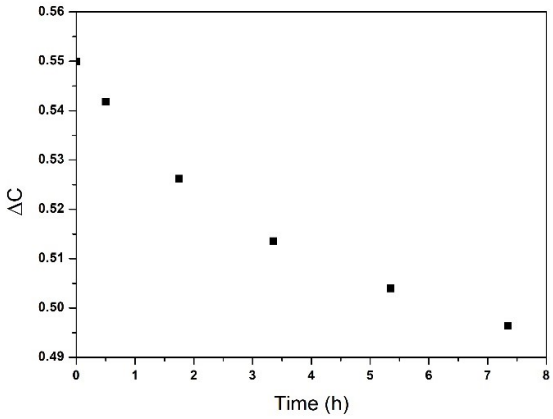

Figure B.2: Driving force versus time

into NaCl concentration (Figure B.1.B). From the difference between NaCl concentration in compartment A and B the driving force over time was calculated and represented in figure B.2. The variation of driving force over the time interval of measurement has been calculated to be 0.02M (4% of the average driving force). For this reason, it was considered constant for the calculations of water mass transfer coefficient.

B.2 Mass transfer coefficient of NaCl

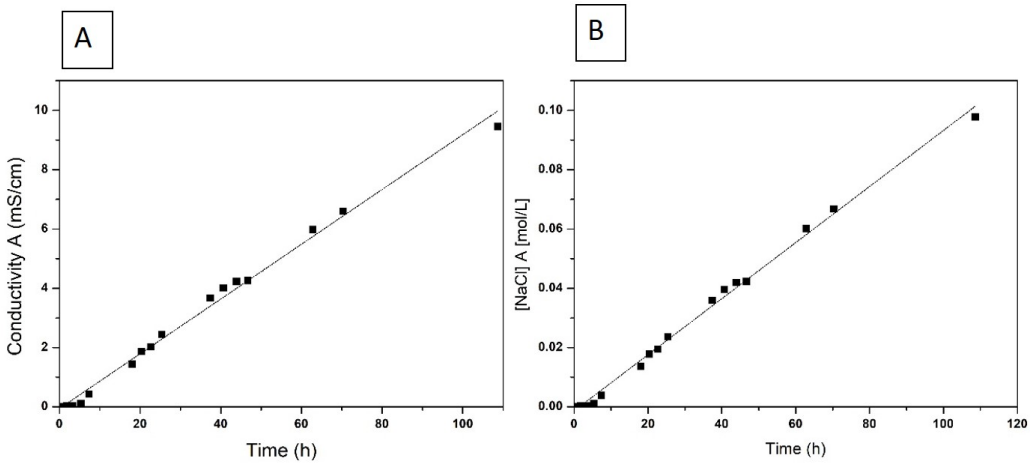

Figure B.3: Conductivity over time in compartment A; B) NaCl concentration over time in compartment A

In Figure B.3 the change of conductivity (A) and NaCl concentration (B) in compartment A over time is displayed. The change of concentration is due to both, increased concentration of NaCl in compartment A and decreased water volume due to its transport to compartment B. Therefore, the flux ($9.28x10^{-4} mol/Lh$) calculated by fitting this curve can be considered apparent.

The real amount of NaCl crossing the membrane has been calculated by multiplying the [NaCl] over time by the corresponding volume of the compartment over time and shown in figure B.4.

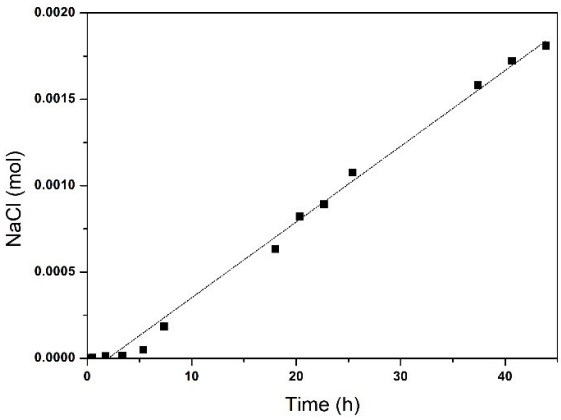

Figure B.4: Amount of NaCl crossing the membrane over time

From Figure B.4, by dividing the slope of the curve by the area of the membrane (A), the molar flux of NaCl (J_{NaCl}) was calculated (eq. B.1).

$$J_{NaCl} = \frac{mol_{NaCl}}{tA} \tag{B.1}$$

The J_{NaCl} can be also defined as:

$$J_{NaCl} = K_{NaCl} \tag{B.2}$$

Where K_{NaCl} is the apparent mass transfer coefficient for NaCl and ΔC is the NaCl concentration difference between the two sides of the membrane. Also in this case, due to the minimal variation of driving force ΔC was considered constant over time (0.52M).

Hence, K_{NaCl} was calculated as:

$$K_{NaCl} = \frac{J_{NaCl}}{\Delta C} \tag{B.3}$$

The value for K_{NaCl} was: $3.92{*}10^{-8} m/s$. This value is two orders of magnitude lower compared to the water flux suggesting that the variation of concentration is mostly determined by the water transport.

References

[1] M. Pessoa-Lopes, J. G. Crespo, and S. Velizarov. "Arsenate removal from sulphate-containing water streams by an ion-exchange membrane process." In: *Separation and Purification Technology* 166 (2016), pp. 125–134. DOI: 10.1016/j.seppur.2016.04.032.